AD-A110 081 NATIONAL BUREAU OF STANDARDS BOULDER CO ELECTROMAGN--ETC F/G 9/5
JOSEPHSON A/D CONVERTER DEVELOPMENT.(U)
OCT 81 C A HAMILTON, R E HARRIS, R L KAUTZ N00014-81-F-0048
UNCLASSIFIED NBSSR-724-29-81 NL

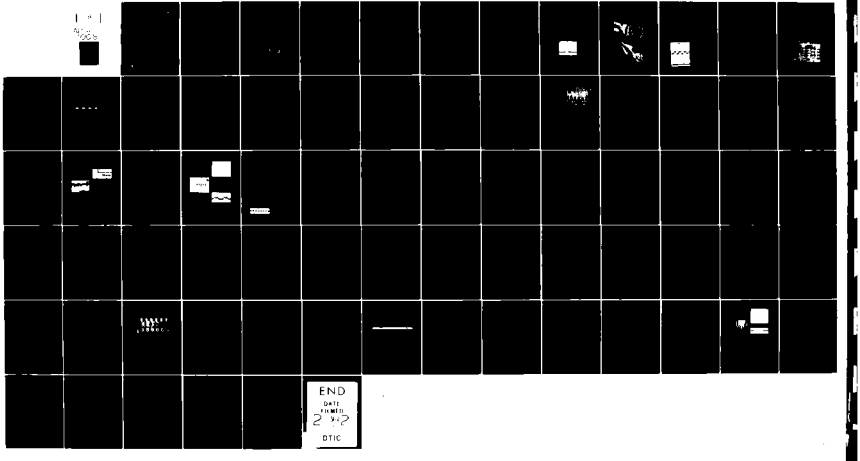

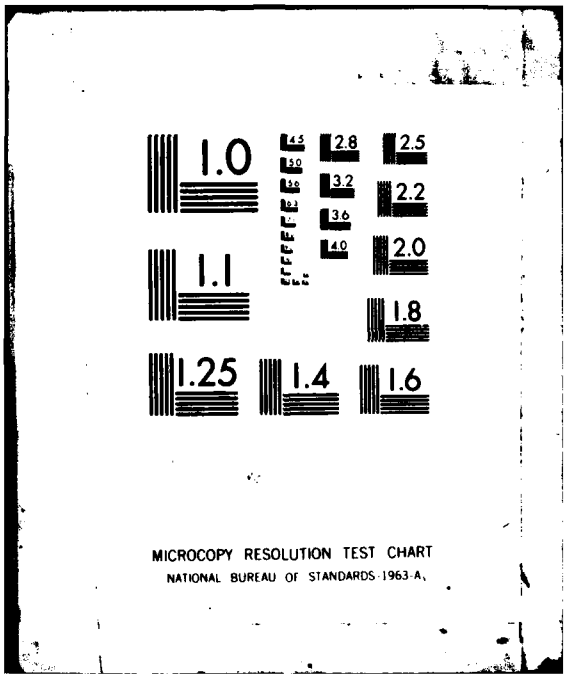
1.0
1.1
1.25
1.4
1.6
1.8
2.0
2.2
2.5
2.8
3.2
3.6
4.0
4.5
5.0
MICROCOPY RESOLUTION TEST CHART
NATIONAL BUREAU OF STANDARDS-1963-A

LEVEL III

12

AD A110081

DTIC FILE COPY

DTIC
ELECTE
JAN 26 1982
S D
D

26 82 05 8

DISTRIBUTION STATEMENT A
Approved for public release;
Distribution Unlimited

JOSEPHSON A/D CONVERTER DEVELOPMENT
ANNUAL TECHNICAL REPORT
to
Office of Naval Research, Code 427
Arlington, VA 22217
May 1, 1980 to April 30, 1981
Contract Number N00014-81-F-0048
Contract Authority NR 383-040

JOSEPHSON A/D CONVERTER DEVELOPMENT

ANNUAL TECHNICAL REPORT

TO

OFFICE OF NAVAL RESEARCH, CODE 427
Arlington, VA 22217

May 1, 1980 to April 30, 1981
Contract Number N00014-81-F-0048
Contract Authority NR 383-040

by
C. A. Hamilton, R. E. Harris, R. L. Kautz,
F. L. Lloyd, and R. L. Peterson
(Report prepared by C. A. Hamilton)

Submitted by:

Electromagnetic Technology Division
Center for Electronics and Electrical Engineering
National Engineering Laboratory
National Bureau of Standards
Boulder, CO 80303
Cost Center No. 7240480

Report No. SR-724-29-81
October 1981

Accession For	
NTIS GRA&I	X
DTIC TAB	☐
Unannounced	☐
Justification	
By	
Distribution/	
Availability Codes	
Dist	Avail and/or Special
A	

Reviewed and Approved by:

R. L. Kamper

Robert A. Kamper, Chief
Electromagnetic Technology Division

SECURITY CLASSIFICATION OF THIS PAGE (When Data Entered)

REPORT DOCUMENTATION PAGE

READ INSTRUCTIONS BEFORE COMPLETING FORM

1. REPORT NUMBER	2. GOVT ACCESSION NO. AD-A110 081
	3. RECIPIENT'S CATALOG NUMBER
4. TITLE (and Subtitle) JOSEPHSON A/D CONVERTER DEVELOPMENT	5. TYPE OF REPORT & PERIOD COVERED Annual Technical for Period May 1, 1980 to April 30, 1981
NBS	6. PERFORMING ORG. REPORT NUMBER SR-724-29-81
7. AUTHOR(s) C. A. Hamilton, R. E. Harris, R. L. Kautz, F. L. Lloyd, and R. L. Peterson	8. CONTRACT OR GRANT NUMBER(s) N00014-81-F-0048
9. PERFORMING ORGANIZATION NAME AND ADDRESS Cryoelectronic Metrology Group Electromagnetic Technology Division National Bureau of Standards, Boulder, CO 80303	10. PROGRAM ELEMENT, PROJECT, TASK AREA & WORK UNIT NUMBERS PE 62762N RF 62-582-001 NR 383-040
11. CONTROLLING OFFICE NAME AND ADDRESS Office of Naval Research, Code 427 Arlington, VA 22217	12. REPORT DATE October 1981
	13. NUMBER OF PAGES
14. MONITORING AGENCY NAME & ADDRESS(if different from Controlling Office) SAME	15. SECURITY CLASS. (of this report) Unclassified
	15a. DECLASSIFICATION/DOWNGRADING SCHEDULE

16. DISTRIBUTION STATEMENT (of this Report)

Approved for public release; distribution unlimited.

17. DISTRIBUTION STATEMENT (of the abstract entered in Block 20, if different from Report)

18. SUPPLEMENTARY NOTES

ONR Scientific Officer
Telephone (202) 696-4218

19. KEY WORDS (Continue on reverse side if necessary and identify by block number)

A/D converter; high speed superconducting electronics; Josephson junctions.

20. ABSTRACT (Continue on reverse side if necessary and identify by block number)

This report describes the fourth year of an effort to demonstrate an ultra-high-speed analog-to-digital converter using superconducting electronics. A converter was fabricated and tested at a sample rate of 4×10^9 samples/second.

DD FORM 1 JAN 73 1473 EDITION OF 1 NOV 65 IS OBSOLETE
S/N 0102-LF-014-6601

SECURITY CLASSIFICATION OF THIS PAGE (When Data Entered)

590891

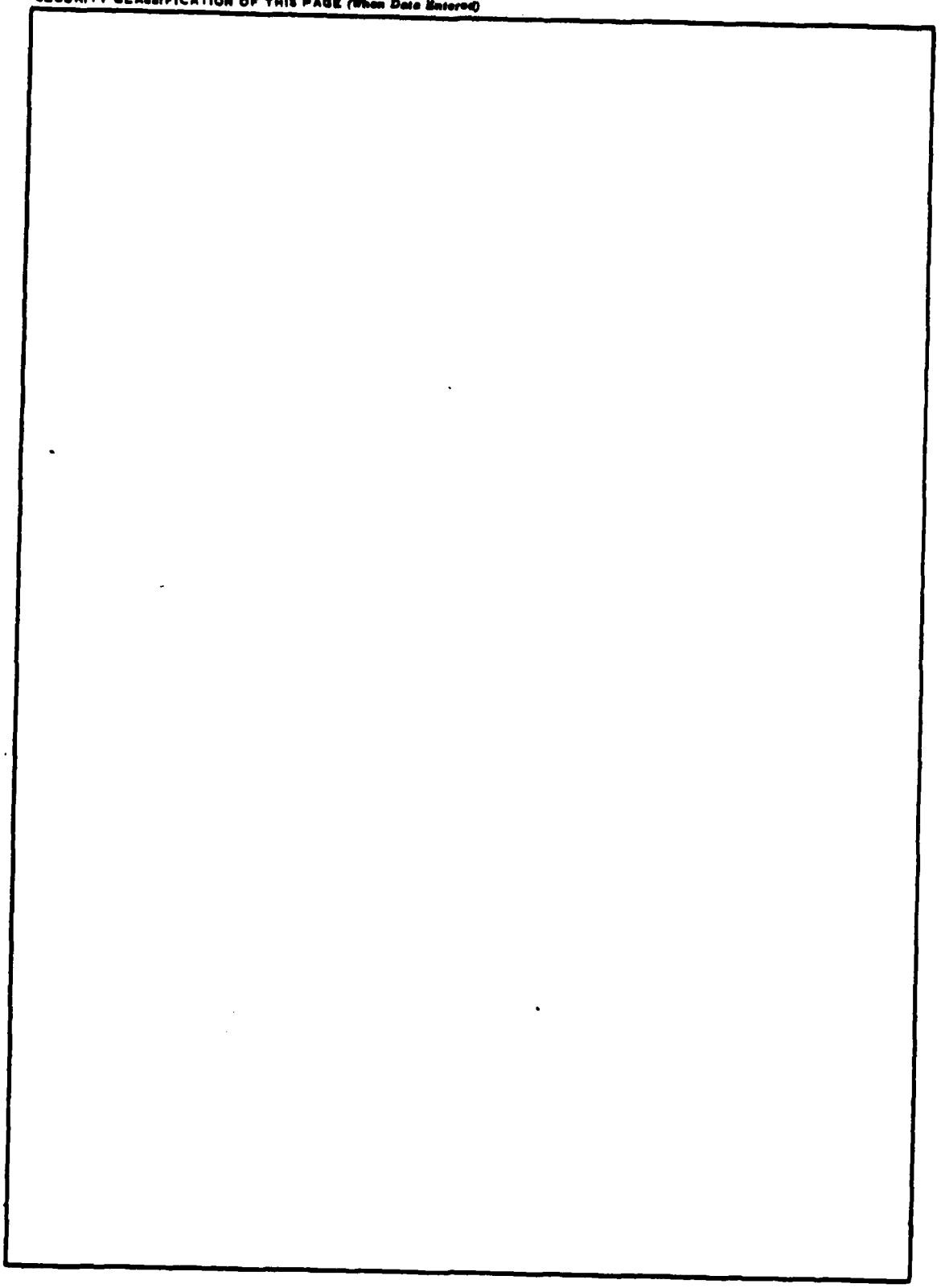

JOSEPHSON A/D CONVERTER DEVELOPMENT

TABLE OF CONTENTS

1.0 INTRODUCTION

This report describes the work performed under contract number N00014-81-F-0048 from May 1, 1980 to April 30, 1981. The general goals of this work are to explore the limits of speed and accuracy for high speed A/D converters which utilize superconducting technology. This goal has been pursued by designing, fabricating and testing an evolving set of ever higher performance devices. The funding this year was expanded to include the specific goal of an 8-bit, 5×10^8 samples/second converter. The most important accomplishments of this year are

1) The redesign of the 6-bit converter and the measurement of comparator operation at 4×10^9 samples/second.

2) The fabrication of a chip holder which allows the testing of our A/D converters at their ultimate operating speed without serious degredation due to the chip holder characteristics.

3) The demonstration of an electronics package for A/D converter testing and automatic maintenance of crucial adjustments.

4) The design of an 8-bit converter for operation at 5×10^8 samples/second. This design necessarily takes much more careful account of noise margins, supply regulation and the dynamic behavior of the SQUID comparators.

The following sections of this report cover these results in more detail and also describe the many related activities including process technology, simulation capability and publications. The success of the 6-bit converter at frequencies up to 4×10^9 samples/second has produced a number of references in the technical trade press. Copies of those we know about are included in Section 6.4.

2.0 A/D CONVERTER

2.1 Comparator Operation at 4 GHz

The most important accomplishment this year is the demonstration of comparator operation at 4 GHz. Three significant changes in the original 6-bit design made this possible: (1) the comparators were converted to current injection logic, (2) the comparators were reduced in size making the complete converter much more compact, and (3) a higher junction current density of 2000 A/cm^2 was used. An example of high speed comparator operation is shown in Fig. 2.1. The top trace is the sinusoidal power supply. The bottom trace is the comparator output for a signal input which is linearly swept between two lobes of the threshold curve. At the beginning of the trace the operating point remains within the first lobe and so no switching occurs. As the signal moves the operating point between lobes, switching begins causing a string of one outputs. Finally, as the second lobe is entered, switching ends. The variable level of the one output is caused by a combination of variable turn-on-delay due to overdrive and the sinusoidal nature of the power supply. This data demonstrates that the comparators work properly at 4 GHz and that they can be turned on and reset at this frequency. As predicted in simulations, at frequencies above 4 GHz, the SQUID comparators begin to punch-through (not reset to the zero voltage state) between cycles. This is the limiting factor in high speed operation of the converter. Achieving higher speed depends largely on our ability to make small, high current density and well matched junctions. The introduction of electron beam lithography into our process should allow substantial progress in this direction.

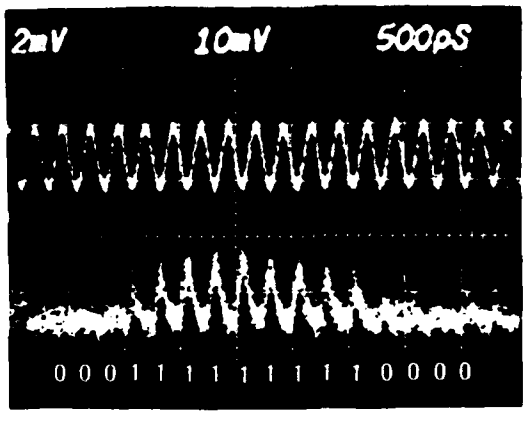

Fig. 2.1 Comparator operation at 4 GHz. Top trace is power supply. Bottom trace is comparator output for a ramped signal input.

2.2 Sample Holder

The data shown in Fig. 2.1 could not have been obtained without a substantial improvement in our sample holder. Past experiments of this sort have always been limited by crosstalk in the sample holder. In the latest design crosstalk has been effectively eliminated by utilizing coplanar striplines to bring signals to and from the chip. These lines eliminate common ground inductances and, with proper spacing, can also greatly reduce coupling due to parasatic capacitance. Photographs of the stripline contact array and assembled chip holder are shown in Fig. 2.2 a and b.

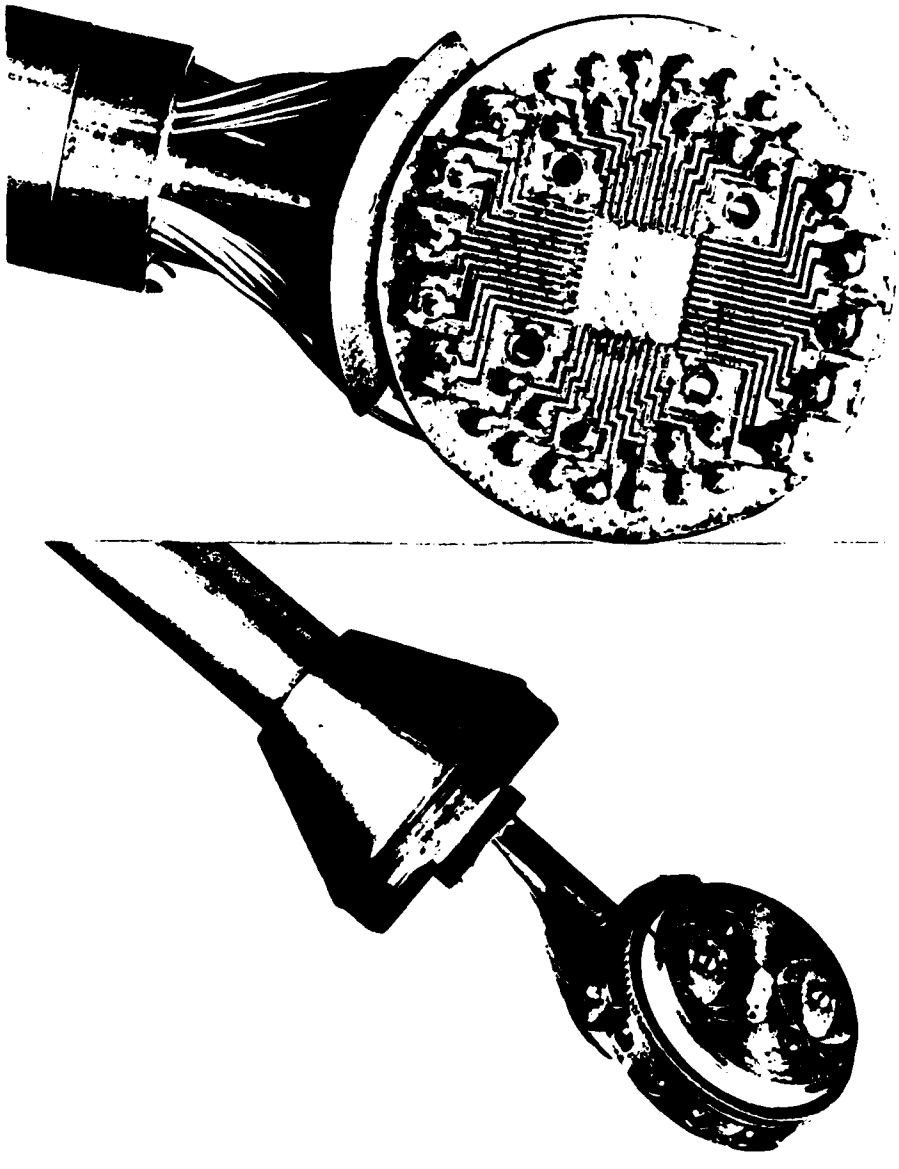

Fig. 2.2 a) Chip mount stripline array and b) assembled chip mount.

A new technique has been used to evaluate the performance of our high speed chip mount. In this procedure, the gate currents of an A/D converter chip are driven with a monopolar sine wave supply. One of the six SQUID comparator outputs is connected to a pass through sampling head which is left unterminated (open circuit). The resulting large reflection coefficient makes the output cable act like a cavity with a set of resonant frequencies given by $N/2\tau$ where N is an integer and τ is the cable delay. When the drive frequency corresponds to one of these resonances each SQUID switching transition will be reflected back to the SQUID at just the right moment to trigger another transition. This mode of operation has three beneficial effects: (1) The reflected signal provides a substantial overdrive which makes the SQUID transitions very fast, (2) The reset transitions are also reflected back and allow the SQUID to reset at higher frequencies than would otherwise be possible, and (3) Time jitter between the sine wave drive and the SQUID output is greatly reduced.

These advantages allow an excellent measure of the bandwidth and crosstalk characteristics of the probe. Some of the results are shown in Fig. 2.3. The top trace is the sine wave power supply. The second trace shows the SQUID switching and resetting at a 4 GHz rate. The third trace shows one of the switching transitions on an expanded time scale. The risetime of approximately 20 ps suggests a probe bandwidth greater than 10 GHz. In the bottom trace the dc bias has been adjusted so that the SQUID will not switch. The remaining signal shows negligible crosstalk from the sine wave supply, even at 4 GHz. Although these results should be regarded as preliminary they suggest that the present probe design is a substantial improvement over earlier versions.

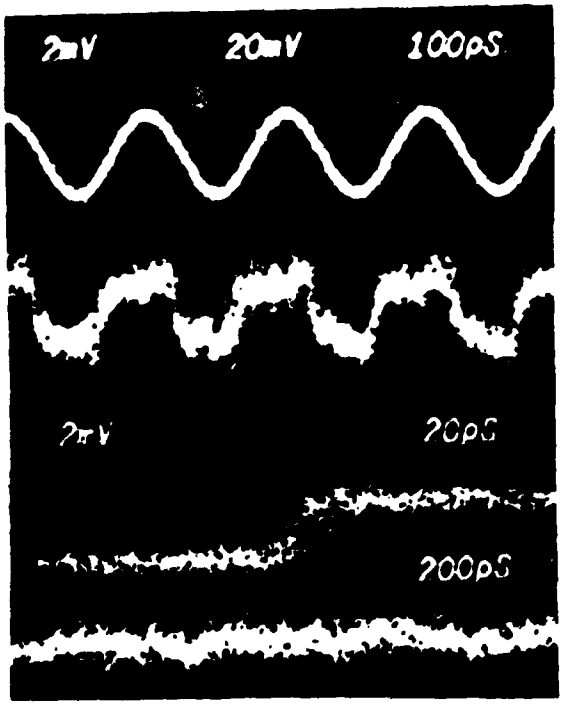

Fig. 2.3 (a) The sine wave supply
(b) SQUID output voltage
(c) A switching transition
(d) Crosstalk level

2.3 Automatic Test Apparatus

Testing of the A/D converters requires the maintenance of many adjustments and the simultaneous observation of 7 or more waveforms. To facilitate this testing we have fabricated a test apparatus which is connected to the converter by a 34 wire ribbon cable and performs the following functions.

(1) Supplies a triangle wave test signal input.

(2) Amplifies the 6-bit outputs and multiplexes them to display all 6 channels on a scope.

(3) In an alternate mode the triangle wave generator and multiplexer can be used to simultaneously display the 6 I-V curves of the SQUID comparators.

(4) Converts the A/D Gray Code output to binary and via a D/A converter produces the staircase function.

(5) Provides manual or automatic adjustment (via 12 interactive servo loops) of all A/D adjustments.

This device shown in Figs. 2.4 a and b has been crucial to our testing efforts. The automatic mode in which all adjustments are servo locked to their correct values has been successfully demonstrated this year.

2.4 8-Bit Converter

A new effort was begun in March of this year to extend our 6-bit converter design to 8-bits. The effort thus far has emphasized an analysis of problems affecting accuracy and a theoretical design which addresses these problems. The critical design considerations include noise margins, power supply regulation, threshold curve critical points and signal line crosstalk. The detailed analysis is given in a paper "Design Limitations for Superconducting A/D Converters," C. A. Hamilton and Frances L. Lloyd, which will be published in the November issue of IEEE Transactions of Magnetics. A preprint is included in this report in Section 7.5. The design for an 8-bit converter, presented in this paper, is presently being implemented. It is expected that an initial layout will be completed in August and the first chips available in September.

2.5 Computational Capability

In support of our A/D converter program we are continually updating our computational and simulation capability. Two significant improvements have been made this year. The threshold curve program written by Robert L. Peterson has been converted to describe the two junction comparators used in our converter (see Fig. 2.5 a). A dynamic simulation has also been added to locate the critical points. These are the points, above which, crossing the threshold curve will induce a transition to the voltage state. In an underdamped comparator, the critical points move down, making the comparator output ambiguous over certain regions of signal input.

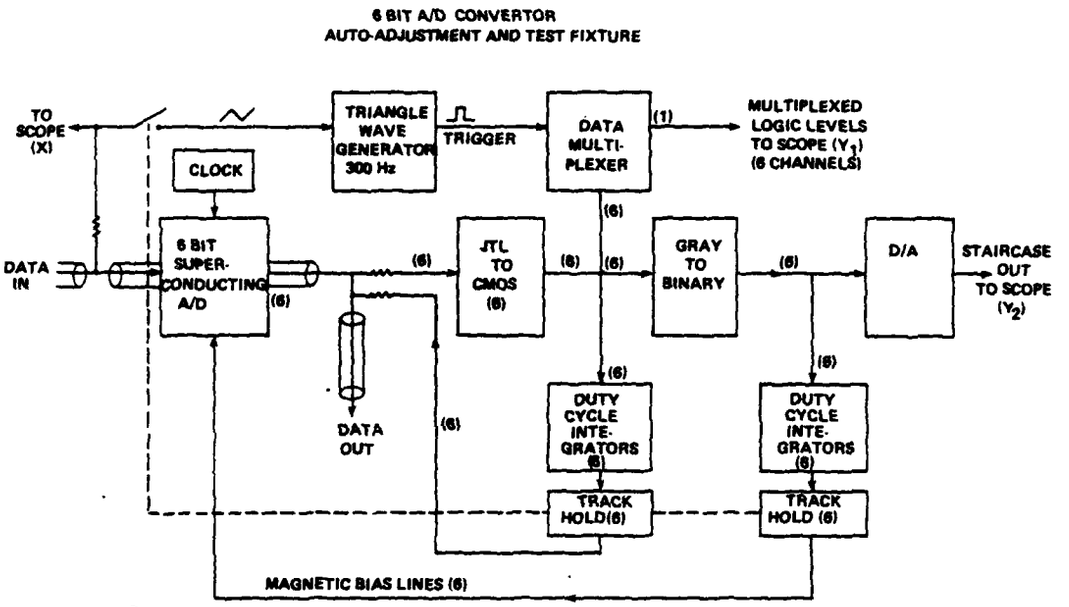

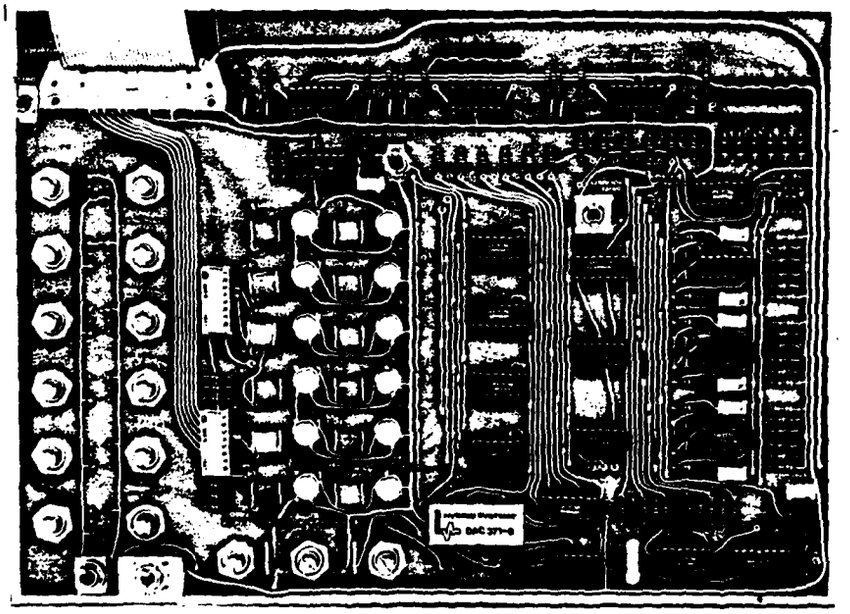

Fig. 2.4 a) Block diagram of auto adjustment test fixture.
b) Photograph of auto adjustment test fixture.

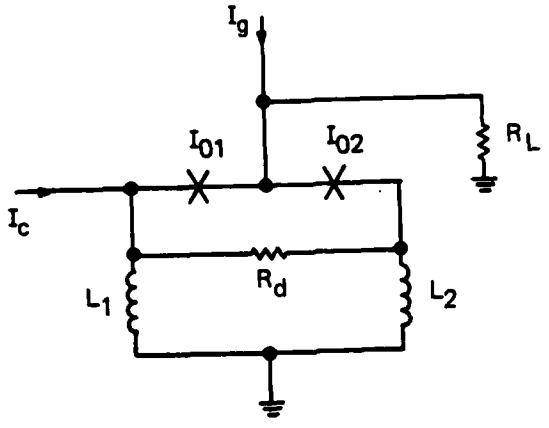

(A)

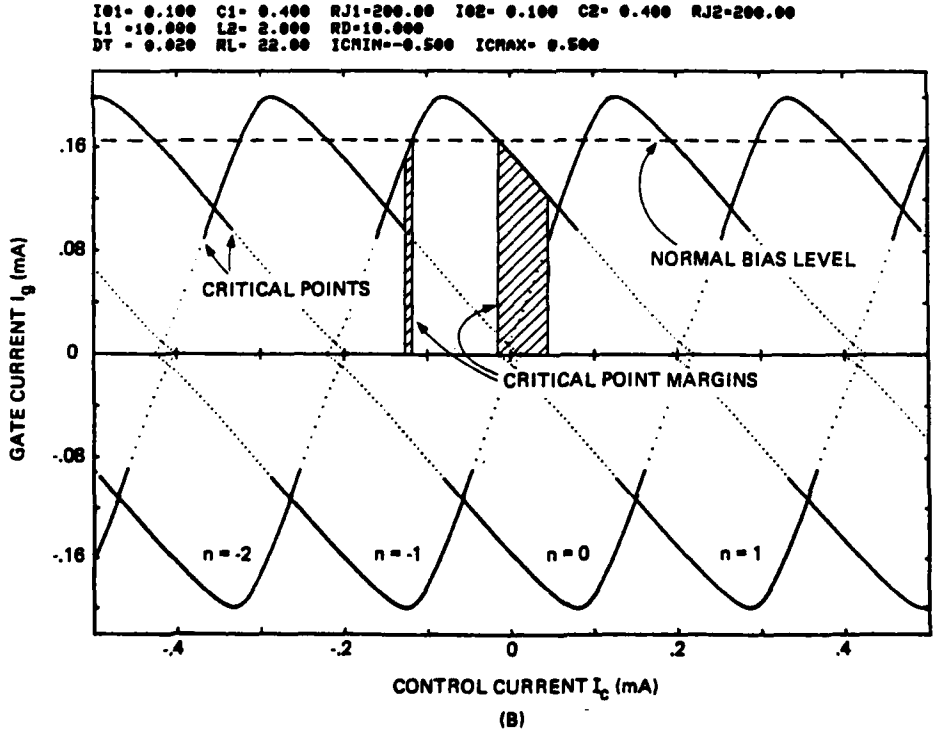

(B)

Fig. 2.5 (A) Circuit diagram for a SQUID comparator and
(B) A typical threshold curve.

The new program has been very useful in designing optimally damped two junction SQUID comparators. An example of the program output is shown in Fig. 2.5 b. The critical points are indicated as the ends of the solid portions of the curve. The shaded area represents the margin between the critical points and the region where ambiguous switching begins. This margin is improved by choosing optimum values of R_d and R_L in Fig. 2.5 a.

We have also been working on the development of a circuit analysis program which is specific to Josephson circuits. This project is being done by a part-time student, Rex Craig, from the University of Colorado. The program combines the numerical analysis methods described in our previous reports (microSCEPTOR) with a generalized nodal input format. The program is now working and is being used for our circuit design problems. This program was used to simulate the probe test experiment previously described. The result is shown in Fig. 2.6 and is in good agreement with the data of Fig. 2.3. Another example simulation is shown in Fig. 2.7 which plots the output voltage (bottom curve) and the voltage across the inductors (top two curves) for the switching transition of a direct injection SQUID. This type of data is essential to evaluate the crosstalk along the signal line of our A/D converter.

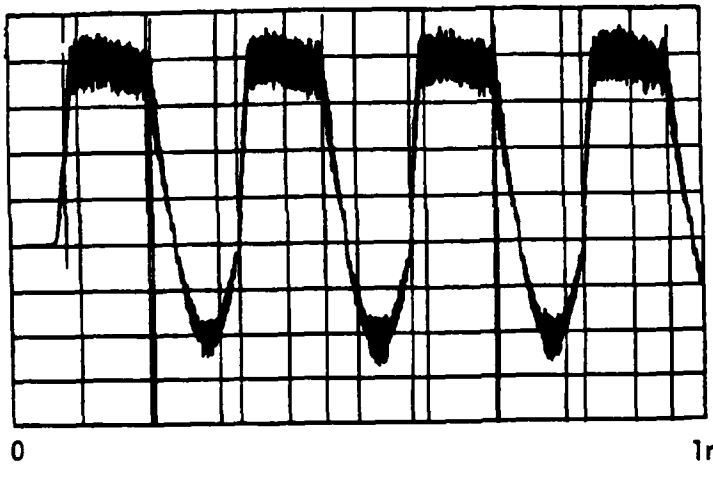

Fig. 2.6 Simulated SQUID output voltage.

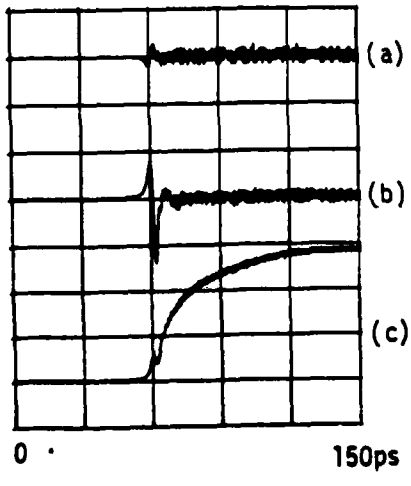

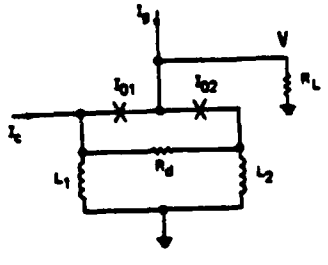

Fig. 2.7 (a) Voltage across L2
(b) Voltage across L1
(c) SQUID output voltage.

3.0 APERTURE TIME

The effort to build a sample and hold circuit based on a shaped power supply waveform has been abandoned as impractical. While the idea works in simulations, the penalty which it extracts in operating margins is fatal to a real circuit.

In our present circuit the data conversion takes place very fast but the converter must be kept active for a much longer time in order to transfer the data to room temperature. If the signal changes during this data transfer time, additional bits may switch, leading to an erroneous code. The error is caused by including a long data transfer time in the aperture time. A solution is to build a very fast latch adjacent to the converter. The converter is then turned on only long enough to transfer data to the latch ($\sim$ 50 ps). The latch can then hold the data, independent of signal changes, for an arbitrarily long time. This is the approach now being tried.

An illustrative circuit is shown in Fig. 3.1. The signal comparator is the same as in previous designs but now its output drives a following latch. The comparator gate current is supplied from a bus which is attached to a shorted stripline stub. Thus the comparators are on only until the reflected signal from the shorted stub returns. By this time, however, the comparator output has been stored in the latch. The aperture time is thus the roundtrip time of the stripline stub which must be at least long enough for the comparators to operate.

We expect to build a circuit of this sort in the next year.

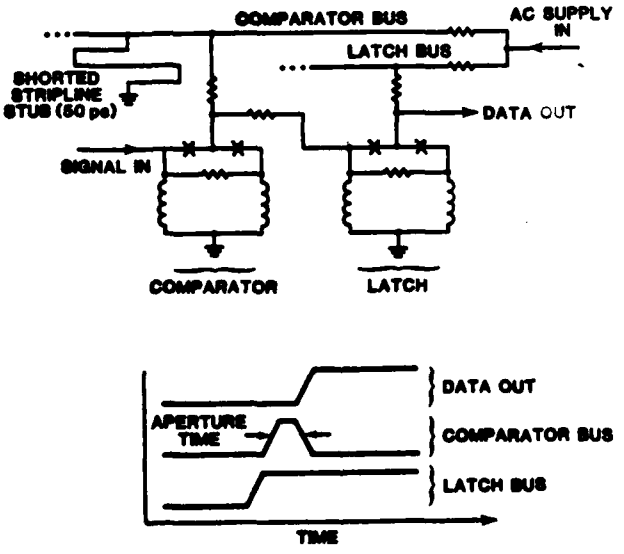

Fig. 3.1 (a) A circuit showing one bit of the A/D converter followed by a fast latch and (b) the timing diagram for this circuit.

4.0 SHIFT REGISTER MEMORY

When spare contact pads are available on the A/D chip, we have included a test shift register memory. This device consists of a series array of AND gates driven by a three phase power supply. Figure 4.1 shows the shift register circuit and how it might be connected to the A/D converter to be used as a serial fast write, slow read memory. As data appear at the A/D comparator outputs, the three phase supply causes this data to ripple through the gate array. When the ac component of the supply is turned off the data remain stored in the gate array.

Tests of the original shift register revealed some problems which have now been corrected. We expect to test a working shift register with a small number of stages in the near future.

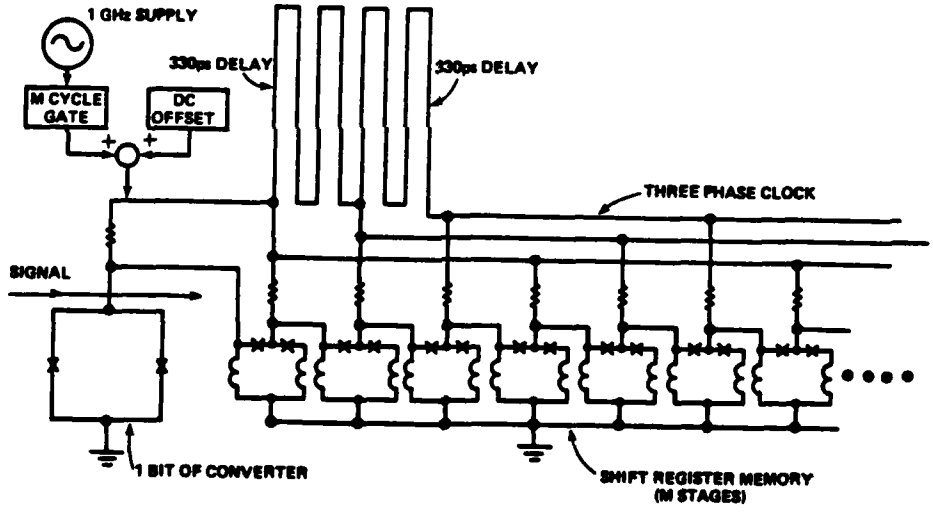

Fig. 4.1 A shift register memory consisting of a series string of AND gates driven by a three phase clock.

5.0 FABRICATION IMPROVEMENTS

We have a continuing effort to increase our microcircuit yield by improving both our fabrication process and our ability to control it. This year several significant strides have been made in this direction.

5.1 Niobium Films

Three important changes have been made in our niobium deposition procedure: (1) New oxidized wafers are now stripped of their SiO_2 coating just prior to insertion in the Nb sputter gun system. This results in better Nb adhesion and also provides a room temperature shorting path through the silicon substrate between all pads. These shorting paths protect against static electricity damage and allow us to verify all probe contacts at room temperature. (2) A heater has been added to the Nb deposition system so that the system parts and wafers can be baked prior to deposition. This has improved the typical resistance ratio of our Nb films from 2.5 to 4.5. (3) An integrating power meter has been added to automatically control the Nb sputter gun so as to achieve more accurate and reproducible thickness.

5.2 Liquid Nitrogen Cooled RF Cathode

A new rf cathode, capable of controlled temperature between -190 C and + 70 C has now been installed in our alloy deposition and rf oxidation system. This has allowed us to produce fine grained electrodes for our Josephson devices.

5.3 Gas Analyzer

A new gas analyzer has also been added to the alloy deposition system. This equipment showed that most of our base pressure was due to water vapor. This has now been corrected with the addition of a liquid nitrogen cooled shroud in the vicinity of the samples. The typical base pressure has now improved by about a factor of four.

5.4 Dicing Saw

After many frustrating delays, we remain optimistic that a Tempress 602 diamond dicing saw will soon be delivered. This will improve yield and the accuracy of the final chip dimensions. This accuracy is very important when the chip must be aligned to 50 or more chip holder contacts.

6.0 INFORMATION EXCHANGE

6.1 Leadership

C. A. Hamilton served as vice chairman for the second Workshop on Digital Devices, Circuits and Systems, Waterville Valley, New Hampshire, September 1981.

C. A. Hamilton is on the organizing committee for the Workshop on High Speed A/D Conversion to be held in San Francisco, CA, February 1982.

R. E. Harris spent the year from July 80 to July 81 as a guest worker at the IBM Research Laboratory in Zurich, Switzerland.

6.2 Invited Talks and Awards

R. E. Harris, "Impact of Superconducting Integrated Circuits on Electrical Measurement," ICCC 80, New York, September 1980.

C. A. Hamilton, "Design Limitations for Superconducting A/D Converters," INTERMAG 81, Grenoble, France, May 1981.

On November 6, 1980, Clark Hamilton, Richard Harris, Frances Lloyd, and Robert Peterson received the Department of Commerce Silver Medal for work on the high speed A/D Converter.

6.3 Publications

1. "Analog Measurement Applications for High Speed Josephson Switches," C. A. Hamilton, Frances L. Lloyd and R. L. Kautz, IEEE Trans. Mag., Vol. MAG-17, pp. 577-582, January 1981.

2. "Impact of Superconducting Integrated Circuits on Electrical Measurement," Richard E. Harris, Proc. IEEE International Conference on Circuits, and Computers, pp. 882-883, October 1980.

3. "Picosecond Applications of Josephson Junctions," D. G. McDonald, R. L. Peterson, C. A. Hamilton, R. E. Harris, and R. L. Kautz, IEEE Trans. on Electron Dev., Vol. ED-27, pp. 1945-1964, October 1980.

4. "Superconducting Electronics," Donald G. McDonald, Physics Today, pp. 36-47, February, 1981.

5. "Design Limitations for Superconducting A/D Converters," C. A. Hamilton, Frances L. Lloyd, IEEE Trans. Mag., November 1981.

6.4 References in the Technical Trade Literature

The progress of our A/D converter program has produced a number of short news items in the technical trade literature. A list of the ones we have found and copies of the articles are given below.

Title	Publication	Date	Circulation
Breakthrough in A/D Conversion to Advance High Speed Testing	Electronic Packaging & Production	2/81	26,057
Supercooled Converter Produces 6-Bits at 2 GHz Rate	Electronics	1/27/81	94,600
A/D Converter	Science Trends	1/19/81	Unknown
A/D Converter	Inside R & D	1/14/81	Unknown
Fast, Faster, & Fastest	Mechanical Engineer	5/81	65,213
NBS Laboratory Unveils Real-Time A/D Converter	Electronic News	2/2/81	74,000
NBS Builds Superfast Data Acquisition System	Instruments & Control Systems	2/81	70,000
Josephson IC Speeds A/D Conversion	Electronics	3/10/81	94,600
Measurement Science is Catching Up	Electronics	7/31/80	94,600

Breakthrough in A/D conversion expected to advance high speed testing

NBS scientists have recently built and tested the fastest known real-time analog-to-digital converter. The NBS superconducting device uses Josephson junctions as its active elements, has six-bit resolution, and in tests has performed two billion A/D conversions per second. It should ultimately be useful for a variety of civilian and military applications involving high-speed measurements and signal processing. One use might be to measure the shape of fast transient phenomena for events lasting only several billionths of a second. The improved time resolution could yield valuable information not readily obtainable by other means. Laser chemistry, radar, communications, and weapons testing are representative of other areas where higher speed measurements could benefit.

Supercooled converter produces 6 bits at 2-GHz rate

Researchers at the National Bureau of Standards in Boulder, Colo., have succeeded in building an experimental Josephson analog-to-digital converter capable of **2 billion 6-bit samples per second—the highest conversion rate ever achieved.** The converter, built of Squids (Supercooled Quantum Interference Devices), works like a flash converter but uses only 6 elements (rather than 36) and fits on a 1-mil² silicon die. A study has shown that an 8-bit part operating at somewhat lower rates is also feasible. The lab setup—consisting of a 2-GHz sine-wave generator, sampling scope, transmission lines, and refrigerator—cost about $60,000.

SCIENCE TRENDS
WASHINGTON, D.C.
WEEKLY

JAN 19 1981

+++ North Carolina may spend $24 million to build a microelectronics center in the hopes of attracting manufacturers in this field. For details, contact Governor's Office, Attn: G. Pearce, Raleigh, NC 27611. Telephone: 919/733-5612. +++ A course on supergravity is to be held April 22-May 6 in Trieste, Italy. Advanced seminars will be given May 4-6. For details, contact International Center for Theoretical Physics, Attn: A. Hamende, Box 586, Strada, Costiera 11, Miramare 34100, Trieste, Italy. +++ A salary survey for engineers in the Wash., DC area is now available to corporations at $25/initial copy and $15/each extra copy, or to individual members at $5 from Institute of Electrical and Electronics Engineers, Attn: Salary Survey Dept., Washington Section Office, 608 H St., SW, Wash., DC 20024. +++ Development of a real-time analog-to-digital converter using Josephson functions, said to be the fastest in existence, was reported by the National Bureau of Standards. For details, contact NBS, Attn: C.A. Hamilton, project leader, Boulder, CO 80303.

What may be the fastest real time analog-to-digital converter in existence has been developed by the National Bureau of Standards at its Boulder, CO, laboratories. In tests it has performed two billion A/D conversions per second.....

.....Key to speed is use of a superconducting device with Josephson junctions as active elements. The converter also uses interference phenomena to simplify circuits. These interference effects permit construction of a converter with only six active elements (one for each bit) to achieve parallel operation with fully decoded output. Normally full parallel operation would require 64 active elements and circuitry for decoding.....

.....The A/D converter fits trends to lower frequency metrology that emphasize handling data in digital form. With digital signals, relatively simple, inexpensive components can preserve signal fidelity. And a range of mathematical transformations can extract desired information from a complex signal. Thus, the transducer which converts the signal into digital form is crucial to system accuracy.....

.....With its speed, the device will permit research into high speed reactions such as fast transient phenomena encountered in fusion experiments lasting several billionths of a second. Laser chemistry, radar and communications also produce fast events that can be analyzed with high speed A/D converters.....

.....Even higher speeds are a real prospect. The present barrier is transmission of signals to and from the chip. Crosstalk in lines to the chip sets the speed limits. But engineering improvements may be able to push speeds higher.....

.....Details: [illegible] Hamilton, National Bureau of Standards, Boulder, CO 80302.

Fast, Faster, and Fastest

Scientists at the National Bureau of Standards (NBS) Laboratories in Boulder, Colo., have built and tested the fastest known real-time analog-to-digital converter. The NBS superconducting unit uses Josephson junctions as its active elements, has six-bit resolution, and has performed 2 billion A/D conversions per second. The device has a variety of applications involving high-speed measurements and signal processing. One use might be to measure the shape of fast transient phenomena in fusion experiments. Such events last only several billionths of a second, and improved time resolution could yield valuable information.

This achievement is a major step in the Bureau's research goal of demonstrating the feasibility of a new generation of measurement instruments based on superconducting integrated circuits. Other facets of this program are high-speed sampling, ultrasensitive magnetometers, microwave mixers, and advanced voltage standards. The project, which is supported by the Office of Naval Research, has the ultimate aim of a three-to-five-fold further increase in performance. At these conversion rates, a fast memory system will have to be added since there are no available devices to accept digital information at such high speeds.

NBS Laboratory Unveils Real-Time A-D Converter

WASHINGTON — The U.S.' Commerce Department's National Bureau of Standards laboratory in Boulder, Col., said it has built and tested "the fastest known real-time analog-to-digital converter," a Josephson junction device with six-bit resolution that can perform two billion A-D conversions per second.

According to the NBS, the converter should ultimately be useful for a variety of civilian and military applications involving high-speed measurements and signal processing.

Possible applications include measurement of the shape of fast transient phenomena encountered in different types of fusion experiments, events which typically last only several billionths of a second. Improved time resolution could improve measurement capabilities, the NBS said. Other applications include laser chemistry, radar, communications and weapons testing.

Chrysler's Heinrich, "they've got a fascinating idea that's caught a lot of people's attention."

Another new entry besides Zenith was made by France's Jaeger, located in Levallois, which officially introduced its electrolytic liquid display [*Electronics*, Jan 27, p. 82]. The electrolytic display uses the dispersion of light caused when a thin silver film is deposited on a clear electrode under the influence of an electric current.

Reversing the current removes the deposited film and erases the display, which otherwise retains its image for several minutes without power. It takes 100 to 200 milliseconds to write and 5% to 10% longer than that to erase. The manufacturer claims that the cell is easier and less expensive to manufacture than liquid crystal. In addition, it promises 10,000 hours of operating time at −40°C to +80°C. **-Gil Bassak**

Instruments

Josephson IC speeds a-d conversion

Dual-slope and flash-conversion techniques for precision digital instrumentation may well be supplanted by methods based on Josephson junction technology. Such supercooled circuitry can switch at picosecond speeds, so it can measure ultrahigh frequency directly.

Working toward that goal, researchers at the National Bureau of Standards have constructed a Josephson-based 6-bit analog-to-digital converter capable of taking 2 billion samples a second [*Electronics*, Jan. 27, p. 33]. "It is a major step in demonstrating the feasibility of a new generation of measurement instruments based on supercooled integrated circuits," an NBS spokesman says.

As the photograph shows, the NBS chip has six conversion units, each based on a two-junction Josephson element. The conversion technique is based on the ability of this element, called a superconducting quantum interference device, or Squid, to switch states each time the magnetic flux in the area between the junctions reaches the critical level of half a flux quantum. "There's nothing in semiconductor technology like it," maintains Clark Hamilton, the project leader at the Boulder, Colo., facility.

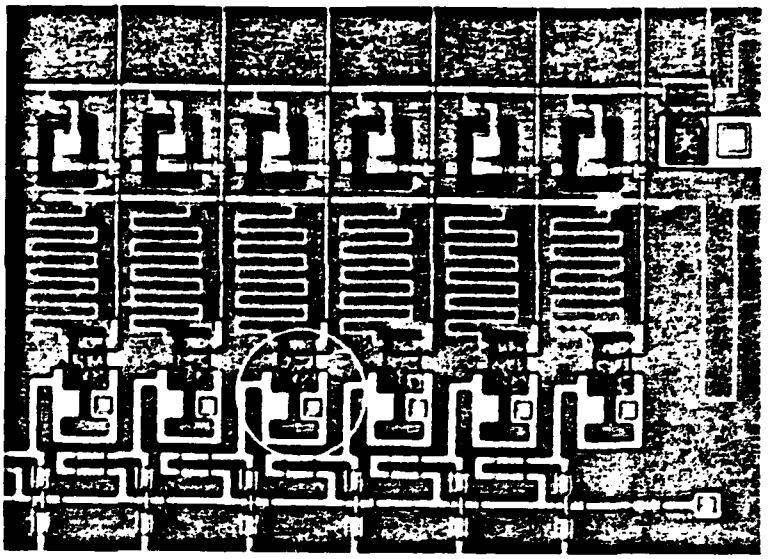

Cool chip. In this NBS a-d converter, each superconducting quantum interference device (circled), containing two Josephson junctions, produces a bit at rates of up to 2 GHz.

The signal to be measured is injected into the groundplane of the IC. The output of each conversion unit changes periodically with the magnitude of the magnetic field, going from 0 to 2 millivolts at one field strength, 2 mV to 0 at the next, and so on. Using Josephson conversion units with different field-strength sensitivities, the converter is able to produce a binary result in parallel, much like a flash converter.

But flash converters have not reached the speed of the 2-gigahertz NBS converter; Analog Devices claims to make the fastest commercial 6-bit flash unit with a 100-megahertz conversion rate. Moreover, flash converters typically use 2^N conversion elements per N bits.

In contrast, the Josephson-based converter needs only N elements, and since each conversion unit is only 1 square mil, the whole converter can fit in about 15,000 mil². "In volume, a chip with the converter alone would cost about 10 cents," Hamilton surmises.

The converter's output has been directly measured at up to 20 million samples per second and found to produce a monotonic staircase. Above that frequency, however, sampling techniques were used because there was no way to capture the converted data in real time.

Memory. To store the data for processing, Hamilton suggests that a shift-register version of the Josephson junction memory that IBM Corp. is building could be put on the chip with the converter. "There's enough space to put probably 500 to 1,000 samples on the same chip," he says.

At IBM's Yorktown Heights, N.Y., research facility, Wilhelm Anacker, head of the Josephson project, points out that, though the memory is fast enough to store the signal, "there may be practical problems with trying to put memories we develop on chips they have developed." Incompatible lithography techniques and process tolerances may prove to be stumbling blocks.

Then, too, the NBS is still working to overcome difficulties in getting the room-temperature signal to the supercooled chip. "Because of a problem with crosstalk in connections to the chip, it is not possible to

know what the signal is that is arriving at the chip at ultrahigh frequencies," Hamilton readily admits. He believes that the transmission problem should be overcome in the not-too-distant future.

However, keeping the chips cool in a practical instrument would not be a problem, owing to the work of another NBS researcher, James Zimmerman. He has already constructed a refrigerator that takes up only 1 cubic foot and can keep the chip at 4 K using only 100 watts.

"Anyone using the machine doesn't have to know that there's something inside working at 4 K," Hamilton says. "The operator just turns it on and waits 5 minutes, as with the old vacuum-tube instruments." -Richard W. Comerford

NBS builds superfast data acquisition system

Scientists at the National Bureau of Standards (NBS) in Boulder, CO, have built and tested the fastest known analog-to-digital (A/D) converter. The NBS device features six-bit resolution and parallel operation, uses Josephson junctions as its active elements, and has performed two *billion* A/D conversions per second in tests.

The converter uses superconducting technology, but its major breakthrough is that it uses unique interference phenomena to simplify the circuit. These interference effects permit the A/D to be built with only six active elements (one for each bit). Normally, full parallel operation requires 64 active elements, plus circuits for decoding.

This achievement is a major step in the Bureau's research program. NBS wants to show that superconducting circuits can be used to develop a new generation of measurement instruments. Other facets of this program involve high speed sampling, ultrasensitive magnetometers, microwave mixers and advanced voltage standards.

The NBS A/D is the product of more than three years of research. Supported by the Office of Naval Research, NBS hopes to increase speed of the A/D by 3-5 times over its present performance. If this goal is met, a faster memory system will have to be added since no available devices can accept digital information at such rates.

Instruments

Measurement science is catching up

High-speed signals of new ICs have labs pushing resolutions of test devices down to a few picoseconds or less

by Richard W. Comerford, Test, Measurement & Control Editor

With the speed of commercial integrated circuits breaking into the nanosecond region, both commercial and research facilities are looking for new ways of accurately and repeatably measuring the high-speed signals produced. At Lockheed Missile and Space Corp.'s Palo Alto (Calif.) Research Laboratory; Tektronix Inc. in Beaverton, Ore.; the National Bureau of Standards in Boulder, Colo.; International Business Machines Corp.'s Thomas J. Watson Research Center in Yorktown Heights, N. Y.; and other such facilities, workers are pushing measurement resolutions down to a few picoseconds or less.

To test gallium arsenide devices, researchers at Lockheed's Microelectronics Center in Sunnyvale, Calif., have used IEEE-488–compatible instrumentation to build a system for testing wafers of large-scale integrated circuits. The system, shown below, has at its heart a Tektronix 7912A digitizer modified by Ray Smith of the company's research lab to work at a minimum bandwidth of 3.5 gigahertz.

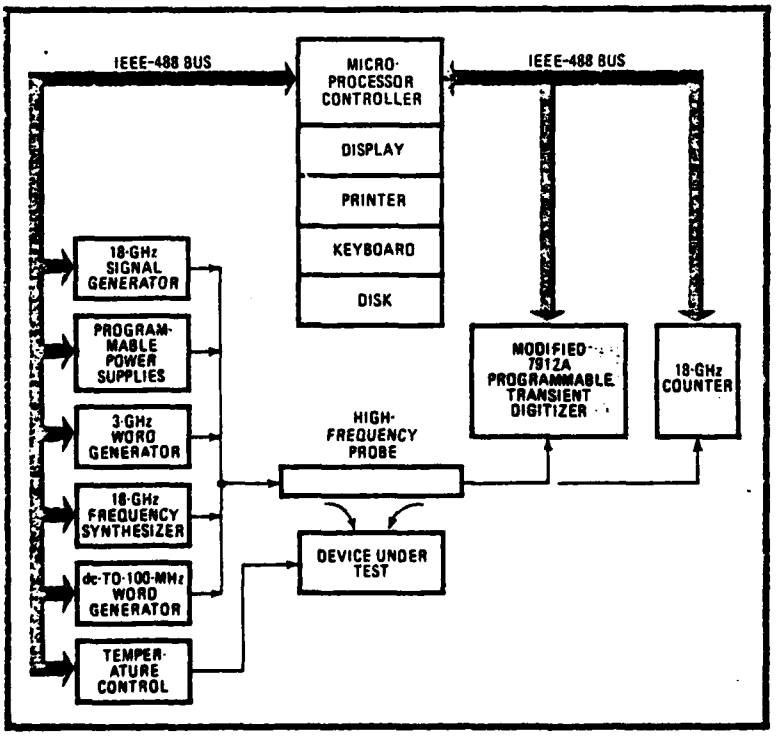

Home brew. Researchers at Lockheed's Microelectronics Center in Sunnyvale, Calif., built this system to test the operation of next-generation high-speed integrated circuits.

Smith's modifications involved changes to the input and output electronics, which resulted in "pushing the [scan converter] tube a bit," the physicist notes, without changing its internal electronics. Smith, who emphasizes that the basic 7912A is a fine instrument, says the change in the unit's vertical input amplification scheme was simple: "We threw it out," he explains. The amplifier limited the 7912A's bandwidth to about 500 megahertz or, at what Smith calls a "brutal" sensitivity of 4 volts/division, to 1 GHz.

The next limiting factor, the tube's native 2.5-GHz bandwidth, was overcome by equalization—attenuating the low-frequency response so that it matched the high-frequency response. Referring to the techniques used in long-distance cable transmission, Smith says, "Usually that's done passively. What we've done is to apply it to the microwave region and we've done so without using an amplifier." The actual circuit details are proprietary, but Lockheed will modify one or two units on an accommodation basis at cost, currently about $15,000.

Without input amplification, it might be expected that the sensitivity of the unit would be extremely low. But to his surprise, Smith found that it was not deflection but the correct location of a trace's charge center that was essential to a digitizing instrument's operation. Finding that center by integrating the trace, as is done in phased-array sonar, resulted in a 2-millivolt sensitivity and an 8-V input range. Signals could therefore be digitized with 12-bit accuracy.

About a year ago, Smith pre-

sented his findings and their result to Tektronix—which verified the modified unit's operation—and offered the company the rights to incorporate the changes. But the timing was not right, according to Jim Cavaretto, business unit manager for signal-processing laboratory oscilloscopes at Tektronix. The company had just spent a lot of time adding programmability and processing capability to the unit, turning it into the 7912AD version, to which Smith's modifications are not readily applicable.

"At the time he approached us," Cavaretto also notes, "we didn't have enough information to determine if we should turn right around and produce another product." Then too, Smith's modifications reduced the 7912's overall throughput—the time it takes to store as well as digitize waveforms—which Cavaretto feels is essential to a general-purpose instrument.

But with the success of instruments like the 7104 1-GHz oscilloscope, Tektronix sees the need to push on. "We're already getting questions and comments that lead us to believe that 1 GHz is certainly not the stopping point," Cavaretto says, and he thinks that scan conversion will be the way to go.

But the silicon target now used in the digitizer "has some inherent limitations in terms of signal-to-noise ratio," he notes, so "in the future, CCD targets may become the vehicle." The charge-coupled devices would be used much as in vidicon cameras today. Then, too, a general-purpose instrument will require high-speed input amplifiers that provide a range of sensitivities, and for that Cavaretto leans toward LSI GaAs devices. "But trying to extend waveform measurement capabilities well into the gigahertz region, regardless of which technology one chooses, is not going to come easily or cheaply," he cautions.

Looking out. While he may come down on the side of direct-reading instruments that use transferred-electron devices and GaAs, Cavaretto keeps a sharp eye on sampling technologies that may up measurement capability, including those based on Josephson devices. "We've spoken with IBM concerning that technology and their need for extremely precise measurement, and we're continuing to try and mold that into a product development strategy."

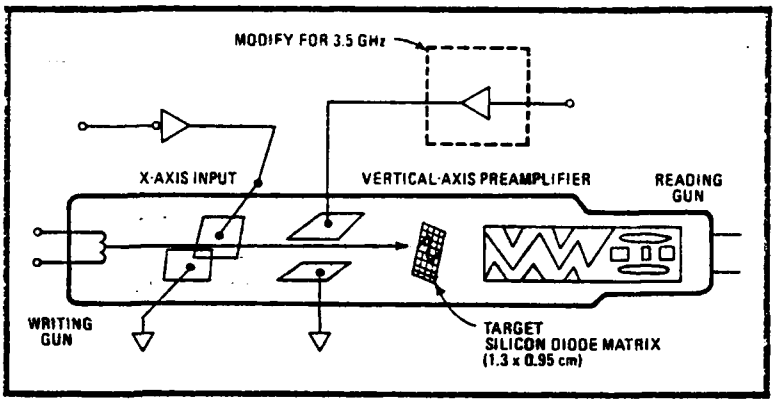

Scan converter. The heart of the 7912A digitizer was modified to increase the operating speed. Such tubes will probably be even further modified, using GaAs devices and CCDs.

IBM's Josephson work is still centered in its research center at Yorktown Heights, and spokesmen for the company continue to stress that the work is experimental. But IBM's recent slew of discussions about Josephson devices could indicate that the move from experimental to rental is not far off. And though the work is essentially devoted to computer efforts, the company also sees its importance to metrology. In fact, the company's most recent announcements have dealt primarily with such applications.

For example, the most recent IBM Josephson announcement has been the experimental demonstration of an ultrashort-pulse generator that makes possible a novel sampling technique for on-chip measurements. Sadeg Faris, the IBM research staff member responsible for the new measuring scheme, explains that for the experiment two pulse generators and a sampling gate were integrated onto a single Josephson chip. The generators were used alternately to provide sample gate triggers and test signals, with the result that "what we measure and what we predict from simulation agree very well," notes Faris happily.

The present circuit's sampling gate has a plasma frequency whose period is about 2 ps. "The plasma frequency really determines the [measurement] bandwidth in our scheme," Faris notes, "it has the capacitance of the device in it. We can make devices that ultimately have zero capacitance—Josephson weak links. Using materials with high temperature coefficients like niobium-germanium, the resolution can be about 0.1 ps."

9 ps at NBS. Similar work is being carried out at the National Bureau of Standards in Boulder. There, researchers have constructed measurement systems using supercooled Josephson logic circuits and a sampling oscilloscope. The sampling system is able to measure with a resolution of 9 ps, three times faster than the sampling scope alone.

Now, the detector on the NBS's supercooled logic must communicate with the sampling logic in the room-temperature scope, unlike the integrated logic that IBM has built. "Since IBM did that [integration] work, we're taking a slightly different direction," says NBS researcher Clark Hamilton. Like IBM, the NBS is headed toward a system that will measure signals transmitted to it from a room-temperature source, work that should be completed in the next few months, Hamilton says.

But IBM does not plan to let the NBS stake out new territory without a fight. Faris notes that work in this direction is also beig done at IBM. He will not say when it is likely to bear fruit, adding that "all I can say is that it's do-able." And though he cannot tie a dollar figure to this type of equipment, he says that "it is practical for most laboratories to do it—I think the semiconductor people, who already have most of the equipment for Josephson device fabrication, should get into it." □

7.0 APPENDICES

7.1. "Analog Measurement Applications for High Speed Josephson Switches," C. A. Hamilton, Frances L. Lloyd and R. L. Kautz, IEEE Trans. Mag., Vol. MAG-17, pp-577-582, January 1981.

7.2. "Impact of Superconducting Integrated Circuits on Electrical Measurement," Richard E. Harris, Proc. IEEE International Conference on Circuits, and Computers, pp. 882-883, October 1980.

7.3. "Picosecond Applications of Josephson Junctions," D. G. McDonald, R. L. Peterson, C. A. Hamilton, R. E. Harris, and R. L. Kautz, IEEE Trans. on Electron Dev., Vol. ED-27, pp. 1945-1964, October 1980.

7.4. "Superconducting Electronics," Donald G. McDonald, Physics Today, pp. February, 1981.

7.5. "Design Limitations for Superconducting A/D Converters," C. A. Hamilton, Frances L. Lloyd, IEEE Trans. Mag., November 1981.

ANALOG MEASUREMENT APPLICATIONS FOR HIGH SPEED JOSEPHSON SWITCHES†

C. A. Hamilton, Frances L. Lloyd, and R. L. Kautz
National Bureau of Standards
Electromagnetic Technology Division
Boulder, CO 80303

Abstract

This paper reviews high speed analog applications of Josephson switching devices. The design and performance of two different analog sampling circuits is described. A method is proposed for delivering room temperature signals to these samplers with 30 GHz or more of bandwidth. An analog-to-digital converter based on quantum interference comparators is also described. This device has achieved conversion rates of 2×10^9 samples per second.

Introduction

The Josephson microcircuit technology being developed for computers has also found numerous applications in analog measurements. These applications include sensitive magnetic field detectors, voltage standards and microwave mixers and amplifiers. This paper will focus on analog applications which specifically make use of the high speed switching behavior of hysteretic Josephson devices. These applications are based on the fact that a Josephson junction or SQUID (Superconducting QUantum Interference Device) made from Josepshon junctions can be used as a current comparator. This current comparator uses the property that a Josephson junction will switch to and remain in the voltage state whenever its critical current is exceeded. Thus, when the current delivered to a Josephson device contains an analog signal component, the existence of a switching transition and/or the time at which it occurs can be used to infer information about the signal. This is the basis for the analog sampling techniques and A/D converter described in this paper.

Analog Sampling

The earliest analog sampling technique utilizing Josephson junctions was proposed by Zappe in 1975.[1] The basis for this technique is shown schematically in Fig. 1. An unknown repetitive signal waveform $I_s(t)$ and a known DC bias current I_b are applied to a Josephson junction J1. At some time, T, the sum of these currents exceeds the critical current, I_o, of the junction and it switches to the voltage state. The time of this switching transition can be accurately measured by observing the junction voltage with a conventional sampling oscilloscope. The signal at time T is thus determined, i.e.

$$I_s(T) = I_o - I_b \quad . \tag{1}$$

The value of the signal at other times is determined by changing I_b and repeating the process. This method can be readily automated so that signal waveforms are plotted directly on an X-Y recorder. Risetimes of as little as 9 ps have been observed in this way.[2] The technique, however, has two disadvantages. First, it can only observe the rising edge of signal waveforms and second, it is ultimately limited by the time jitter of the room temperature sampling equipment.

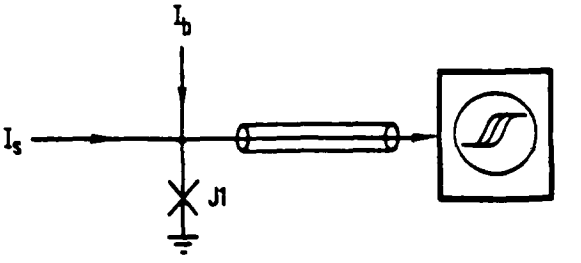

Fig. 1 A single junction current comparator used as an analog sampler.

Both of these disadvantages can be remedied by adding a very short sampling pulse, I_p, to the current supplied to the Josephson comparator.[3,4,5] The idea is shown in Fig. 2a. The sampling pulse is arranged to occur at a variable time T, which spans the region of interest of the repetitive signal waveform. The maximum signal level is restricted so that the signal alone is never sufficient to switch the comparator. Figure 2b shows the three components and resulting total current flowing through the comparator. By observing whether or not the comparator switches, the dc bias I_b can be adjusted to a threshold level such that

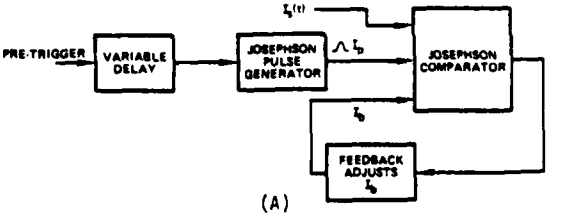

(A)

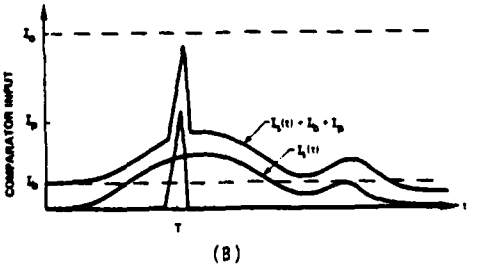

(B)

Fig. 2(a) A sampling circuit based on a Josephson comparator and a pulse generator and
(b) The current waveform at the comparator.

†Contribution of the U. S. Government, not subject to copyright.

0018-9464/81/0100-0577$00.75 © 1981 IEEE

$$I_s(T) + I_p + I_b = I_o \quad . \qquad (2)$$

Since I_p, I_b, and I_o are known, the signal at time T is determined. By sweeping T through the signal, the entire waveform can be mapped out. This method is also readily automated to directly display the unknown signal on an oscilloscope or X-Y recorder. Faris and Tuckerman have developed a system based on this technique with a time resolution of about 6 ps.[4,5]

Room Temperature Signals

The time resolution made possible by these techniques has so far only been available for signals generated on the same chip with the sampling circuit. NBS is currently engaged in a program to make these sampling methods available for signals generated at room temperature. The technical challenge, in this case, is to deliver the signal to the sampling circuit through a transmission path with 30 GHz or more of bandwidth. Our approach is illustrated by Fig. 3 which is a photograph of the sampling circuit mount. The

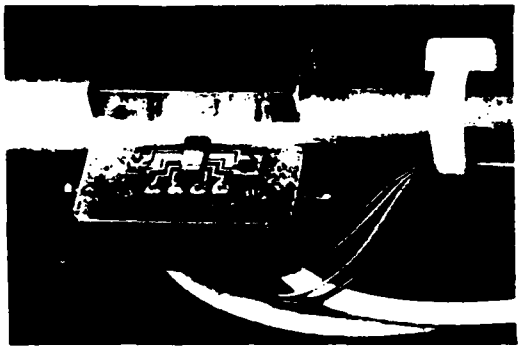

Fig. 3 A photograph of the mount used to couple the coaxial line signal to the sampling circuit on the chip. This is a "pass through" sampler since the signal is relatively unaffected by the presence of the sampling circuit.

signal is transmitted into the 4 K environment over 70 cm of precision 50 Ω, 7 mm or 3 mm coaxial line. The 10-90% step response of this line is estimated to be 5 ps.[6] A 2 mm wide chip containing the sampling circuit is inserted through a slot in the side of the coax line. The chip is shown face down. Conventional pressure contacts are made to the exposed part of the chip outside the coaxial line. The sampling circuit, which is located as close to the center conductor as possible, is shown in Fig. 4a. This circuit was fabricated using an eight level fabrication procedure described elsewhere.[7] Figure 4b is a photograph of the sampler. The Josephson comparator is, in this case, a fractional turn double junction SQUID. Signals on the coaxial line produce magnetic fields which couple to this SQUID. A coil, located outside the coax line and below the chip, provides a magnetic field bias. This design has the advantage of being a pass through sampler since the signal is essentially unaffected by the presence of the sampling circuit.

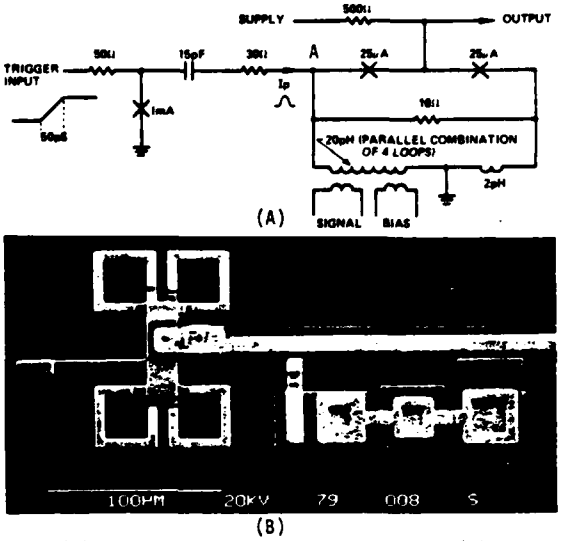

Fig. 4(a) The sampling circuit diagram and (b) a photograph of the circuit.

The SQUID comparator has a design trade-off resulting from the following requirements:

1). Sensitivity to the input signal on the coaxial line requires a large SQUID loop and therefore a large inductance, L.

2). Noise immunity requires junction critical currents, I_o, of the order of 20 μA or more.

3). The LI_o product must be less than $\phi_o/2$ or the SQUID can trap flux quanta at zero current bias resulting in a multiple valued critical current.

By using four parallel loops for the SQUID, modest sensitivity can be achieved while maintaining sufficiently low inductance. The effective area of this SQUID is the area of one loop, while the inductance is one forth the inductance of one loop. Since the SQUID loops are small compared to the separation between the inner and outer coax conductors, the sensitivity of the SQUID to the voltage on the line may be readily derived to be

$$\frac{\mu_o A}{2\pi r Z_o \phi_o} \text{ flux quanta/volt} , \qquad (3)$$

where A is the loop area, r is the radius from the coax center to the SQUID, Z_o is the coax impedance and ϕ_o is the flux quantum. Our loops have an area of 24 μm x 24 μm and are located at a radius of 0.7 mm. This yields a predicted sensitivity of 1.6 ϕ_o/V which is in good agreement with the measured sensitivity of 1.76 ϕ_o/V. The design value of I_o is 25 μA.

An appropriate sampling pulse is created by using a properly timed trigger signal to switch a single junction into the voltage state. The switching transition is differentiated with a small capacitor thus producing a pulse whose width equals the rise time of the transition. This pulse is injected directly into the SQUID inductance. The SQUID comparator is thus subjected to magnetic fields from the signal, the biasing coil, and the pulse. Since the SQUID has a threshold magnetic field for switching into the voltage state, it operates as a magnetic field comparator and can therefore be used to determine the signal waveform as previously described.

Simulations

The time resolution of this circuit is limited by the sampling pulse width, the amplitude of the signal relative to the pulse and the response time of the SQUID comparator. Figure 5 shows the simulated response to a square signal pulse input for current densities of 750 and 2000 A/cm^2. Junction capacitance is taken as 4 μF/cm^2 and the signal and magnetic field bias are treated as injected currents at node A. The trigger risetime is set at 50 ps.

In these simulations, a trigger time and trial bias are selected and the time dependent behavior of the circuit is calculated for about 300 ps. At the end of this time a new bias is selected based on whether or not the SQUID switched. After seven such time runs the threshold bias value is determined within 1% thus yielding one point on the response curve. The trigger time is then advanced 1 ps and the process is repeated. The simulations show that a step response time of about 5 ps can be achieved with 2000 A/cm^2 junctions. A simple technique for making such multiple simulations is described in the Appendix. Unfortunately, fabrication difficulties have, at the time of this writing, prevented the experimental demonstration of this circuit.

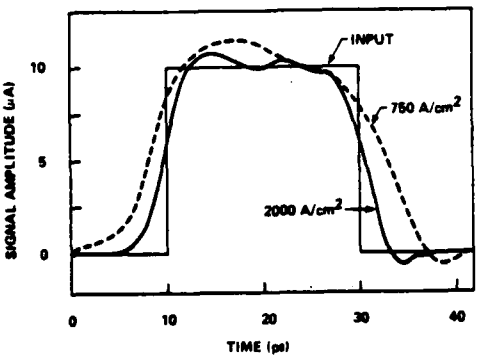

Fig. 5 Simulated sampler response to a square input pulse for circuits with current densities of 750 and 2000 A/cm^2.

A/D Conversion

Josephson device comparators have also found application in ultra high speed analog-to-digital converters. The periodic nature of the threshold current in a dc SQUID offers a unique method of performing A/D conversion.[8,9,10]

The circuit for a double junction SQUID comparator is shown in Fig. 6c and its I-V curve in Fig. 6a. For currents below the maximum threshold current, I_{mo}, the device has zero voltage drop. When I_{mo} is exceeded the SQUID switches very rapidly (10-30 ps depending on overdrive) along the load line to the energy gap voltage (V_G = 2.9 mV). As shown in Fig. 6b, the threshold current I_m has a maximum value I_{mo} and a periodic dependence on a control current I_c which is magnetically coupled to or directly injected into the SQUID. Thus, by applying a signal, I_c, to the control input and pulsing the SQUID current I_g to a predetermined level, (see Fig. 6b), the SQUID is a comparator which, as shown in Fig. 6d, has the unique property that its digital output, V, is a periodic function of the analog signal input, I_c. This is exactly the property required for an A/D converter since each digital output of an A/D converter is a periodic function of the signal input with the period changing by a factor of two from one bit to the next.

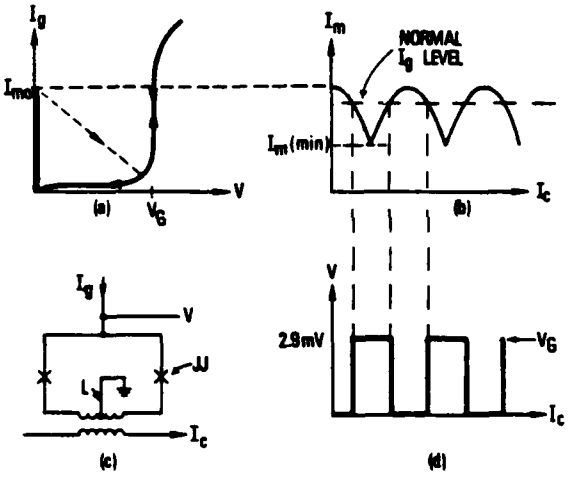

Fig. 6(a) The I-V curve of a double junction SQUID, (b) the dependence of the critical current I_m on a control current I_c, (c) the circuit diagram of a SQUID, and (d) the input-output characteristic of a SQUID comparator.

Figure 7a is the circuit diagram for a 6-bit converter using this idea. The required variation in periodicity is achieved by using a resistor ladder to divide the input signal by a factor of two for each successive SQUID. Another variation of this circuit uses a magnetically coupled signal with variable mutual inductance to achieve the binary ratios.[9,10] When a conversion is to be made a current pulse, I_g, is applied to the power supply line so that all SQUIDs are biased to the level shown in Fig. 6b. Each SQUID for which this bias level exceeds the threshold curve will switch to the voltage state producing a 2.9 mV pulse on its output line. These pulses are a digital representation of the analog signal. For continuous operation the supply line is driven by a pulse train, or at the highest speeds by an offset (monopolar) sine wave.

This A/D converter operates in a fully parallel fashion and requires only one SQUID comparator for each bit of accuracy. Figure 7b is a photo of the circuit.

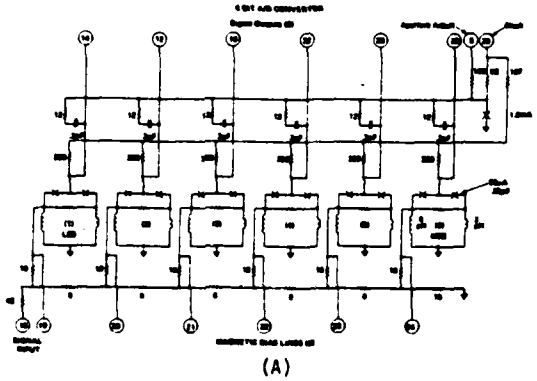

(A)

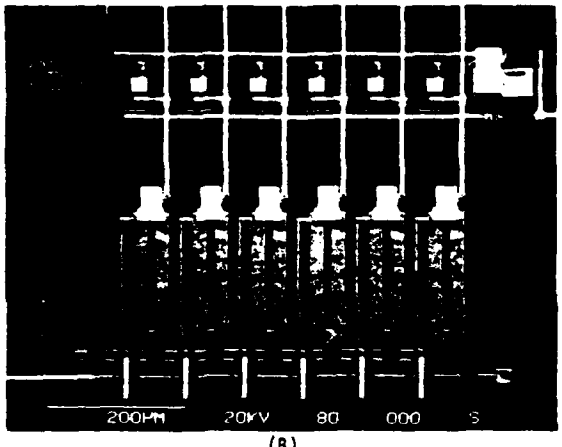

(B)

Fig. 7a The circuit diagram of a superconducting A/D converter using direct injection SQUIDs and (b) a photograph of the circuit.

Experimental Results

Figure 8a shows the six bit patterns as a function of analog signal level. Note that the output is in Gray code so that perfect alignment of the threshold levels is not required. In Fig. 8b the Gray code is converted back to an analog signal. The monotonic staircase verifies that the accuracy of the converter is ± 1 LSB (least significant bit).

Crosstalk between the chip leads causes considerable difficulty in testing this device at very high speed. For this reason a mount has been designed in which the pads on the chip are pressed against the ends of 8 differential microstrip line pairs which are etched on G-10 circuit board. Six millimeters away from the chip, each stripline pair converts to 50 Ω coax. The coax shields are tied together only at the superconducting ground plane on the chip.

Even with these measures, crosstalk from the high level ac power supply (30 mV) exceeds the output signal levels (2.9 mV) at sample rates above 2×10^9 per second. We are currently not able to fully verify the operation of the converter at this rate. However, by synchronizing

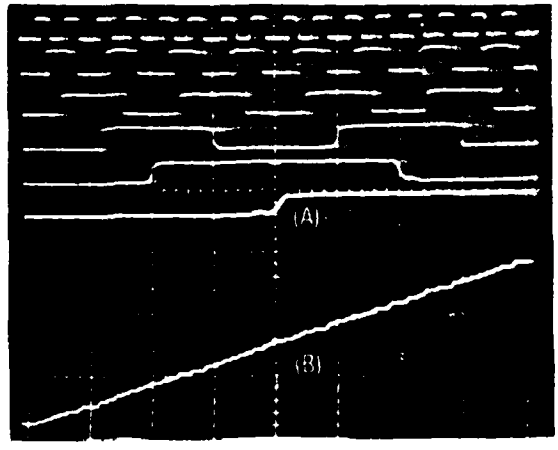

Fig. 8(a) The six digital outputs as a function of signal input, and (b) the digital value of the output as a function of the signal (staircase function).

a signal waveform with the 2 GHz power supply, it is possible to use a sampling oscilloscope to observe the digital data on the output lines. Figure 9 shows the data on one of the six output lines for eight successive samples of a 6 ns wide signal waveform. The crosstalk has been electronically subtracted from this data. It is clear that the full utilization of this A/D converter will require either a greatly improved sample holder and interface electronics or some data rate reduction on the chip. The ultimate speed achievable with this type of converter is determined by the turn-on-delay of the interferometers and the time required to reset them to zero voltage state at the end of each cycle.

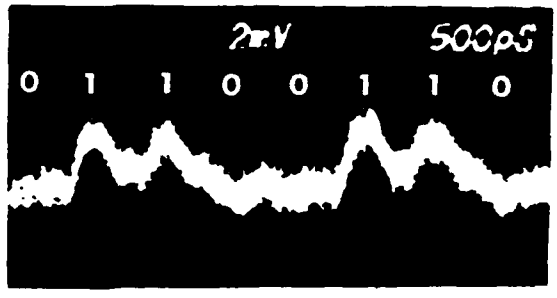

Fig. 9 The digital output data on one of the six output lines as a function of time. Eight successive samples are shown.

Aperture Time

A useful addition to this A/D converter is the sampling circuit shown at the top of Fig. 7a and b. This circuit is analogous to the circuit of Fig. 4 in that it uses the switching transition of a single junction to add a narrow pulse to the power supply waveform. As shown in Fig. 10 the peak amplitude of the pulse is set at the required bias level for the six SQUIDs. Following the pulse, the supply returns to a value below the "floor" of the threshold curve. At this lower bias value the SQUIDs retain the output data and are insensitive to changes in the signal

level. The converter thus has an aperture time equal to the width of the sampling pulse.[11] Simulations have verified the performance of this circuit although the operating margins are significantly less than for the A/D converter without the sampling circuit.

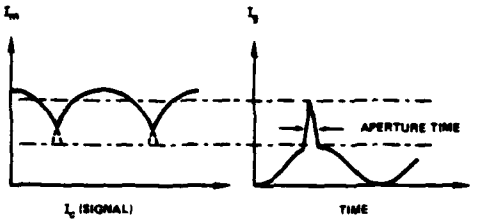

Fig. 10 The pulsed power supply waveform used to achieve a short aperture time.

Shift Register Memory

The most useful addition to the present A/D converter would be an on-chip memory which could be loaded at the full sampling rate and then read out slowly for data analysis. This would, in effect, be a transient digitizer on a chip. Such a memory has been contemplated in a shift register form consisting of long strings of gates driven by a three phase power supply. While requiring three SQUIDs per memory bit, this design is conceptually simple and can be operated by offset sinewave supplies up to frequencies of 10 GHz.

Figure 11a shows one possible arrangement in which the three phase supply is generated by on-chip delay lines and the gates are direct injection SQUIDs. As data appear at the A/D output, the three phase supply causes it to ripple through the strings of SQUIDs. If the sinewave supply is turned off while maintaining the dc offset, the data are retained in the memory and can be recovered by application of a low frequency three phase supply. Currently, quasi-static tests are being made on single cells of this memory. A photograph of eight gates in the shift register memory is shown in Fig. 11b.

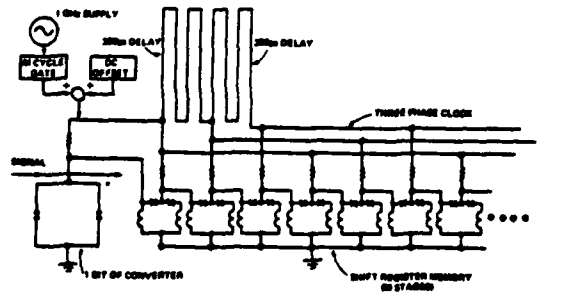

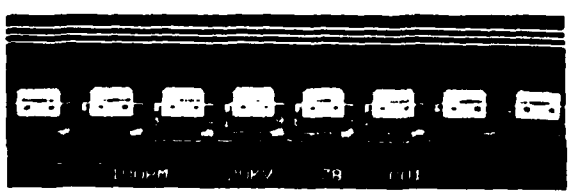

Fig. 11(a) One bit of an A/D converter with a shift register memory and (b) a photograph of eight of the shift register memory gates.

Acknowledgements

The authors are indebted to Don Sullivan, Richard Harris, Rex Craig, and Jim Andrews of NBS and Hans Zappe of IBM for discussions which contributed to this work. This program was partially supported by the U. S. Office of Naval Research under Contract Nos. N00014-79-F-0020 and N00014-80-F-0012.

Appendix

Generalized network analysis programs are extensively used to predict the behavior of Josephson circuits. Certain problems which involve extensive reruns or repetitive circuits may best be solved by another approach outlined below. Examples of such problems are the dynamic calculation of threshold curves and the simulation of a many stage shift register.

The approach is based on the assumption that for short times capacitors can be treated as voltage sources and inductors and junctions treated as current sources. By redrawing the circuit with these substitutions it is usually trivial to solve for the current into capacitors and the voltage across inductors. A simple time integration is then used to update the capacitor voltages and inductor currents and the process is then repeated. An example, consisting of a Josephson relaxation oscillator is shown in Fig. 12. The solution procedure in computer format is:

1. $v_L = V_d - V_c$
2. $i_c = I_L - V_c/R - I_o \sin\phi$
3. $I_L = I_L + v_L \Delta t/L$
4. $V_c = V_c + i_c \Delta t/C$
5. $\phi = \phi + (2e/\hbar)V_c \Delta t$
6. $t = t + \Delta t$
7. Plot I_L vs t
8. GO TO 1

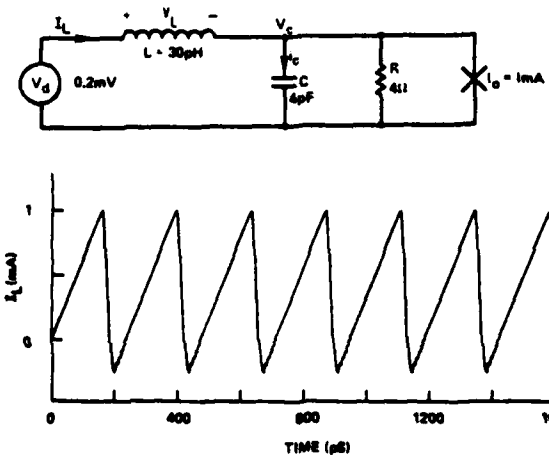

Fig. 12(a) A circuit for a Josephson relaxation oscillator and (b) the calculated inductor current as a function of time.

Lines 1 and 2 solve the circuit and lines 3-5 perform a simple integration to update the values for the three energy storage elements (C, L, and JJ). The result of this procedure using $\Delta t = 0.02$ ps is shown in Fig. 12b. The crude (rectangular) integration procedure used is perfectly adequate for most problems. For example, the calculation of Fig. 12b is accurate to 1% for $\Delta t < 0.2$ ps. A trapezoidal integration yields negligible increase in accuracy and increases the calculation time per increment.

The usefulness of this procedure is in problems where a simple circuit solution like that shown above can be embedded in a larger program to make many runs as a function of some circuit parameter or to simulate many simple circuits connected together. For example, the circuit equations to solve the shift register of Fig. 11a with 20 stages and over 200 components require only 15 lines of FORTRAN code.

References

1. Hans H. Zappe, "A Subnanosecond Josephson Tunneling Memory Cell with Nondestructive Readout," IEEE J. Solid State Circuits, Vol. SC-10, pp. 12-19, 1975.

2. C. A. Hamilton, F. L. Lloyd, R. L. Peterson, and J. R. Andrews, "A Superconducting Sampler for Josephson Logic Circuits," Appl. Phys. Lett., Vol. 35, pp. 718-719, 1979.

3. C. A. Hamilton, "A Sampling Circuit and Method Therefor," U. S. Patent Application Serial No. 853,354, 1977, (Allowed).

4. Sadeg M. Faris, "Generation and Measurement of Ultrashort Current Pulses with Josephson Devices," Appl. Phys. Lett., Vol. 36, pp. 1005-1007, 1980.

5. David B. Tuckerman, "A Josephson Ultrahigh-Resolution Sampling System," Appl. Phys. Lett., Vol. 36, pp. 1008-1010, 1980.

6. Donald R. Holt and Norris S. Nahman, "Coaxial-Line Pulse-Response Error Due to a Planar Skin-Effect Approximation," IEEE Trans. on Instrumentation and Measurement, Vol. IM-21, pp. 515-519, 1972.

7. J. H. Greiner, C. J. Kircher, S. P. Klepner, S. K. Lahiri, A. J. Warnecke, S. Basavaiah, E. T. Yen, John M. Baker, P. R. Brosious, H. C. W. Huang, M. Murakami, and I. Ames, "Fabrication Process for Josephson Integrated Circuits," IBM J. of Research and Development, Vol. 24, pp. 195-205, 1980.

8. H. H. Zappe, "Ultrasensitive Analog-to-Digital Converter Using Josephson Junctions," IBM Tech. Disc. Bull., Vol. 17, pp. 3053-3054, 1975.

9. R. E. Harris, C. A. Hamilton, and F. L. Lloyd, "Multiple-Quantum Interference Superconducting Analog-to-Digital Converter," Appl. Phys. Lett., Vol. 35, pp. 720-721, 1979.

10. C. A. Hamilton and Frances L. Lloyd, "A Superconducting 6-Bit Analog-to-Digital Converter with Operation to 2×10^9 Samples/Second," IEEE Electron Dev. Lett., Vol. EDL-1, pp. 92-94, 1980.

11. D. J. Herrell, private communication.

ICCC80

IMPACT OF SUPERCONDUCTING INTEGRATED CIRCUITS ON ELECTRICAL MEASUREMENT

Richard E. Harris

Electromagnetic Technology Division
National Bureau of Standards

Boulder, CO 80303

ABSTRACT

The remarkably high speed, high sensitivity, and low dissipation of superconducting electronic devices has led the National Bureau of Standards to investigate the use of circuits containing these devices in new measurements and standards. Using a fabrication technology [1] much like that described in the literature [2,3], a number of new high performance devices have been developed. In addition a small low power refrigerator has been developed which may make convenient packaging of these devices possible.

MEASUREMENTS AND STANDARDS

Devices for measurement and standards developed to date are for remarkably fast analog sampling, analog-to-digital conversion, microwave detectors, very high sensitivity magnetic field sensors, and a new approach to a voltage standard.

High speed electrical measurements are of crucial importance to the development of superconducting technology because conventional instruments have insufficient speed to diagnose the behavior of the new circuits. Thus high speed analog sampling devices have been developed both by NBS [4] and IBM [5,6]. The shortest rise-time yet reported [4] is only 9 ps. More sophisticated techniques [5,6] have made possible the measurement of complicated waveforms. These techniques have improved the speed of measurement over commercially available sampling oscilloscopes by a factor of about 3.

High speed analog-to-digital conversion is also important in diagnoses of high speed circuits, but has an additional important role in future communications and radar. To date the fastest analog-to-digital converter [7,8] produces 6-bit digital values of an analog signal at a rate of about 2 GHz. This device is not yet an operational system, still requiring the addition of a high speed sample-and-hold and a memory which can acquire the high rate data. Nevertheless it represents a significant advance in high speed data acquisition made possible by superconducting technology.

This technology has also made possible improved, low noise microwave detection [9]-[11]. Such microwave detectors have been examined at 36 GHz and found to approach the quantum limit for both heterodyne and video detection. In addition conversion gain has been observed for the first time in superconductor-insulator-superconductor junction detectors. While the initially observed gain is modest, its observation holds considerable promise for the future.

Historically still other devices, based on point contact SQUIDs (Superconducting Quantum Interference Devices), have demonstrated the applicability of superconducting electronics to measurements and standards. These devices have been applied to a variety of applications [12] including rf power and attenuation measurement, noise thermometry, current comparison, and null detection. Integrated circuit technology is now allowing still further improvement of these devices [13,14], to the point that they now approach limits set by the Heisenberg uncertainty principle in sensitivity.

The present United States legal volt is maintained using the Josephson effect, as are the legally defined voltage standards in many other countries. Such voltage standards produce only a few millivolts of output voltage which must usually be compared with standard cell outputs of about one volt. These comparisons require expensive resistance bridges. While it might seem rather simple, using superconducting integrated circuits, to simply add the voltages from many Josephson devices in series, practical problems prevent doing so. A recent development [15] has provided an approach to higher output voltages, while maintaining the full accuracy of the standard. Laboratory standards based on the approach may have significantly reduced cost, compared to present Josephson standards. The common use of the standards may become practical.

CH1511-5/80/0000-0882 $00.75

REFRIGERATION

The practical utilization of these remarkably fast devices depends upon the availability of simple inexpensive refrigeration. Recently [16,17] a refrigerator has been developed which appears to satisfy both of these requirements. The refrigerator, which operates on a Sterling cycle, was developed for high sensitivity superconducting magnetic field sensors. It is therefore non-magnetic and constructed from fiberglass and plastic. To date it has achieved a lowest temperature of about 6.5 K. An additional stage, tested separately, has reached 3 K with its high temperature end cooled by other means to about 10 K. Combined in a practical system these devices could adequately cool the electronic circuits discussed above.

The author is grateful for the hospitality of the IBM Zurich Research Laboratory, Rüschlikon, Switzerland, during the preparation of this manuscript.

REFERENCES

[1] Havemann, R.H., Hamilton, C.A., and Harris, R.E., "Photolithographic Fabrication of Lead Alloy Josephson Junctions," J. Vac. Sci. Technol. 15, pp. 392-395, (1978).

[2] Greiner, J.H., Kircher, C.J., Klepner, S.P., Lahiri, S.K., Warnecke, A.J., Basavaiah, S., Yen, E.T., Baker, John M., Brosious, P.R., Huang, H.-C.W., Murakami, M., and Ames, I., "Fabrication Process for Josephson Integrated Circuits," IBM J. Res. Dev. 24, pp. 195-205, (1980).

[3] Broom, R.F., Jaggi, R., Mohr, Th. O., and Oosenbrug, A., "Effect of Process Variables on Electrical Properties of Pb-Alloy Josephson Junctions," IBM J. Res. Dev. 24, pp. 206-211, (1980).

[4] Hamilton, C.A., Lloyd, F.L., Peterson, R.L., and Andrews, J.R., "A Superconducting Sampler for Josephson Logic Circuits," Appl. Phys. Lett. 35, pp. 718-719, (1979).

[5] Faris, S.M., "Generation and Measurement of Ultra-Short Current Pulses with Josephson Devices," Appl. Phys. Lett. 36, pp. 1005-1007, (1980).

[6] Tuckerman, David B., "A Josephson Ultra-High Speed Sampling System, Appl. Phys. Lett. 36, pp. 1008-1010, (1980).

[7] Harris, R.E., Hamilton, C.A., and Lloyd, F.L., "Multiple-Quantum Interference Superconducting Analog-to-Digital Converter," Appl. Phys. Lett. 35, pp. 720-721 (1979).

[8] Hamilton, C.A., and Lloyd, F.L., "A Superconducting 6-Bit Analog-to-Digital Converter with Operation to 2 × 10**9 Samples/Second," IEEE Trans. Electron Device Lett., EDL-1, pp. 92-94, (1980).

[9] Richards, P.L., Shen, T.M., Harris, R.E., and Lloyd, F.L., "Quasiparticle Heterodyne Mixing in SIS Tunnel Junctions," Appl. Phys. Lett. 34, pp. 345-347, (1979).

[10] Richards, P.L., Shen, T.M., Harris, R.E., and Lloyd, F.L., "Superconductor-Insulator-Superconductor Quasiparticle Junctions as Microwave Photon Detectors, Appl. Phys. Lett. 36, pp. 480-482, (1980).

[11] Shen, T.M., Richards, P.L., Harris, R.E., and Lloyd, F.L., "Conversion Gain in Millimeter Wave Quasiparticle Heterodyne Mixers," Appl. Phys. Lett. 36, pp. 777-779, (1980).

[12] Kamper, R.A., "Superconducting Devices for Metrology and Standards," in Superconductor Applications: SQUIDs and Machines, ed. by B.B. Schwartz and S. Foner, Plenum, New York, pp. 189-244, (1977).

[13] Correlli, P., and Cromar, M., "Low Inductance dc SQUIDs with High Energy Sensitivity," in Proceedings of the 1980 Applied Superconductivity Conference, Santa Fe, New Mexico, to be published.

[14] Ketchen, M.B., "Dc SQUIDs 1980: the State of the Art," Proceedings of the 1980 Applied Superconductivity Conference, Santa Fe, New Mexico, to be published.

[15] Kautz, R.L., "On a Proposed Josephson Effect Voltage Standard at Zero Current Bias," Appl. Phys. Lett. 36, pp. 386-388, (1980).

[16] Zimmerman, J.E., and Sullivan, D.B., "A Milliwatt Sterling Cycle Cryocooler for Temperatures Below 4 K," Cryogenics 19, pp.170-171, (1979).

[17] Sullivan, D.B., and Zimmerman, J.E., "Very Low Power Sterling Cryocooler Using Plastic and Composite Materials," Int. J. Refrig. 2, pp. 211-213, (1979).

Picosecond Applications of Josephson Junctions

DONALD G. MCDONALD, ROBERT L. PETERSON, CLARK A. HAMILTON, MEMBER, IEEE, RICHARD E. HARRIS, AND RICHARD L. KAUTZ

Invited Paper

Abstract—The behavior of simple superconducting circuits in the picosecond regime is described in a comprehensive way, with primary emphasis being given to the step function and pulse responses of these circuits. Topics receiving detailed discussion include Josephson-junction modeling with both the microscopic and shunted-junction models. Limitations of the shunted-junction model are explored by comparing it with experimental results and with the microscopic model. An approximate evaluation is given of the important dynamical properties of junctions made with the dominant fabrication technology (Pb-alloy systems), as a function of tunneling barrier thickness. Rounding out the device aspects of the discussion, we describe in detail the properties of superconducting microstrip transmission lines, with an emphasis on their high-speed behavior. Turning to simple circuits we review experimental results on the measurement of picosecond regime transient signals. The concept of turn-on delay is analyzed anew, providing simplified and extended results. Details of concepts for pulse height and pulsewidth measurements are explored, leading to the conclusion that the time resolution of superconducting circuits is limited to approximately the period of one plasma oscillation. With present Pb-alloy fabrication technology this limit is 2 ps.

I. Introduction

JOSEPHSON JUNCTIONS are now being used for the generation, detection, and measurement of pulses and switching transients with durations as short as about 10 ps. Our purpose here is to present a unified picture of the more basic developments in this area, including some new results. The earliest developments were the microscopic theories of superconducting tunnel junctions by Riedel [1] and Werthamer [2], which predicted essentially a flat spectral response out to the frequency of the energy gap, where a somewhat enhanced response was expected. At frequencies above the gap, the superconducting response goes monotonically to zero, but with measureable effects extending out to several times the gap. Experimental investigations of the bandwidth of Josephson junctions were first carried out in the frequency domain, perhaps most importantly at 891 GHz (30 percent above the gap), where it was found that the response was indeed close to that at low frequencies. These experiments were done with point-contact devices for which it was known, from the analyses of Stewart [3] and McCumber [4], that the capacitance was quite small.

In the early years of the Josephson effect it was commonly thought that the response time of tunnel junctions would be severely limited by the capacitance associated with the exceedingly thin tunneling barrier. Basavaiah, Eldridge, and Matisoo [5] corrected this misconception by experimentally evaluating phenomenological tunneling theory and producing, for the first time, a clear picture of the relationship between tunneling barrier thickness and current density. From this it was only a small step to relate current density to junction response time, from which it became clear that the picosecond regime should be accessible with tunnel junctions.

The evolving development of high-quality superconducting integrated circuits, discussed in detail in this Special Issue, creates the possibility of practical utilization of nearly 1 THz of bandwidth in electronic systems. In the following we will more thoroughly examine the experimental and theoretical basis for the quantitative views expressed here. We will also present new results regarding turn-on delay, pulse detection, and pulsewidth measurement, with an emphasis on performance at the highest possible speeds. The order of discussion which follows is: II. Experimental Results, III. Theoretical Basis, IV. Switching Time, V. Pulse Generation, Detection, and Measurement, VI. Transmission Lines, and VII. Discussion. Our discussion emphasizes single-junction devices rather than multijuction SQUID's both because the former are simpler to analyze and to fabricate and because they probably give the fastest response, though the latter point has not been proven. We have also chosen to largely omit discussion of nonlatching devices [6] and of the resetting (or punchthrough) problems [7]. Finally, discussion of noise was omitted since fundamental physical noise will not ordinarily dominate the circuits of interest. More germane to the irregularities of practical circuits is the problem of reflections from impedance mismatches, which are nearly always present.

II. Experimental Results

Although most of our discussion will be about the time-domain response of superconducting circuits, it is appropriate to begin with a brief review of experiments in the frequency domain, both because they gave the first experimental evidence of high-frequency response and because time-domain measurements are still limited to times greater than about 10 ps, whereas frequency-domain measurements using far infrared lasers probe the subpicosecond regime.

A. Bandwidth Measurements in the Frequency Domain

The most direct proof of the large bandwidth of Josephson junctions comes from a rather simple point of view. We take

Manuscript received May 17, 1980; revised July 2, 1980. This research was partially supported by the Office of Naval Research under Contract N000-14-80-F-0012.

The authors are with the U.S. department of Commerce, National Bureau of Standards, Boulder, CO 80303.

the low-frequency description of the Josephson effect and ask at what frequency does it break down? Fortunately Josephson junctions have a special property which allows this to be done with little uncertainty.

The low-frequency form of the Josephson equations relating current I to voltage V is

$$I = I_o \sin \phi \tag{1}$$

$$\dot{\phi} = \frac{2e}{\hbar} V \tag{2}$$

where the dot means d/dt and e and $\hbar$ are the usual fundamental constants. These equations predict that if a superconducting junction is dc biased at voltage V_b, the phase ϕ will advance uniformly in time, and the current I will oscillate with amplitude I_o at frequency

$$f_J = \frac{2e}{h} V_b \quad \left(\frac{2e}{h} = 484 \text{ GHz/mV}\right). \tag{3}$$

A more complete theory of junctions, which will be discussed later, makes it clear that it is the quantity I_o, the junction critical current, which eventually begins to decrease with frequency. That is not at all surprising since one would not expect to be able to produce significant optical frequency current, for example, from a state of matter which has a binding energy of only a few millivolts.

The experimental problem then is to measure I_o as a function of frequency. Since the frequency range of interest exceeds 1 THz it could be a difficult practical problem.

B. Josephson, in his original paper on superconducting tunneling [8], suggested an indirect method for observing the supercurrent I_o at microwave frequencies. This method, first successfully used by Shapiro [9], is based on the simultaneous application to a junction of dc bias and microwave radiation. The basic idea is that for proper adjustment of V_b the frequency of the Josephson oscillation f_J will be equal to the frequency f_a of the applied radiation. Since the Josephson junction is a nonlinear device, it will produce a beat frequency current at the difference frequency $f_J - f_a$, which in this case is at zero frequency. The result is a current step on the I-V characteristic. This situation can be analyzed using (1) and (2) with

$$V = V_b + V_1 \cos(2\pi f_a t + \theta_1). \tag{4}$$

From this analysis it is found that the induced dc is

$$I_{dc}(f_J = f_a) = 2I_o J_1(2eV_1/hf_a) \tag{5}$$

where J_1 is the first-order Bessel function of the first kind. Thus I_{dc}, considered as a function of V_1, has a maximum value of $1.16\,I_o$. The analysis given here omits the shunt capacitance and shunt resistance of real junctions. Simulations by Russer [10] and Kautz [11] have shown that the induced dc given by (5) is an upper bound which is closely approached in the right circumstances. The upper bound suffices for our purposes so we will not consider in detail the effects of the shunts.

Experiments of this type specifically designed to explore the bandwidth of the Josephson effect were reported several years ago by McDonald *et al.* [12], [13] and more recently by Weitz, Skocpol, and Tinkham [14]. Perhaps the most direct evidence for large-amplitude Josephson oscillations

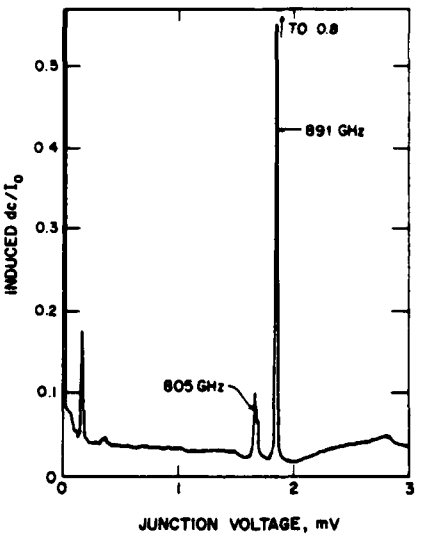

Fig. 1. Experimental results for the induced dc in a Josephson junction with applied radiation at 891 and 805 GHz. Spectral features appear at 1.84 and 1.66 mV, corresponding in (3) to Josephson oscillations at the frequencies of the applied radiation. The feature at 0.18 mV is not due to applied radiation but corresponds to the difference frequency of the applied signals.

at a frequency in the vicinity of the energy gap is illustrated [12] in Fig. 1. The experimental technique which was used for acquiring these data largely removed the background I-V curve from the data and emphasized the induced dc. This was an experiment in which a Josephson junction was simultaneously irradiated at 891 and 805 GHz. As the voltage across the junction was slowly increased, the frequency of the Josephson oscillation increased according to (3) until, at a voltage of 1.66 mV, this oscillation phase locked with the applied far-infrared laser radiation at 805 GHz and produced a zero-frequency beat current which is illustrated in the figure. As the voltage was increased further, the Josephson oscillation phase locked with the 891-GHz radiation at 1.84 mV and again produced a zero-frequency beat, but this time of greater amplitude because of higher intensity radiation (larger V_1). In effect, the junction acts as a spectrum analyzer of unusually large bandwidth. Our main interest, however, is in the result that the junction gives a large response at this extremely high frequency; in fact, the magnitude of the response is $0.8\,I_o$. Considering this result, as well as other more extensive data [14], we conclude that the Josephson response is ~70 percent of the upper bound of (5).

The principal frequency of this experiment, 891 GHz, is somewhat above the energy gap of 675 GHz of the superconductor (Nb) used in the experiment. Thus in an approximate way, considering the possible deleterious effects of shunt impedances, heating [15], and noise rounding [16], [15], we conclude that the Josephson effect operates at nearly full amplitude in the vicinity of the energy gap, a very high frequency for electronics. More generally, it has been found experimentally that I_o decreases above the gap frequency such that by approximately 12 times the gap it is no longer observable above the noise [12]-[14].

These high-frequency experiments were done with point-

contact junctions to accommodate the far-infrared radiation. Closely related experiments with tunnel junctions lead to the same conclusions [18], [19].

Also consistent with the discussion given here is the study of self-resonances in Josephson interferometers by Zappe and Landman [20]. They conclude that the simple model of the Josephson effect is applicable up to frequencies at least as high as 300 GHz.

B. Time-Domain Experiments

The early high-frequency experiments with Josephson devices suggested their use as very fast logic switches. Matisoo [21] demonstrated this potential in the first important time-domain experiment. This experiment placed an upper limit of 800 ps on the transition time of a Josephson tunnel junction for switching from the zero-voltage state to the energy-gap voltage. After many improvements in fabrication and testing, Jutzi [22] published data in 1972 which put an upper limit of 34 ps on the switching time of a small-area junction with a critical current density of 1000 A/cm^2. The most recent published data for Josephson logic devices indicate switching times of about 7 ps and total logic delay of as little as 13 ps per gate [23].

The fact that Josephson devices can produce and detect these exceedingly fast signals gives them the potential for improving the state of the art in very-fast-waveform analysis. To understand how this might be done we can consider, as a first approximation, a Josephson junction to be a device which switches from zero voltage to the energy-gap voltage V_g (~3 mV) at the instant its critical current is exceeded. This model is discussed more fully in Section IV. Since the transition is very rapid, a Josephson junction can act as a comparator to determine the *time* at which some threshold is crossed. Also, Josephson devices which operate in a latching mode can be used to detect and remember an extremely short excursion above an arbitrary threshold level. Both of these properties are used to measure the waveforms of repetitive analog signals.

Fig. 2(a) shows one common way this is done [24]-[26]. The unknown repetitive signal I_s, together with a bias current I_b, is applied to a tunnel junction $J1$. When the sum of these two currents exceeds the critical current I_o of $J1$, it will switch causing a voltage transition to be transmitted to room-temperature apparatus where its time of arrival is measured. Since the bias and the critical current of $J1$ are known, the signal level at the time the detector switches can be estimated. Thus by measuring the delay in the $J1$ transition as a function of bias, rising edges on the signal may be mapped out. In practice this may be automated so that the unknown signal is traced out directly on an X-Y recorder. Hamilton *et al.* [26] used this method to observe the rise time of a 4200-A/cm^2 junction adjacent to the sampler (see Fig. 2 (b)). The two traces, recorded about 1 min apart, are for increasing and decreasing bias. They are different because time drift in the room-temperature electronics decreases the apparent rise time in one case and increases it in the other. Assuming constant time drift, the correct rise time is the average or about 9 ps. This result represents the combination of the actual signal rise time and the time-jitter limited system response of about 7 ps. Simulations of this circuit show that there is a turn-on delay between the time that I_o is exceeded and the switching transition of $J1$. This turn-on delay depends on the degree of overdrive of $J1$, among other factors (see Section IV). When I_b is high, the overdrive is high and the turn-on delay is minimal. As I_b decreases, the turn-on delay increases. The result is that signals observed with this technique are distorted, with the observed signal rise time being a few picoseconds greater than the actual rise time.

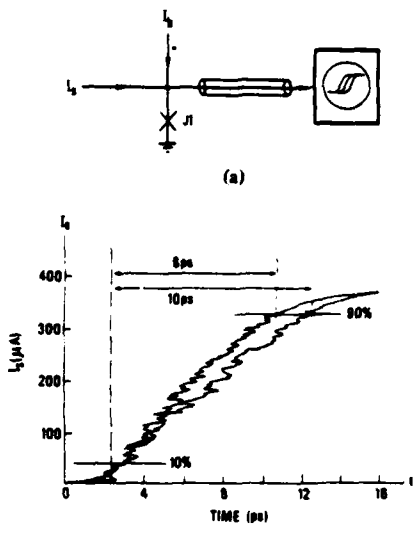

Fig. 2. (a) Sampling circuit for measuring the rise time of a signal I_s. A sampling oscilloscope in a servo-loop is used to automatically measure the time at which the signal plus the bias cause $J1$ to switch. I_s is reproduced by plotting the bias versus switching time. (b) Measured waveform, using the above technique, of the switching transition of a Josephson junction.

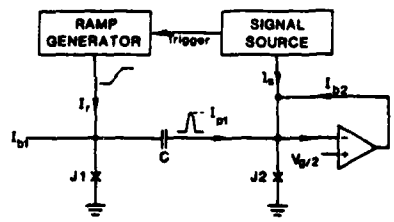

Fig. 3. Sampling circuit for measuring an arbitrary-signal waveform I_s. A sharp pulse of amplitude I_{p1} is obtained by differentiating, in an RC network, the switching transition waveform of junction $J1$. This pulse and the unknown signal I_s are applied to a detector junction $J2$ which, through I_{b2}, is then adjusted to the threshold for switching. The resulting value of I_{b2} is the essential information needed for determining the value of I_s at the time the pulse occurs. The entire signal waveform is measured by sweeping the time at which the pulse occurs.

The character of the distortion of the signal is consistent with the theoretical turn-on delay formula (23). Whether the agreement is quantitatively accurate is impossible to say because of the amount of jitter present. In addition to the jitter problem, this technique is further limited in that it can only observe rising edges of the signal.

Both of these limitations may be removed by another method [27], [28] depicted in Fig. 3. In this circuit, the current

through $J1$ is the sum of a dc bias I_{b1} and a fast ramp $I_r = \alpha t$. $J1$ will switch to the voltage state when $I_{b1} + I_r = I_{o1}$, producing a voltage transition at a time $T = (I_{o1} - I_{b1})/\alpha$. This voltage transition is differentiated by a capacitor C to produce a sampling pulse of maximum value I_{p1}. This pulse is applied to junction $J2$. $J2$ also receives current from the signal $I_s(t)$ and a second bias source I_{b2}. The maximum values of I_s and I_{b2} are arranged so that I_{o2} can never be exceeded except at the instant of the sampling pulse. Thus if $I_{p1} + I_s(T) + I_{b2} > I_{o2}$, $J2$ will switch producing an output voltage $V_o = V_g$. If $I_{p1} + I_s(T) + I_{b2} < I_{o2}$ the output voltage is zero.

The output voltage, averaged over many repetitions of the signal, is compared with a value $V_g/2$ and the amplified difference is used to drive I_{b2}. This servo-loop automatically adjusts I_{b2} to the threshold value where $J2$ is switching half the time and $I_{p1} + I_s(T) + I_{b2} = I_{o2}$. Since I_{p1}, I_{b2}, and I_{o2} are known, the signal $I_s(T)$ is determined. The complete signal waveform may be recovered by sweeping I_{b1} and plotting the computed signal $(I_{o2} - I_{p1} - I_{b2})$ versus equivalent time $(I_{o1} - I_{b1})/\alpha$. Note that this circuit works in a repetitive mode where $J1$ and $J2$ are reset to the zero-voltage state between each signal recurrence. The reset circuits are not shown in Fig. 3. In practice, the sampling pulse may be created in several different ways and the detector junction $J2$ may be a Josephson interferometer. Faris [28] and Tuckerman [29] have used this principle in a general waveform sampling circuit with an estimated time resolution of 6 ps.

In order to produce an undistorted picture of the signal with this technique, the maximum value of $I_s(t) + I_{p1}$ must occur at the same time as the maximum of I_{p1}. Since I_{p1} is rounded on top, any variation of $I_s(t)$ across the rounded top of I_{p1} will cause the maxima not to coincide and thus lead to distortion in the observed signal. The magnitude of this distortion depends on the width of I_{p1} and the amplitude of $I_s(t)$ relative to I_{p1}. In practice, this error can be reduced to a few picoseconds [28]. A second source of distortion results from the finite response time of the detector junction $J2$. Discussion of this point will be left to Sections IV and V which consider, in detail, the dynamics of Josephson junctions used as latching detectors.

III. Theoretical Basis

The design of circuits involving Josephson junctions is facilitated by the availability of accurate models for the junctions. The most commonly used model is a phenomenological description known as the RCSJ model, or resistively and capacitively shunted junction model first described by Stewart [3] and McCumber [4]. Following a brief description of this model, we discuss certain features of the more complex microscopic theory on which it is based. The microscopic theory is of practical importance because it provides a basis for testing the phenomenological model in areas that are experimentally difficult, such as the picosecond regime.

A. RCSJ Model

Stewart and McCumber used (1) and (2) to describe supercurrent flow in a Josephson junction and added a resistive shunt to account for normal current at finite voltages. A capacitive shunt was also needed because of the physical nature of a tunnel junction. Their circuit model is illustrated in Fig. 4(a). In order to encompass the idea of switching from the zero-voltage state to the energy-gap voltage V_g, the shunting resistance can be made voltage dependent, as illustrated in Fig. 4(b). We designate this junction resistance as R_J.

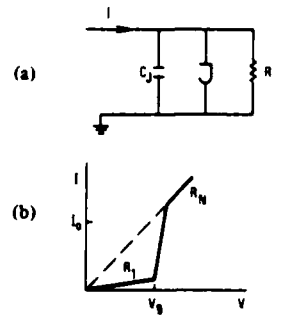

Fig. 4. Schematic representation of the RCSJ model. (a) The "J" symbol represents the supercurrent path which has current $I_o \sin \phi$. C_J is the intrinsic junction capacitance and R may be either the voltage-dependent resistance R_J or a parallel combination of R_J with an external shunt capacitance. (b) The voltage-dependent resistance R_J has three segments. Below the energy gap voltage V_g the resistance is R_1. Above V_g is a low-resistance region which is followed by a higher resistance designated as R_N, the junction normal-state resistance. R_J is an approximation to the quasi-particle I-V characteristic of the microscopic model.

If the RCSJ model is driven by a current source $I(t)$ the circuit equation for the case with no load conductance is

$$I(t) = C_J \dot{V} + V R_J^{-1} + I_o \sin \phi. \tag{6}$$

Much of the analysis to be discussed here will involve junction behavior at voltages below the energy gap, in which case $R_J = R_1$ (see Fig. 4 (b)). Restricting analysis to this region, one may write (6) in the form

$$\frac{I(t)}{I_o} = \omega_p^2 (R_N C_J)^2 \frac{d^2\phi}{d\theta^2} + \frac{R_N}{R_1} \frac{d\phi}{d\theta} + \sin \phi \tag{7}$$

where R_N is the junction normal state resistance and ω_p is the plasma frequency [30]

$$\omega_p \equiv (I_o/C_J\bar{\phi}_0)^{1/2} \tag{8}$$

where $\bar{\phi}_0 \equiv \hbar/2e$. The dimensionless time $\theta \equiv (\pi/2)\,\omega_g t$, where $\omega_g = 2I_o R_N/\pi\bar{\phi}_0$. Equation (7) contains the three time scales of a Josephson junction related to ω_p, $R_N C_J$, and to ω_g. We note, incidentally, that these time scales are not independent, in fact $\omega_p^2 R_N C_J \simeq \omega_g$.

The ω_g time scale is based on the quantity $I_o R_N$. As will be seen later when discussing the microscopic theory of a Josephson junction, the quantity $I_o R_N = \pi\Delta/2e$ where Δ is the energy gap. Thus $I_o R_N$ is determined by a microscopic quantity and we shall, therefore, refer to θ as the microscopic time. On the other hand, the quantities ω_p and $R_N C_J$ both depend on capacitance, or in other words, on the presence of a macroscopic dielectric layer, so we shall refer to the corresponding time scales as the macroscopic scales. These three time scales will be examined in more detail in the following two subsections.

B. Microscopic Theory

Josephson, in his original work on superconducting tunneling [6], described the consequences of (1) and (2). It remained for others to evaluate the theory for frequencies in the vicinity

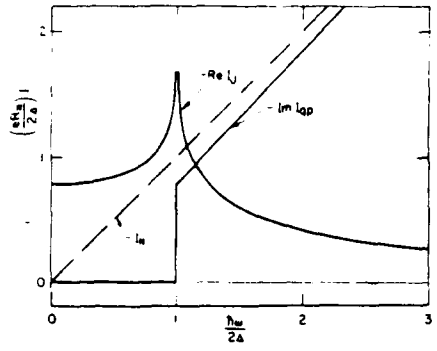

Fig. 5. Results of the microscopic theory of Josephson junctions. The illustrated functions reveal the frequency dependence of the supercurrent and the voltage dependence of the quasi-particle current as described in the text.

of the energy gap of the superconductors making up the junction. That was subsequently done by Reidel [1], and more completely by Werthamer [2], who were, in turn, followed by other significant contributors [31]-[34]. Because the microscopic theory includes detailed effects which are not present in the phenomenological theory it is more complex and less straightforward to interpret. Here we will discuss only those aspects of the microscopic theory which are conceptually relevant to picosecond response. Further details are presented in Appendix I.

Initially, the microscopic theory was presented in a frequency-domain formulation. This theory describes only the tunneling current but the capacitive current can be added exactly as for the phenomenological model. The tunneling current is the sum of two currents: one of normal electrons called the quasi-particle current and described by $I_{qp}(\omega)$ and one of paired electrons called the supercurrent and described by $I_J(\omega)$. Although both I_{qp} and I_J have real and imaginary parts, which are all required for the complete theory, it is Im I_{qp} and Re I_J which provide the theoretical basis for the phenomenological theory. These functions are shown in Fig. 5. The junction critical current of the phenomenological model is the low-frequency limit of Re I_J

$$I_o = -\lim_{\omega \to 0} \operatorname{Re} I_J(\omega) = \frac{\pi\Delta}{2eR_N}. \tag{9}$$

The right-hand equation is correct for superconductors with weak electron-phonon coupling but requires a correction factor for strongly coupled materials [35], [36]. The frequency dependence of $I_J(\omega)$ is the frequency dependence of I_o, which was discussed in Section II. The peak in Re I_J at the energy gap describes an internal microscopic resonance called the Riedel peak which has been experimentally verified [18], [19].

The phenomenological resistive current VR_J^{-1} in (6) appears in the microscopic theory as Im $I_{qp}(\omega)$. When the full microscopic theory is used to calculate an I-V curve [37] the abrupt rise in Im $I_{qp}(\omega)$ of Fig. 5 occurs at a voltage $V = V_g \equiv 2\Delta/e$, the energy-gap voltage. Thus the phenomenological resistive current is Im $I_{qp}(V)$. Indeed, this function provides a highly accurate description of experimentally measured current-voltage characteristics [38].

In our later discussions, the plasma frequency plays an important role. Physically, this frequency represents the resonance between the junction capacitance C_J and the Josephson inductance which is derivable from (1) and (2)

$$L_J \equiv \bar{\phi}_0 / I_o. \tag{10}$$

In the context of the microscopic theory one should note, first of all, that the analog of I_o, i.e., $I_J(\omega)$, is frequency dependent so the inductance should also be frequency dependent. Secondly, $I_{qp}(\omega)$ has a reactive part which will affect the resonance. As will become especially clear when we discuss the theory of pulse detection, the plasma frequency is the natural frequency for small oscillations of junction voltage about the zero-voltage state. Consequently, we use small-signal theory [34] to calculate the effective inductance in the microscopic model including the above effects, with the result

$$[L_{\text{eff}}(\omega)]^{-1} = \frac{e}{\hbar} \operatorname{Re}\{-[I_J(0) + I_J(\omega)] + [I_{qp}(0) - I_{qp}(\omega)]\}. \tag{11}$$

In the limit as ω goes to zero, the I_{qp} terms cancel and, using (9), L_{eff} becomes L_J of (10). If L_{eff} is evaluated at 0 K it is found that the singularity in Re $I_J(\omega)$ at the energy gap is canceled by a singularity in Re $I_{qp}(\omega)$ at the same frequency. L_{eff} increases monotonically from its minimum value L_J at $\omega = 0$, reaches a value of 1.57 L_J at the energy-gap frequency, and asymptotically approaches a linear dependence on ω, $L_{\text{eff}}(\hbar\omega \gg \Delta) = L_J\hbar\omega/\Delta$. The increase of inductance with frequency simply means that the additional parallel resistive and capacitive current paths dominate the circuit at high frequencies.

Including high-frequency effects, the plasma frequency is given by $(L_{\text{eff}}C)^{-1/2}$. Therefore, as C is reduced so as to make ω_p approach the energy-gap frequency ω_g, one sees that L_{eff}, which is always $\geq L_J$, makes ω_p smaller than expected without high-frequency corrections. This result has implications for the later discussion in Section V where it is found that the plasma frequency is directly related to the time resolution of superconducting circuits.

Returning to the general subject of the microscopic theory, we note that only a few evaluations of it have been made. These include detailed evaluations of a) I-V curves as a function of $R_N C_J$ [37], [39], [40], b) a proposed technique for producing picosecond pulses [41], and c) the impulse response of a Josephson junction [42]. Since the last reveals the microscopic limitations of the pulse response of junctions most clearly, we confine our attention to it here.

A Josephson junction, or any physical system for that matter, does not respond instantaneously to an applied stimulus. Delays arise from the interactions of electrons within the superconducting electrodes of a junction. These microscopic delays represent a fundamental limitation to device response.

To illustrate the intrinsic delay in a Josephson junction, Harris [42] has calculated the idealized impulse response of a hypothetical junction which has no capacitance. The calculation was based on a reformulation of the microscopic theory in the time domain which is discussed further in Appendix I. In this calculation, the stimulus is a voltage pulse described as a delta function. The amplitude of the pulse is

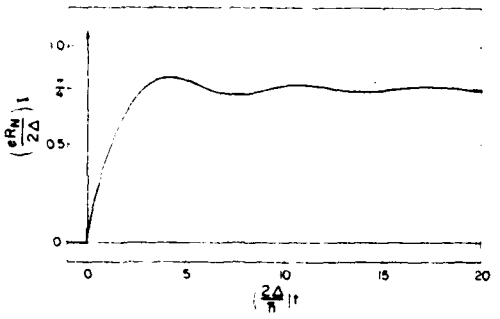

Fig. 6. Theoretical impulse response of a tunnel junction without capacitance. The current calculated from the microscopic model is illustrated for a voltage impulse applied at a time zero. The amplitude of the impulse was adjusted to produce a phase shift of $\pi/2$.

adjusted to produce a phase shift of $\pi/2$ in ϕ. The resulting current in the junction is illustrated in Fig. 6. The calculation reveals three significant aspects of the response. First, the instantaneous response at time zero is linearly related to the driving voltage and is a result of the resistive nature of the I-V curve for large-bias voltages. Second, after this response comes a rapid rise, on a time scale of $\hbar/2\Delta$ which is about 0.23 ps for the Pb-alloy junctions we will discuss in the next section. This rise reveals the intrinsic response time of the junction. It is a very fast response, about a factor of 25 faster than any observed to date. As shown in Appendix I, this delay arises from both the supercurrent I_J and the quasi-particle current I_{qp}. Third, at later times, the current oscillates at the gap frequency $2\Delta/h$. This is just the appearance in the time domain of the previously mentioned internal resonance named after Riedel. An important question is now apparent: how close can real devices, which suffer from macroscopic limitations, come to this limiting response time?

C. Macroscopic-Junction Properties

Several intrinsic macroscopic parameters are needed for evaluating the behavior of real Josephson junctions. We will summarize the general formulas for these quantities and evaluate them for Pb-alloy technology. Following that, we return to a discussion of the macroscopic time scale suggested by the differential equation (7) of the RCSJ model.

The macroscopic properties of interest are the response time $R_N C_J$, the plasma frequency ω_p, the critical current density j_c, and the Josephson penetration depth λ_J, all of which are interrelated. These quantities are independent of junction area except for the plasma frequency, which is proportional to $(I_o/C_J)^{1/2}$, according to (^). This ratio is independent of area if the current density is uniform. Another point of interest, which we discuss in due course, is that the plasma frequency is maximized, for a given capacitance, if the current density is uniform. The Josephson penetration depth is a measure of the maximum size a junction can have and still retain uniform current density [43]. Consequently, we use (8) combined with (12) below to compute the plasma frequency with the proviso that the junction size not exceed λ_J by λ_J.

Basavaiah, Eldridge, and Matisoo [5] empirically related critical current density to tunneling-barrier thickness d using the following relationship:

$$j_c = \frac{c_1}{d} \exp(-c_2 d) \tag{12}$$

where c_1 and c_2 are constants to be determined.

The next relationship of interest is between j_c and the junction normal state resistance R_N. For a junction using electrodes of identical superconductors at zero temperature we have

$$R_N = \frac{c_3}{A} \frac{\pi}{4} \frac{2\Delta}{j_c e} \tag{13}$$

where A is the junction area. This formula is similar to (9) but includes the strong coupling [29], [30] correction c_3. If $T > 0$, c_3 also includes a minor temperature correction. For dissimilar electrode materials, we use an approximate expression obtained by replacing 2Δ with $\Delta_1 + \Delta_2$, rather than the exact but more complicated result of Ambegaokar and Baratoff [44].

Combining (13) with the usual expression for capacitance, $C = \epsilon_r \epsilon_0 A/d$, the expression for $R_N C_J$ is obtained

$$R_N C_J = \epsilon_r \epsilon_0 c_3 \frac{\pi}{4e} \frac{2\Delta}{j_c d}. \tag{14}$$

The Josephson penetration depth is given by

$$\lambda_J^2 = \frac{\bar{\phi}_0}{\mu_0 (\lambda_1 + \lambda_2 + d) j_c} \tag{15}$$

where μ_0 is the magnetic permeability of vacuum, and λ_1 and λ_2 are the magnetic penetration depths of the base and upper superconducting electrodes of the Josephson junction.

For evaluation of the foregoing formulas, the constants c_1, c_2, c_3, Δ, ϵ_r, λ_1, and λ_2 must be determined. In general, one would expect these constants to depend on the alloy composition of the base and upper electrodes of the junction and the details of the procedure for producing the tunneling barrier. Recent work of Greiner, Kircher, and Ames [45], and of Baker, Kircher, and Matthews [46] has begun to clarify what factors are important in the fabrication procedure. Unfortunately, not all of the material constants we need have been determined for the alloys of greatest interest [45] so we are forced to assume typical values taken from several different sources.

We begin with the constants in the relationship between j_c and d of (12). For this, we use tunneling barrier data from the work of Eldridge and Matisoo [47] which used Pb-In alloy for the base electrode and Pb for the upper electrode. In this work, the barrier is described in terms of various fractional concentrations of In and Pb in the oxide and we somewhat arbitrarily choose the data for 6.5 percent In and 93.5 percent Pb. Equation (12) has been fitted by a least squares procedure to these data to yield $c_1 = 2.207 \times 10^5$, $c_2 = 1.57872$ for d, and j_c in units of nm and A/cm^2, respectively. With these constants, (12) gives j_c to within 5 percent of the experimental data [40] over the range from 1 to 1000 A/cm^2.

The dielectric constant of the tunneling barrier can be

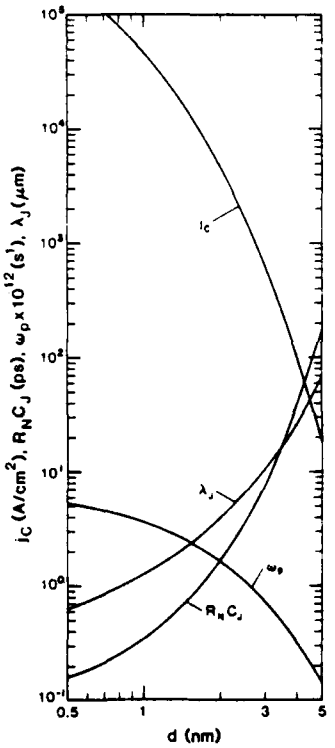

Fig. 7. Macroscopic properties of small Pb-alloy Josephson junctions. The critical current density j_c, the time constant $R_N C_J$, the plasma frequency ω_p, and the Josephson penetration depth λ_J are shown as functions of tunneling barrier thickness d.

evaluated from the recent data of Gheewala [48]. He reports a critical current of 50 μA for a junction with 2.5-μm diameter and 0.2-pF capacitance. Using the corresponding j_c of 1019 A/cm^2, the barrier thickness is evaluated from (12), and the dielectric constant $\epsilon_r = 12.7$ comes immediately from the standard capacitance formula. (Note that this value of ϵ_r is obtained by combining data for two different alloy systems and consequently has considerable, but unknown, uncertainty associated with it.) A working rule of thumb for capacitance is 4 pF/1 mA of critical current at 1000 A/cm^2.

An *I-V* curve for the most recent alloy system of Greiner *et al.* [45] allows the evaluation of additional constants. From the voltage of the steep rise of the quasi-particle current, our own data give $2\Delta/e = 2.9$ mV. For a critical current of 0.177 mA, we measure a normal-state resistance $R_N = 8.0\ \Omega$, which from (14) gives a value of $c_3 = 0.62$. Values of the magnetic penetration depths are taken from [45]: $\lambda_1 = 137$ nm, $\lambda_2 = 202$ nm.

These constants allow computation of the graphs shown in Fig. 7. It should be understood that these graphs are only approximate since they are based on data from more than one alloy system. Nevertheless, we take them to be representative of the properties of Pb-alloy junctions and find them to be useful for design analysis.

Most of the detailed analysis in subsequent sections involves junction behavior at voltages below the steep rise of the quasi-particle current at the energy gap. For this case, the appropriate RC time is not $R_N C_J$ but rather $R_1 C_J$, where R_1 is the resistance below the energy gap of Fig. 4(*b*). Thus to obtain the physical RC time, the graphical data for $R_N C_J$ of Fig. 7 must be multiplied by R_1/R_N, a number which depends on the fabrication process. For example, in our laboratory R_1/R_N was typically 5 when a PbAu upper electrode was used but a PbBi upper electrode at the present time gives a representative value of 17.

Using data from Fig. 7 one can readily establish that the quantity $\omega_p R_1 C_J \gg 1$ for the entire range of the figure. That means that junctions operating in the subgap resistance region have plasma oscillations that are only lightly damped, a fact that has significant consequences in the study of pulse coincidences in a detector in Section V.

We observe from Fig. 7 that $R_N C_J$ and ω_p refer to substantially different numerical time scales. Consequently, we must consider which is physically more important.

In the RCSJ model, Fig. 4(a), there are three parallel current paths, namely, those through R_1, C_J, and the Josephson inductance L_J given by (10). For effective high-speed action of a Josephson junction in a switching circuit L_J must not be heavily shunted by R_1 or C_J. The plasma frequency, by definition, is the frequency above which the impedance of C_J is less than that of L_J. Using the graphical data of Fig. 7 it can readily be determined that at the plasma frequency the capacitance heavily shunts R_1. Thus R_1 plays only a small role in the high-speed dynamics. From these considerations it becomes clear that ω_p and not $R_N C_J$ should be the basis for the physically more important time scale for Josephson junctions without external shunts of low impedance.

Earlier we found the microscopic response time of a Pb-alloy junction to be $\hbar/2\Delta = 0.23$ ps. The corresponding limiting macroscopic time is approximately $\tau_p \equiv 2\pi/\omega_p$. In order to have the macroscopic and microscopic response times approximately equal, we find that the plasma frequency must be approximately equal to the energy-gap frequency $\omega_g \equiv 2\Delta/\hbar$. In this regime, the RCSJ model has inaccuracies of about 30 percent which we will largely ignore. More importantly, we note that the current density required for such a high ω_p would be well in excess of 10^5 A/cm^2 for Pb-alloy technology. Such high j_c means that nonequilibrium and self-heating effects would be significant. Even though current densities in excess of 10^5 A/cm^2 have been achieved [49], little is known about the dynamical properties of such junctions. Consequently, it must be left as an open question whether or not the macroscopic and microscopic speeds can be made comparable.

An example of what *is* achievable and in agreement with the RCSJ model, comes from the work of Broom, Jutzi, and Mohr who used junctions with current densities of 28 000 A/cm^2 in a memory cell [50]. Heating effects were sufficiently large in this case that the *I-V* curve was traced by a pulsed method to reduce errors from self-heating of the junction. Taking this example as a rough estimate of the maximum j_c that is practical without using extra thick electrodes or special substrates [51], Fig. 7 gives the corresponding $\omega_p = 3 \times 10^{+12}\ s^{-1}$. This is a factor of ten below the plasma frequency needed to make the macroscopic and microscopic response times equal.

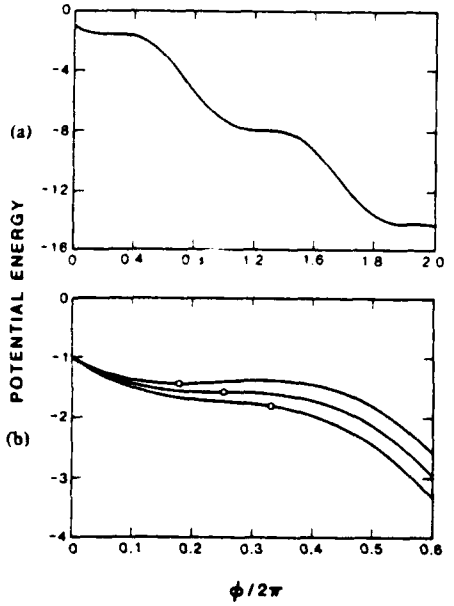

Fig. 8. The potential energy washboard. (a) The potential energy of (17), normalized to ω_p^2, is plotted against $\phi/2\pi$ for $I_b = I_o$. (b) Comparison of potential energies of three values of I_b/I_o: top curve, 0.9; middle curve, 1.0; bottom curve, 1.1. The circles on the upper and middle curves show the initial position and potential energy of the system "particle." The circle on the lower curve lies at $\frac{1}{2}$ rad beyond $\pi/2$.

IV. Switching Time

The switching time of a junction from the zero-voltage state to the energy-gap voltage divides roughly into two parts, a turn-on delay time during which the voltage remains small, and a rise time during which the voltage is rapidly increasing, as illustrated in Fig. 9. The analysis of these given here is based on the RCSJ model. For the period during which the voltage remains below the gap voltage, one may use (6) with R_J replaced by R where R is the parallel combination of the subgap resistance R_1 and a possible load resistance R_L. Setting $I(t) = I_b(t)$ in (6), we note that if $I_b(t)$ changes sufficiently slowly then (6) can be written in the form of an energy equation

$$\frac{d}{dt}(\mathcal{T} + \mathcal{U}) = -\frac{\dot{\phi}^2}{RC_J} \tag{16}$$

where the kinetic and potential energies, $\mathcal{T}$ and $\mathcal{U}$, are, respectively, $\mathcal{T} = \frac{1}{2}\dot{\phi}^2$ and

$$\mathcal{U} = -\omega_p^2(\cos\phi + (I_b/I_o)\phi). \tag{17}$$

These equations suggest the helpful analogy of a particle of unit mass subject to a viscous retarding force, sliding down a potential energy "washboard." Fig. 8 illustrates the potential energy as a function of ϕ and I_b. Clearly, there is no stable position for the particle if $I_b > I_o$. Consideration of the washboard picture helps one to understand qualitatively many features of the RCSJ model, including the switching behavior of a junction. For example, the particle initially moves slowly until the downward curvature of the potential is reached. This corresponds to the turn-on delay period, which was first discussed by Harris [52]. Subsequently, the particle accelerates

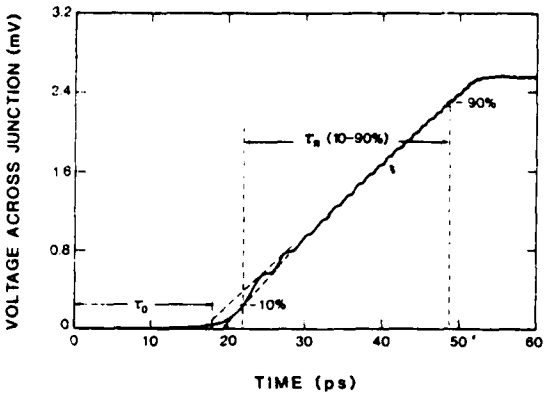

Fig. 9. Switching curve (from simulations) for a current-biased junction, stepped from $I_b = I_o$ to 1.01 I_o, illustrating both the turn-on delay and rise-time portions. $I_o = 0.0796$ mA, $C_J = 1.0$ pF, $V_g = 2.5$ mV, $R_1 = 200\ \Omega$, $R_L = \infty$. The method used for determining τ_D from the switching curve is shown. The 10-90-percent voltage levels on the rise-time portion are also indicated. For weak coupling $R_N = \pi V_g/4I_o = 24.7\ \Omega$, so $R_N C_J = 24.7$ ps. Compare with τ_R (10-90 percent).

until either its terminal velocity is reached, corresponding to a voltage $I_b R$, or the velocity corresponding to the gap voltage is reached. This defines the rise time of the switching process. Fig. 9 shows a simulation which illustrates this behavior. We will develop formulas for the turn-on delay τ_D and the rise time τ_R for lightly and moderately loaded circuits. The sum of these is the approximate switching time.

A. Turn-on Delay of a Josephson Junction

Suppose that the current $I_b(t)$ is increased slowly from zero so that the junction phase ϕ will be about $\pi/2$ when I_b reaches I_o. At that point, I_b is then abruptly stepped to $I_o(1 + \delta_0)$ where δ_0 is the fractional overdrive. This is a bit artificial in that in practice I_b typically ramps up through I_o at a finite rate. One technique which approximates this case is that in which a junction is biased at a constant current below I_o, and then triggered by a current pulse resulting from the switching of another junction, as discussed in Section II-B. We will shortly generalize to the case where the initial I_b is below I_o. The effects of a finite ramp rate will, however, not be taken up here.

In (6) we thus use $I_b = I_o(1 + \delta_0)$ for $t > 0$, and have $\phi(0) = \pi/2$. We set sin ϕ equal to unity and consider the evolution of V until ϕ advances by one-half radian. The supercurrent term is in error by just 12 percent at the end of this period, so that the estimated time for ϕ to get to $\pi/2 + \frac{1}{2}$ is quite accurate. Fortunately, $\phi = \pi/2 + \frac{1}{2}$ is also about the place where $\dot{\phi}$ begins increasing significantly, as simulations show. We thus take this time as an estimation to τ_D. From (6) we then easily obtain, provided $\tau_D \ll RC_J$,

$$\tau_D = \omega_p^{-1}\delta_0^{-1/2} \tag{18}$$

where ω_p is given in (8).

Harris [52] has published an expression for the turn-on delay time for this case. He approximated sin ϕ by the first two terms in its Taylor expansion, integrated the resulting expression exactly in terms of elliptic integrals, and approximated the latter by simpler functions. From this result he calculated

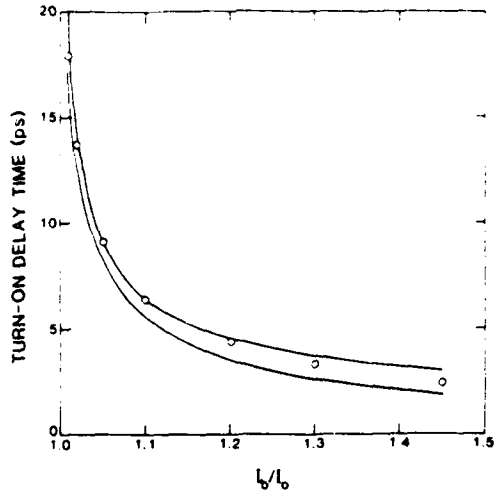

Fig. 10. Turn-on delay as determined from (18) (upper curve), (19) (lower curve), and from simulations (circles). The junction parameters are those of Fig. 9. I_b is stepped from I_o.

the time required for the phase to advance to $3\pi/2$. He subtracted from this the time required for the phase to advance the same amount if only the junction capacitance were being charged. His result, again for $\tau_D \ll RC_J$, is

$$\tau_D = \frac{1}{\omega_p}\left[\frac{2.61}{\delta_0^{1/4}}\tan^{-1}\left(\frac{1.13}{\delta_0^{1/4}}\right) - \left(\frac{2\pi}{1+\delta_0}\right)^{1/2}\right]. \quad (19)$$

Fig. 10 compares (18) and (19). Also shown are values of τ_D taken from numerical simulations. The latter have been determined by extrapolating the rise-time portion of the curve down to the time axis. Typically, there is a few-percent uncertainty in this, both because of the superimposed Josephson oscillations, and because the rising portion is not a straight line even with the oscillations removed. The points shown in Fig. 10 were determined from the midpoint of two straight lines drawn tangent to the first two maxima and minima, as shown in Fig. 9.

As is seen in Fig. 10, (18) is more accurate than (19) in the region of about 1-50-percent overdrive. Outside this region, Harris' expression is more accurate. Thus from 1-50-percent overdrive, (18) would be preferred for reasons of both accuracy and simplicity. Below 1 percent, turn-on delay becomes a more serious problem, and one may prefer to use (19); the simple formula overestimates τ_D there. Above about 50 percent, τ_D is typically very small compared to the rise time and, therefore, of decreased significance.

Now we remove the restriction that I_b is initally at I_o. Let $I_b(t<0) \equiv I_{bi} \leq I_o$, and $\phi(0) \equiv \phi_i = \sin^{-1}(I_{bi}/I_o)$. There are two new effects to consider now. One is that the particle in the washboard model must travel a longer distance if the same "final" position is used to define the delay time. The other is that the initial potential energy is now greater, giving the particle more velocity after the step, thus decreasing the delay time. This is illustrated in Fig. 8(b). The latter effect usually dominates.

We write $I_{bi} = I_o(1-\delta_i)$ and $I_b(t>0) = I_o(1+\delta_0)$ where $\delta_i \geq 0$ and $\delta_0 > 0$. Our procedure is, in effect, to approximate $\sin\phi$ by its initial value and to drop the damping term V/R from (16), which thus gives a constant acceleration to the system particle and an easy determination of τ_D. Lest this seem too crude, we shall show that the same result is obtained by expanding $\sin\phi$ through the term linear term in $\phi - \phi_i$, followed by some usually excellent approximations and the assumption that $\tau_D \ll RC_J$ as in the preceding case. When $\sin\phi$ is thus expanded, the potential energy of (17) is changed to a typically shallow parabola. Equation (6) then describes a damped harmonic oscillator

$$I_o(1+\delta_0) = C_J\dot{V} + V/R + I_o\sin\phi_i + (\phi - \phi_i)I_o\cos\phi_i. \quad (20)$$

This has the solution

$$\phi(t>0) = \phi_i + \frac{\delta_0+\delta_i}{\cos\phi_i}\left[1 - e^{-t/2RC_J}\cdot(\cos\omega t + (2\omega RC_J)^{-1}\sin\omega t)\right] \quad (21)$$

where

$$\omega = (4R^2C_J^2\omega_p^2\cos\phi_i - 1)^{1/2}/2RC_J \simeq \omega_p(\cos\phi_i)^{1/2}. \quad (22)$$

Thus ω is essentially the phase-dependent plasma frequency. The approximate equality in (22) is quite typically valid: If we take V_g/I_o as a minimum value for R (to ensure switching to the gap), the condition for the validity of the approximate equality is $\cos\phi_i \gg \bar{\phi}_0 I_o/4C_JV_g^2$. For the junction of Fig. 9, this becomes $\cos\phi_i \gg 10^{-3}$, or $\delta_i \gg 10^{-6}$. Clearly, R may be considerably less than V_g/I_o, as in high-speed latching logic, without practically invalidating the approximation of (22).

The coefficient of $\sin\omega t$ in (21) is very small under the same conditon. Thus the initial motion of ϕ results principally from the $\cos\omega t$ term. Expanding $\cos\omega t = 1 - (\omega t)^2/2$, and defining τ_D as the time at which ϕ reaches $\pi/2 + \frac{1}{2}$, as before, we find

$$\tau_D = \frac{1}{\omega_p}\left[\frac{1+2(\pi/2-\phi_i)}{\delta_0+\delta_i}\right]^{1/2}. \quad (23)$$

This is a simple generalization of (18) to which it reduces as I_{bi} goes to I_o. Unless ϕ_i is far from $\pi/2$, the numerator is not very sensitive to the precise value of δ_i, but the denominator can be very sensitive to δ_i, confirming our earlier remarks concerning the relative effects of the initial position and potential energy.

Equation (23) underestimates the delay time for small overdrives, as determined from simulations. The reason is that the approximations used in the above analysis are equivalent to taking the acceleration of ϕ as unchanged from its initial value during the motion. For $\delta_i = 0.1$, the result of (23) for the junction of Fig. 9 is about 30 percent low for $\delta_0 = 0.01$, correct for δ_0 about 0.2, and progressively too high beyond that. It is not difficult to refine the approximation at the expense of a more complicated formula. However, since different methods for defining τ_D can give values differing by several percent, and since one is ordinarily only interested in estimating τ_D, the estimate of (23) is surely adequate for most purposes.

Thus in summary, the total size of the step rather than just the amount of overdrive is the important quantity in the

turn-on delay resulting from a step increase in I_b. Further, τ_D is modified by the initial phase.

Discussions of the turn-on delays in single-junction and two-junction SQUID's are given in Appendixes II and III.

B. Rise Time

The rise time τ_R refers to the time duration of the rapidly rising portion of the switching transition illustrated in Fig. 9. We shall show that the rise time of the RCSJ model is approximately $R_N C_J$ where R_N is the normal state resistance of the junction. Although this result is widely known, it is often misquoted. It needs to be emphasized that the resistance here R_N is *not* the actual resistance R shunting the junction.

During the steep rise of the transition the sin ϕ term of (6) is rapidly oscillating so that the current $I_o \sin \phi$ averages nearly to zero. Equation (6) with the sin ϕ term neglected describes the charging of the junction capacitance. The solution to this equation is

$$V(t) = I_b R[1 - \exp(-t/RC_J)] \tag{24}$$

if the bias current has the value I_b which does not change significantly during the rapid rise. We choose $t = 0$ as the time when the significant acceleration begins. If $I_b R$ is less than the gap voltage V_g, the voltage rises only to $I_b R$ with time constant RC_J. However, if V_g is less than $I_b R$, the rise time τ_R at which the gap is reached is

$$\tau_R = -RC_J \ln(1 - V_g/I_b R). \tag{25}$$

If, moreover, $V_g \ll I_b R$ we see that

$$\tau_R \simeq \frac{C_J V_g}{I_b} = \frac{4}{\pi} R_N C_J \frac{I_o}{I_b} \tag{26}$$

where we have used the relation $V_g = 4I_o R_N/\pi$ from (9). Thus if $I_b \sim I_o$ and $V_g \ll I_o R$, the 10–90-percent rise time will be close to $R_N C_J$. This may be verified in Fig. 9. For strong coupling superconductors, the 10–90-percent rise time will be somewhat longer than $R_N C_J$.

V. Pulse Generation, Detection, and Measurement

In this section we adopt the primitive view that pulses have only two characteristics of interest, a height and a width. As a reasonable approximation to practical pulses we use the Gaussian pulse shape for most of the analysis. The main problem of interest is to develop the concepts needed for measurements of pulses that are available on a repeating basis.

A. Pulse Generators

Probably the simplest means of producing pulses in superconducting electronics is the circuit of Fig. 2(a). The junction $J1$ is assumed to be initially in the zero-voltage state with $I_s(t) + I_b < I_o$. The switching transition of the hysteretic junction $J1$ occurs very shortly after $I_s(t)$ exceeds $I_o - I_b$. The resulting increased impedance of $J1$ diverts the bias current down the transmission line producing the rising edge of the pulse. If the shunt impedance across the junction is low enough [53] the junction will not stay in the switched position, i.e., it will not latch, but will go back to the zero-voltage state producing the trailing edge of the pulse.

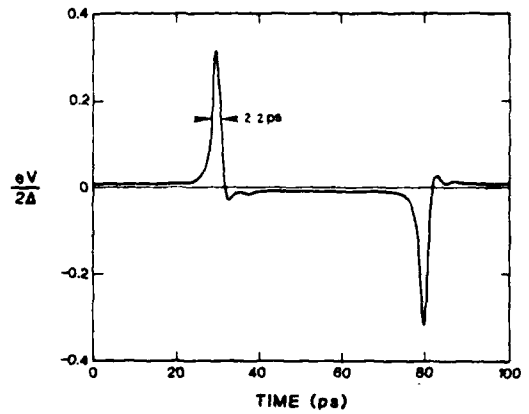

Fig. 11. One period of the voltage across the load resistance of the microwave driven pulser with an applied frequency of 10 GHz. The microscopic theory of junctions was used to calculate this waveform. The resulting pulsewidth is 2.2 ps with the following circuit parameters: $R_N C_J = 3.24$ ps, $R_N/R_L = 4$.

A related technique for producing especially narrow pulses is to pass the rising edge of the switching transition through a differentiating network, as indicated, for example, as part of Fig. 3.

Faris [28] and Tuckerman [29] have recently demonstrated a pulse generator, based on a SQUID interacting with another junction, which produced 12-ps wide pulses.

Several years ago Peterson and McDonald [54] proposed a conceptually different form of pulse generator based on a Josephson junction driven only by a microwave current source and loaded by a shunt resistor. In this circuit the junction may be either hysteretic or nonhysteretic without changing the qualitative behavior of the circuit. A train of alternating positive and negative pulses is produced when the drive current amplitude just exceeds I_o and encounters a strong nonlinearity. One cycle of the pulse train is shown in Fig. 11. This design is notable in part because it has been analyzed using the microscopic theory of junctions [35] to calculate the resulting pulsewidths. A comparison of the waveforms calculated using the microscopic theory and the RCSJ model is one of the few benchmark comparisons between the two theories. The differences between the waveforms are approximately 15 percent for pulsewidths of 4.7 ps and about 35 percent for the narrowest pulsewidths of 0.8 ps.

The original analysis did not consider the details of pulse detection and measurement. The need to understand these processes provided the primary motivation for the analysis which follows. In all of the simulations which follow, the effects that would arise in practice from parasitic inductance and finite source and load impedances are neglected. The goal is to describe the main qualitative features of pulse interactions with detectors.

B. Pulse Detectors

The elementary problem considered here is represented in Fig. 13(a), in which a current source $I_p(t)$ provides a single pulse to a Josephson-junction detector, and a current source I_b provides dc bias. We then ask under what circumstances

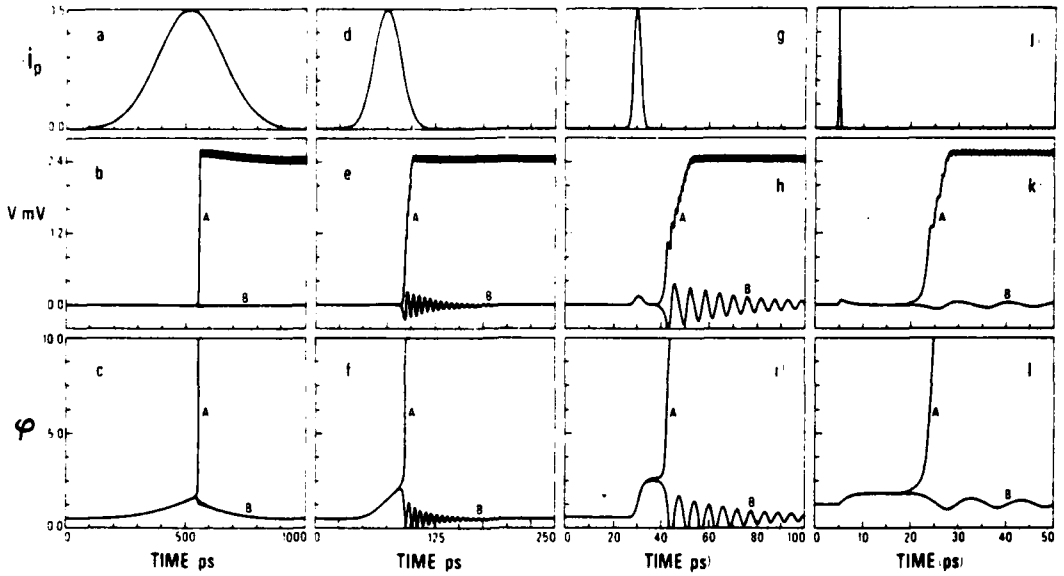

Fig. 12. Calculated detector responses for four different applied pulsewidths. The applied current pulses are shown at the top of each column of illustration with the corresponding detector responses arranged below. The detector properties and the applied pulse heights ($i_{p1} = 0.5$) are the same in all cases. The response of the junction voltage V and the phase ϕ (radians) are illustrated for bias levels just above threshold (labeled A) and for just below threshold (labeled B). For the four columns, reading from left to right, the pulsewidths are: 324, 32.4, 3.24, and 0.324 ps; and the bias levels above and below threshold are: 0.500215, 0.500214; 0.502139, 0.502138; 053905, 0.53904; 0.95528, 0.95527 mA. The detector properties are $I_o = 1$ mA, $R_N = 1.578\ \Omega$, $R_1/R_N = 5$, $C_J = 2.05$ pF.

does the junction voltage V switch from zero to the energy-gap voltage? The basis for our analysis is (6) with the driving current $I(t) = I_p(t) + I_b$.

If the pulse rise time is slow enough, the detector will switch as soon as $I_p(t) + I_b = I_o$, assuming $I_b < I_o$. However, if the pulse rise time is too fast or if the pulsewidth is too narrow, large deviations from this limiting case are suggested by the qualitative ideas of the washboard model. The emphasis in the present discussion will be on determining the minimum value of I_b for which switching occurs, i.e., the threshold condition, with a particular pulse amplitude and pulsewidth. In a subsequent section, the measurement of pulsewidth is explored.

Initially, we consider simulations in which the applied pulse has a Gaussian shape described as

$$i_p(t) = i_{p1} \exp\left\{-(4 \ln 2)\left(\frac{t - t_0}{W}\right)^2\right\} \cdots \quad (27)$$

where $i_p(t) \equiv I_p(t)/I_o$, $i_{p1} \equiv I_{p1}/I_o$, t_0 is the time of arrival of the center of the pulse at the detector, and W is the full width of the pulse at a current level of $\frac{1}{2} i_{p1}$.

Fig. 12 is a composite illustration of the calculated responses of a detector junction to pulses of four different widths. The driving pulses are shown in the first row of illustrations. The junction properties and the pulse amplitudes, $i_{p1} = 0.5$, are the same for all cases. Various junction responses are shown for biases i_b just below and just above threshold for switching. Although both bias levels are very close to threshold, the corresponding graphs qualitatively represent the general behavior for any values of i_b below and above threshold, respectively.

In the second row of illustrations it is seen that for i_b below threshold the voltage stays near zero and undergoes damped plasma oscillations after excitation by the applied current pulse. For i_b above threshold, the voltage rises rapidly from zero to the energy-gap value V_g. Josephson oscillations driven by V_g are evident after the junctions switch in all cases, but the time scale is too coarse for their resolution in the two leftmost illustrations of this group. These figures clearly illustrate why a Josephson junction is useful as a pulse detector: The device permanently changes its voltage state after the passage of a brief transient event if the pulse height, pulsewidth, and bias have the proper relationship. Of course this is much the same as the operation of a Josephson latching logic gate.

In the third row of Fig. 12, the time dependence of the phase ϕ of the junction is shown for each of the four driving pulsewidths. For the curves corresponding to bias values below threshold, the phase is driven to some maximum positive value by the applied pulse and then undergoes damped plasma oscillations in returning to its equilibrium position. The plasma oscillations, which seem like an unimportant detail, assume major importance when we consider the detection of pulse coincidences in a later section. An extensive numerical study of the phase supports the general idea that a junction

will switch if the phase reaches a certain universal critical value. Thus if one could watch the evolution of the phase in time using this critical phase idea, one would know well in advance whether or not the voltage was committed to a trajectory to V_g. The critical phase is $\pi - \phi_b$, where ϕ_b is the phase due to the steady bias

$$\phi_b = \sin^{-1} i_b. \tag{28}$$

This idea is central to the detailed models that will be used to analyze threshold-switching conditions. Zappe has used a similar argument when analyzing response to a current step [53]. We note that the critical phase idea originates from considerations with ideal pulses. If a pulse is complex, i.e., if it goes alternately both positive and negative, for example, the critical phase idea may not apply. This is only to say that the direction of motion of a pendulum can always be reversed regardless of its position relative to a critical angle.

The switching process for pulse detectors involves a turn-on delay and a rise time which are qualitatively the same as discussed in Section IV. These delays are particularly evident for the switching transition of Fig. 12 (k), the simulation with the narrowest driving pulse. The formulas given in Section IV for the turn-on delay are derived for the case in which the applied current remains at a constant level above the critical current, thus continually feeding energy into the system and shortening the turn-on delay. Turn-on delay expressions for the pulsed case can be derived. However, they are not simple and we will not present them here.

In summary, Fig. 12 illustrates the behavior of the detector biased near threshold for a variety of pulsewidths. The relationship between pulse height, pulsewidth, threshold bias, and the properties of the detector junction will now be analyzed by considering three different cases: 1) Static Limit, 2) Impulse Approximation, and 3) Square Pulse Approximation.

1) Static Limit: This limit applies to very broad pulses, broad in comparison with a junction plasma period $\tau_p \equiv 2\pi/\omega_p$. With the pulse current rising sufficiently slowly it is obvious that the junction will switch very soon after $i_p(t) + i_b$ exceeds unity. The pendulum analog [55] provides a simple interpretation for this case. This analog is based on the observation that the differential equation for the angle of deflection of a simple pendulum is similar to (7) for the phase of a Josephson junction if one makes a suitable identification of the analogous variables. The torque τ_b, analogous to the driving current, is balanced by gravitational torque so that the bias angle ϕ_b in the analogous cases is

$$\phi_b = \sin^{-1}\left(\frac{\tau_b}{mgl}\right) = \sin^{-1} i_b \tag{29}$$

where mg is the gravitational force on the pendulum of length l. Since the torque required to hold the penulum statically at angle ϕ_b is proportional to $\sin \phi_b$, it is clear that the torque increases for angles from zero up to $\pi/2$ and then decreases for larger angles. Thus for any torque $\tau_b < mgl$ there are two angular positions where that torque can hold the pendulum: ϕ_b and $\pi - \phi_b$. However, the upper position is unstable and random fluctuations in position will cause the pendulum to go "over the top." Thus our hypothesis is that if the pendulum can ever reach $\pi - \phi_b$, the mirror image position of ϕ_b for reflection in a horizontal plane, then continuous rotation of the pendulum will be initiated (assuming no damping), which is analogous to switching to the energy gap in a Josephson junction.

In the static limit the V and $\dot{V}$ terms (which are equivalent to $\dot{\phi}$ and $\ddot{\phi}$ terms) in (6) are negligible. An examination of this equation leads to the conclusion that in the static limit the critical angle idea has a special twist. It becomes obvious that in order for a slow pulse to carry the pendulum to the mirror position with the lowest possible (threshold) bias level, the pendulum must reach $\phi = \pi/2$ in coincidence with the pulse maximum.

The simulations in the first column of Fig. 12, with a pulsewidth of 324 ps, are close to the static limit. Threshold bias is between the two illustrated bias levels of 0.500214 and 0.500215. Thus we see immediately that the threshold bias $i_b(\text{Th})$ is very near the simple relation $i_b(\text{Th}) + i_{p1} = 1$, since $i_{p1} = 0.5$.

2) Impulse Approximation: Another limiting case which can be evaluated in detail is for extremely narrow pulses, the impulse approximation. In this case the current very rapidly rises and falls back to i_b before the junction can respond. All of the charge q_p in the impulse goes onto the capacitor, charging it to voltage V_m and providing an amount of energy $\frac{1}{2} C_J V_m^2$ for driving the system.

$$q_p = \int_{-\infty}^{\infty} I_p(t)\, dt = C_J V_m. \tag{30}$$

In the pendulum analog, an impulse of torque is applied but it is over before the pendulum has time to move. In the limiting case, the pendulum undergoes a step-function change in angular velocity. Based on our previous discussion of the analog, which ignores dissipation, we see that the system will go into a state of steady rotation if the impulse causes the pendulum to reach the mirror-image position.

Another source of energy is the bias supply. To calculate this energy, it is appropriate to integrate from the initial phase ϕ_b to the phase of the image position $\pi - \phi_b$

$$\int_{\phi_b}^{\pi-\phi_b} I_b V(t)\, dt = \bar{\phi}_0 I_b \int_{\phi_b}^{\pi-\phi_b} d\phi = \bar{\phi}_0 I_b(\pi - 2\phi_b). \tag{31}$$

The only other energy in the system is the analog of the potential energy of the pendulum [42], which is given by: $-\bar{\phi}_0 I_o \cos \phi$. As the pendulum is raised the potential energy continuously increases. The change in potential energy between ϕ_b and $\pi - \phi_b$ is $2\bar{\phi}_0 I_o \cos \phi_b$.

Ignoring dissipation, conservation of energy requires that the energy in the impulse plus the energy supplied by the bias equals the change in potential energy

$$\frac{1}{2}\frac{q_p^2}{C_J} + \bar{\phi}_0 I_b(\text{Th})\{\pi - 2\phi_b(\text{Th})\} = 2\bar{\phi}_0 I_o \cos \phi_b(\text{Th}) \tag{32}$$

at threshold.

For a Gaussian pulse described by (27)

$$q_p = 1.064\, i_{p1} W. \tag{33}$$

Combining (32) and (33) and changing to reduced variables gives

$$i_{p1}^2 = \frac{1.767}{\omega_p^2 W^2}\ \{2\cos\phi_b(\mathrm{Th}) - i_b(\mathrm{Th})[\pi - 2\phi_b(\mathrm{Th})]\}. \tag{34}$$

This is the desired relationship between pulse height i_{p1} and bias at threshold $i_b(\mathrm{Th})$ for a narrow pulse of width W. A clearer idea of what "narrow' pulse means will be obtained by comparing this formula with detailed simulations.

Fig. 12 (j)-(l) illustrates an example calculation for which the impulse approximation is reasonably accurate. For this case, the pulsewidth $W = 0.063\,\tau_p = 0.324$ ps, and the pulse height $i_{p1} = 0.5$. Fig. 12 (k) illustrates the time dependence of the detector voltage for biases of 0.95527 and 0.95528, which are just below and just above threshold.

Setting $i_b(\mathrm{Th}) = 0.95528$, the value for i_{p1} at threshold can be calculated from the impulse approximation formula, (34). The result is $i_{p1} = 0.4505$, which is about 10 percent off the simulation value of 0.5.

This simulation differs from the static limit in that the sum $i_b(\mathrm{Th}) + i_{p1} = 1.455$ instead of simply 1. Greater variations of the sum $(i_b + i_{p1})_{\mathrm{Th}}$ are found if i_b is held fixed and the threshold pulse height is evaluated. The required pulse height diverges as W^{-1}, according to (34).

A physically more interesting difference from the static limit is illustrated in Fig. 12 (l) where the time development of the phase is shown. For i_b *just barely below threshold*, ϕ advances to a maximum of 1.865 radians and then falls back and undergoes damped plasma oscillations. The maximum advance of the phase is very close to the image position $\pi - \phi_b = 1.872$ radians, validating the physical significance of that position.

The plasma oscillations are much more evident below threshold in the impulse limit than in the static limit, Fig. 12 (c). This behavior is readily understood from a Fourier analysis of the two different input pulses. The bandwidth of the pulses (defined as the frequency at which the frequency distribution has fallen to $\frac{1}{2}$ its maximum value) is

$$f_{1/2} = \frac{2\ln 2}{\pi W}. \tag{35}$$

In approximating the static limit we had $W = 324$ ps, implying $f_{1/2} = 1.36$ GHz. The pulse used in the impulse limit has $W = 0.324$ ps, and $f_{1/2} = 1360$ GHz. For both of these simulations, which differ only in the applied pulsewidth, the plasma frequency is 194 GHz. Comparing the two values of $f_{1/2}$ with the plasma frequency it is obvious that the wide pulse has very little energy available for exciting plasma oscillations, whereas, in the narrow-pulse case the plasma frequency is well inside the bandwidth of the pulse so substantial energy is available. Excitation of plasma oscillations takes on much greater importance when we deal with pulsewidth measurements in the next section, so it is important to understand what produces them.

3) Square Pulse Approximation: The static limit and the impulse approximation leave the intermediate cases unevaluated on a quantitative basis. To obtain workable formulas for these cases it is necessary to relinquish the Gaussian description of the pulse in favor of a simpler pulse shape. Dhong and Van Duzer [56] have shown that analytical results for threshold conditions with arbitrary pulsewidths can be obtained if the driving pulse has vertical sides and square corners. For describing this pulse we use the same notation as for the Gaussian pulse, i.e., it has a maximum current, normalized to I_o, of i_{p1} and a width W. In this calculation, the system is initially assumed to be dissipationless but a correction is made for that later. Using the washboard model, described earlier, and energy conservation, the phase ϕ_W which must be reached by the end of the square pulse in order to have continuing movement down the washboard is

$$\phi_W = \frac{-\pi i_b + (2i_b + i_{p1})\phi_b + 2\cos\phi_b}{i_{p1}}. \tag{36}$$

Using a linearized sin ϕ term, expanded about ϕ_b, the differential equation (6), with $I(t) = I_p(t) + I_b$, can be solved for the time dependence of the phase *during* the pulse

$$\phi = -\left(\frac{i_{p1}}{\cos\phi_b}\right)\cos\omega_p' t + \left(\frac{i_{p1}}{\cos\phi_b} + \phi_b\right), \quad 0 < t \leq W \tag{37}$$

where $\omega_p' \equiv \omega_p\sqrt{\cos\phi_b}$. ($\omega_p'$ is a generalization of the plasma frequency ω_p which explicitly includes the phase dependence of the effective inductance of a Josephson junction.) Solving (37) for t and then setting $t = W$ so that $\phi = \phi_W$ yields

$$W = \frac{2}{\omega_p'}\sin^{-1}\sqrt{\frac{(\phi_W - \phi_b)}{2i_{p1}}\cos\phi_b}. \tag{38}$$

Combining the threshold relationship (36) with (38) allows the calculation of the pulsewidth W at threshold for a given bias and pulse height, assuming no damping.

Including a correction for damping, Dhong and Van Duzer [56] obtained the following expression for the pulsewidth at threshold:

$$W' = W + \frac{\bar{\phi}_0(\phi_W - \phi_b)}{I_o R_1(-i_b + \sin\phi_W)}. \tag{39}$$

This relationship has been evaluated for a number of values of pulsewidth with fixed pulse height $i_{p1} = 0.5$. The results are displayed in Fig. 13 along with several data points from an evaluation of the impulse approximation formula, (34). In the figure these points are to be compared with the results of circuit simulations represented by the solid line.

The square pulse approximation predicts the threshold current to an accuracy of 10 percent or better, as compared with the simulations, over the pulsewidth range $0.09\,\tau_g < W < 0.5\,\tau_g$. This approximation diverges from the simulations for small pulsewidths because the correction term for dissipation becomes comparable to W. For large pulsewidths it diverges from the simulations because the linearization of sin ϕ becomes inaccurate. The impulse approximation is comparably accurate for $W < 0.25\,\tau_g$. One caution that should be observed is that the RCSJ model is not expected to be very accurate for

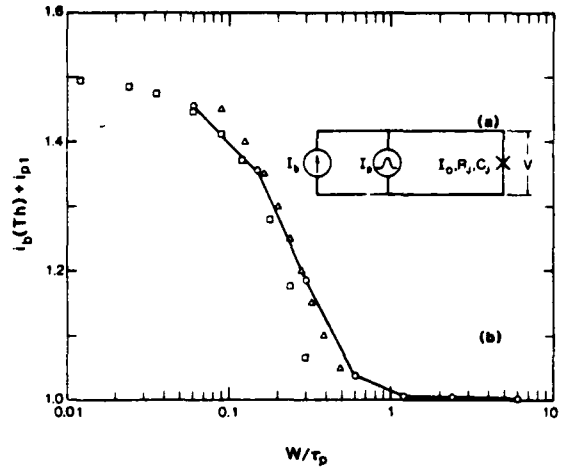

Fig. 13. (a) Circuit diagram for simulations of detector response. I_p is a current source for a Gaussian pulse and I_b is the constant bias supply. The × symbol represents the Josephson junction, which is described by the RCSJ model. (b) Calculations of detector threshold bias i_b(Th) as a function of pulsewidth W. For all points in this graph the pulse height is $i_{p1} = 0.5$. The circles, connected by a solid line, represent data from the RCSJ model, the squares are calculations from the impulse response (34), and the triangles are calculations using the square pulse approximations (39). The maximum threshold current for $i_{p1} = 0.5$ is 1.5, the value closely approached by the impulse approximation at the narrowest pulsewidths. The detector parameters are the same as for Fig. 12.

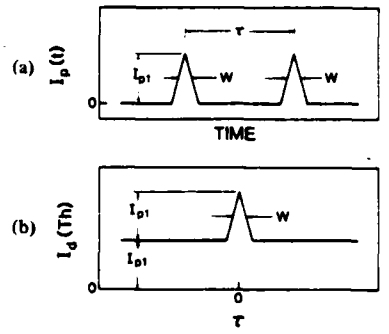

Fig. 14. Response of an idealized linear detector. (a) $I_p(t)$ is the current to the detector. This current has the form of two identical triangular pulses with delay time τ between them. (b) Threshold bias of the detector I_d(Th) plotted versus τ, showing the "image" of the pulses of (a).

pulsewidths of the order of 1 ps or less, the regime where the microscopic frequency dependence of the superconducting response becomes significant. In a related problem [41] for which comparisons with the microscopic model were made for an 0.8-ps pulsewidth, the differences between the models were about 35 percent.

The most important general conclusion from Fig. 13 is the observation that the static limit is a good approximation for pulsewidths greater than or equal to one plasma period, i.e., for $W \geq \tau_p \equiv 2\pi/\omega_p$. In this region the Josephson pulse detector is linear, by which we mean that at threshold a change in i_{p1} can be compensated for by an equal but opposite change in i_b following the relationship $(i_b + i_{p1})_{Th} = 1$. In the next section we argue that τ_p, and, therefore, the minimum pulsewidth for linear detection, can be as small as 2.1 ps. For narrower pulses, nonlinear threshold conditions apply as described by (39) for intermediate pulsewidths and (34) for the narrowest pulses.

C. Pulsewidth Determination

The Josephson pulse detector described in the preceding section is a very simple device. Given such a device one can measure its critical current density and from that infer its $R_N C_J$ and ω_p from Fig. 7. However, if this detector is used to detect pulses of unknown width and amplitude, what can be learned about the pulses? About all one can measure is the bias threshold for detection of the pulses, but that tells very little about them since the switching may be due to wide pulses of relatively low amplitude or from narrower pulses of higher amplitude. Knowledge of the detector response time does not change the situation. However, if the pulsewidth could be measured, the pulse amplitude could be inferred.

Before describing a technique for pulsewidth measurement, it is instructive to consider a hypothetical situation in which two triangular shaped current pulses are applied to an ideal threshold detector. For simplicity, the widths W and the amplitudes I_{p1} of the two pulses are equal. Fig. 14(a) is a plot of current in the detector as a function of time for a particular delay τ between the centers of the pulses. The idealized detector is a device which instantly switches the state of its output terminals (and remains switched) if an adjustable current level I_d is exceeded at its input terminals. Consider the input to the detector to be repeatable and the detector to be resettable so that one can experimentally determine, for a given τ, the maximum value of I_d for which threshold is crossed by the input signal.

The result of such an idealized experiment is shown in Fig. 14(b). If the pulses are well separated in time, the maximum value of I_d for detection, I_d(Th), is equal to I_{p1}. As τ is decreased, the pulses begin to overlap but I_d(Th) does not change until one pulse begins to overlap the *center* of the other pulse. The maximum value of I_d(Th) is $2I_{p1}$ and occurs for $\tau = 0$. The result of this idealized experiment is an image of one of the pulses in the I_d(Th) versus τ plot. The image pulse has an offset baseline but the pulse shape is unchanged.

The scheme for using Josephson junctions for pulsewidth measurements is similar to the idealized case just described but there are significant differences. The idealized device is linear in that a change in the bias I_d produces an exactly equal change in the current required to reach threshold. For a Josephson junction, that is true only in the static limit. In both the square pulse approximation (39) and the impulse approximation (34) the relationships between I_b and I_{p1} at threshold are nonlinear. With the idealized detector, the fidelity of the image of the driving pulse is a result of the linearity of the detector. With a nonlinear detector, distortion in the pulse image can be expected.

Our investigations of this procedure are limited to a circuit like the pulse detection circuit of Fig. 13 with the addition of a second Gaussian pulse source. We confine our attention to calculating the switching threshold of the detector as a func-

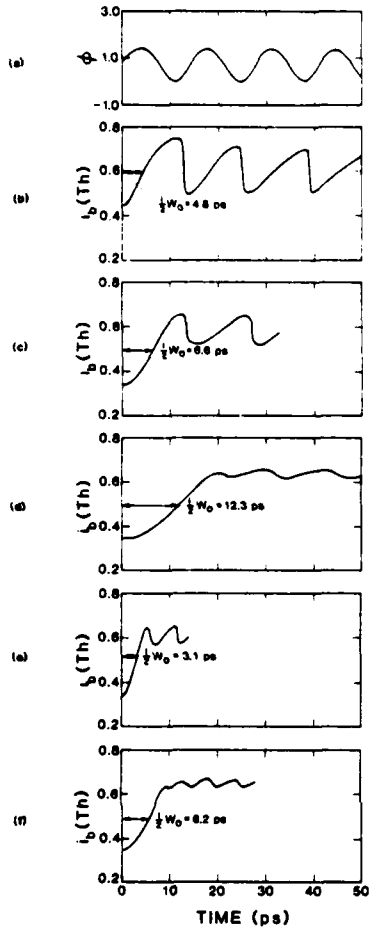

Fig. 15. Pulsewidth measurement simulations. (a) Time dependence of a lightly damped plasma oscillation excited by a single pulse of width $W = 4.72$ ps, with its center arriving at the detector at time zero. (b)–(f) Interference patterns. These patterns are graphs of the threshold bias as a function of delay time between the arrival of identical pulses at the detector. In all cases, the pulse amplitude $i_{p1} = 0.33$. The broadly structured interference pattern of (b) is a reflection of the plasma oscillations in (a). For illustrations (b)–(d) the detector characteristics are unchanged; the applied pulsewidths have the values 4.72, 9.54, and 19.0 ps, respectively. The illustrated values of $\frac{1}{2}W_0$ are the half-widths of the "images" of the applied pulses. The junction parameters are $I_o = 1$ mA, $R_N = 1.412\ \Omega$, $R_1/R_N = 17$, $C_J = 10.1$ pF, and $\omega_p = 0.548 \times 10^{12}\ s^{-1}$. For the illustrations (e) and (f) the plasma frequency of the detector has been increased. The applied pulsewidths are 4.72 and 9.43 ps, respectively. The junction parameters are $I_o = 1$ mA, $R_N = 1.412\ \Omega$, $R_1/R_N = 17$, $C_J = 1.63$ pF, and $\omega_p = 1.37 \times 10^{12}\ s^{-1}$.

tion of time delay between two pulses for delays of up to a few times the pulsewidth. In essence, this is a study of the interference pattern of two pulses applied in coincidence, or near coincidence, to a nonlinear detector. This is a special case of the waveform-measurement technique shown in Fig. 3 in which the signal is identical to the sampling pulse.

For simplicity, the two Gaussian pulses have the same amplitudes, $i_{p1} = i_{p2} = 0.33$, and the same widths $W_1 = W_2 = W$. Our first simulations of this type of experiment, Fig. 15(b), produced a surprisingly broadly structured interference pattern. In this plot of I_b (Th) versus delay time between first and second pulses, the image of the pulse is a negatively directed peak at zero delay. Only the pattern for positive delay times is displayed since the pattern is symmetric about zero delay. This case is for $W = 4.72$ ps, $\tau_p = 11.5$ ps, and $R_1 C_J = 243$ ps. Note that the width of the central minimum in Fig. 15(b) is $W_0 = 9.6$ ps. For the present, we ignore the broad structure and ask how does W_0 change as the width of the applied current pulses is changed? In Fig. 15(c), W has been approximately doubled to 9.54 ps and it is found that the central minimum did increase in width but only by about 38 percent instead of the anticipated factor of 2. Thus it is clear that the detector is not responding in a simple way, and that the broad structure in the interference pattern cannot be ignored.

Evidently this structure is due to plasma oscillations. These oscillations are less damped here than in Fig. 12 since R_1 is now larger. In Fig. 15(a), the time dependence of ϕ is shown with only the first of the two pulses applied. It is immediately obvious that the ringing behavior is present for the time delays of Fig. 15(b), and is of the correct frequency to cause the observed structure. Thus our conclusion is that the plasma oscillations are so strong, particularly in Fig. 15(b), that the system is not very sensitive to the applied pulsewidth.

In Fig. 15(d), the width of the pulse is increased to 19.02 ps and the plasma oscillations are clearly less important than in the preceding two figures. It is revealing to calculate the bandwidth of this pulse. Using (27) the result is $f_{1/2} = 23$ GHz. This is low compared with the plasma frequency of the detector which is about 87 GHz. Consequently, there is very little energy available to excite the plasma oscillations. Thus it becomes clear why the extended structure in Fig. 15(b) diminishes as wider pulsewidths are used.

The oscillatory behavior of the interference pattern for large delay times is much reduced in Fig. 15(d) as compared with the graph immediately above it. At the same time we note that W_0 changes essentially by a factor of 2 between these two figures. Thus the width of the pulse image now changes in proportion to changes in the driving pulsewidth, which is the desirable result. This behavior is correlated with the pulsewidth W becoming comparable to and greater than the period of a plasma oscillation τ_p.

To further substantiate this point of view, additional simulations were done for the narrow pulsewidth, 4.72 ps, used for Fig. 15(b) but now applied to a junction with a shorter plasma period, $\tau_p = 4.76$ ps. The result is the considerably lower level of plasma oscillations evident in the interference pattern Fig. 15(e) as compared with Fig. 15(b). Furthermore, it is now found that when the applied pulsewidth is increased by a factor of 2, to 9.43 ps, the width of the pulse image also increases by a factor of 2, as is seen by comparing Fig. 15(e) and (f).

Thus the interference pattern provides a sensitive means of measuring pulsewidth if $W \geq \tau_p$. We note in passing that our empirically derived criterion for sensitive pulsewidth measurements can also be expressed in the frequency domain. Using (38) we obtain for Gaussian pulses, $f_p/f_{1/2} \geq 2.27$, where f_p is the plasma frequency in hertz. This result is similar to our earlier observation that if the plasma frequency is well above

the spectrum of the applied pulse, then the plasma oscillations are not highly excited and simple behavior results. However, the width of the pulse image W_0 is not necessarily numerically equal to the pulsewidth W. The widths of the interference patterns in Fig. 15(d) and (f) are about 1.3 times the driving pulsewidths. It is expected that for larger pulsewidths the pulse image will more nearly approximate the driving pulse. Without further theoretical development, detailed simulations are required to determine the driving pulsewidth from the interference pattern. An experiment of this type has been done by Faris in which a pulsewidth of 26 ps was measured with little distortion [28].

We are now in a position to consider the minimum measureable pulsewidth for Josephson detectors driven by current sources. The previously discussed maximum current density of 28 000 A/cm^2 corresponds, in Fig. 7, to a plasma period of 2.1 ps. Therefore, the minimum measurable pulsewidth is also 2.1 ps if the change in the width of the pulse image must be proportional to the change in the width of the pulse. Narrower pulses can be measured if a less sensitive relationship between image width and pulsewidth is acceptable. Whether or not that might be the case depends on the experimental signal-to-noise ratio which is beyond the scope of the present article.

VI. Superconducting Striplines at High Frequencies

In previous sections we have detailed the speed limitations of the Josephson junction in various applications. A limitation which remains to be considered is that imposed by the interconnections between junctions in circuits.

As was realized early on [57], the operation of Josephson circuits at high speeds requires that the junctions be interconnected using transmission lines with matched loads. This arrangement prevents multiple reflections of the signals and, assuming an ideal transmission line, allows full utilization of the devices' switching speed. Swihart has shown [58] that at frequencies well below the superconducting energy-gap frequency, the striplines used to interconnect superconducting microcircuits are nearly ideal, having low loss and low dispersion. However, at frequencies approaching the energy gap, both attenuation and dispersion can be significant for striplines having lengths typical of microcircuit dimensions [59].

The speed limitations imposed by superconducting striplines were explored theoretically by Kautz [59] using the theory of Mattis and Bardeen for the conductivity of a superconductor. Fig. 16 shows the attenuation and phase velocity of an example stripline chosen to be typical of those used in superconducting microcircuits. Results are shown for temperatures of 4.2 K at which the line is superconducting and 9.2 K at which the line is normal. Above the energy-gap frequencies of the Nb- and Pb-alloy conductors, 720 and 610 GHz, respectively, at 4.2 K, the attenuation and phase velocity are nearly the same for the superconducting and normal states. Well below the gap frequency, the superconducting line shows its superiority, having an attenuation orders of magnitude lower than the normal-state line and virtually no dispersion. Below about 10 GHz, the attenuation and dispersion of the superconducting line are low enough that lines 1 cm or less in length can be considered ideal. At frequencies approaching the gap, however, both attenuation and dispersion become significant even for a 1-cm length of line.

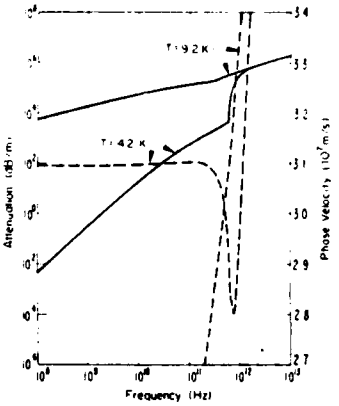

Fig. 16. Theoretical attenuation (solid line) and phase velocity (dashed line) for an example superconducting stripline at 4.2 K and for the same stripline in the normal state at 9.2 K. The example stripline consists of a 0.4-μm-thick Nb ground plane, a 0.1-μm layer of Nb_2O_5 dielectric (assumed lossless), and a 0.4-μm-thick Pb-alloy strip (assumed wide compared to the dielectric thickness).

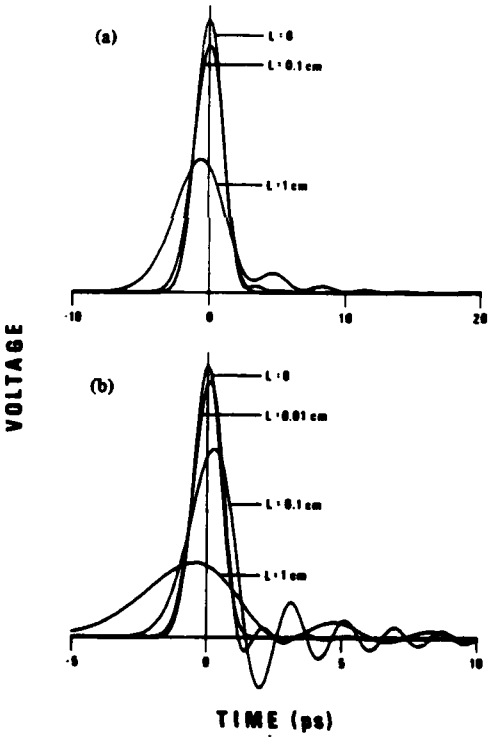

Fig. 17. Simulated pulse propagation on the example stripline described in Fig. 16. The histories of two pulses are shown in (a) and (b), respectively, by plotting the pulse shape at various distances L along the line. The pulses are originally Gaussian shaped, at $L = 0$, with $W = 2.4$ ps in (a) and 1.2 ps in (b).

The effects of attenuation and dispersion at these high frequencies on pulses is shown in Fig. 17. Here we see the evolution of two pulses which are initially Gaussian, with

widths $W = 2.4$ and 1.2 ps, as they propagate along the example stripline. For these pulses, virtually all of the energy is contained in frequency components below the energy gap, 99 percent of the energy being below 290 and 580 GHz for the 2.4- and 1.2-ps pulses, respectively. As Fig. 17 shows, the 2.4-ps pulse can travel no further than about 0.1 cm without significant distortion, while the limit for the 1.2-ps pulse is about 0.01 cm. Thus for microcircuit applications, the quality of the example line is excellent for pulsewidths down to a few picoseconds but for shorter pulses becomes rapidly unsatisfactory.

Finally, we examine the extent to which the high-frequency limit of the example stripline can be increased by changing its materials, temperature, or dimensions. Use of a superconductor with a larger energy gap, for example, leads to a direct increase in the high-frequency limit. Unfortunately, such large-gap superconductors are refractory and difficult to work with. Lowering the operating temperature leads to a dramatic decrease in attenuation below the gap frequency but reduces the dispersion only slightly. If the example stripline is operated at 1.0 K then the subgap attenuation does not exceed 10^{-2} dB/m but dispersion at frequencies just below the gap still prevents propagation of subpicosecond pulses over significant distances [59]. Finally, because both the attenuation and the frequency-dependent terms of the phase velocity are inversely proportional to the dielectric thickness, use of a thicker dielectric yields an overall improvement in pulse propagation [60]. Increasing the dielectric thickness by a factor of 10, for example, provides a 10-fold increase in the distance a given pulse can propagate before it becomes severely distorted. However, for the level of miniaturization required in a complex microcircuit, the dielectric can probably be no thicker than 1 μm and subpicosecond pulses will propagate no more than a centimeter without distortion. Thus the energy-gap frequency represents a firm upper limit for pulse propagation in superconducting microcircuits.

VII. Discussion

The behavior of superconducting circuits in the picosecond regime has been studied in only a few experiments. Consequently, in assessing picosecond applications of these circuits, we must rely heavily on circuit simulations. There are two models available for simulating the active part of the circuit: the RCSJ model and the microscopic model.

The RCSJ model is a simplification of the microscopic model and is used almost exclusively in the work reported here, partly because it requires much less computer time, but also because it is technically adequate. To establish its adequacy we compared it with frequency-domain experiments in Section II-A, and we compared it with the microscopic model in two areas: the evaluation of the Josephson inductance in Section III-B and the calculation of picosecond waveforms in Section V-A. We summarize these results as follows: for electrical responses that occur in time intervals of a few picoseconds or longer, the RCSJ model is adequate for practical purposes. However, as shorter time periods are considered it should be recognized that the RCSJ model is increasingly inaccurate, with waveform errors as large as approximately 35 percent at 0.8 ps. We conclude that all of the time-domain experiments that we discussed are justifiably analyzed with the RCSJ model.

Within the limitations of the RCSJ model we examined the step-function response of a junction and derived a simplified formula for the turn-on delay τ_D associated with switching from the zero-voltage state to the energy-gap voltage. The theory of turn-on delay was also extended to include arbitrary initial bias levels instead of only the single case of initial bias equal to the critical current. It was shown that the total step height of the bias current, rather than simply the amount of overdrive, is important in determining τ_D. A simple expression for the delay until the first appearance of a voltage pulse in a single-junction SQUID was also developed.

Detailed consideration was then given to the theory for measurements of the height and width of pulses using a latching Josephson detector. Formulas were derived for the switching threshold condition for three ranges of pulsewidths. We found the threshold condition to be especially simple for pulsewidths $W \geq \tau_p$, where τ_p is the period of a plasma oscillation. The simple threshold condition is a linear relationship, $(i_b + i_{p1})_{Th} = 1$. With the RCSJ model, any width of pulse will switch the detector if it has sufficient amplitude but the threshold conditions are nonlinear for $W < \tau_p$. The transmission lines limit the minimum pulsewidth to about 1 ps.

Simulations show that pulsewidth measurements can be made by studying the detector response for pulses arriving in near coincidence at the detector. It was found that this technique gives a sensitive measure of pulsewidth as long as $W \geq \tau_p$, the same criterion as for the detector to be linear.

For pulsewidths less than τ_p, the technique no longer proportionately measures the width of the pulse and becomes increasingly insensitive to pulsewidth as the width is decreased.

These results suggest a model in which the detector junction is an ideal instantaneously responding device in series with a low-pass filter which is resonant at the plasma frequency. The Q of the filter is determined by the loading across the junction. Thus most of the ringing reflected in Fig. 15(b) can be suppressed by adding a resistor, but frequencies above ω_p cannot be readily observed.

We conclude that the plasma period τ_p is an approximate measure of the highest time resolution that can be achieved in time-domain measurements. (Obviously, a more complete understanding must include consideration of signal-to-noise ratio.) Because of self-heating effects, τ_p cannot be made smaller than about 2 ps with present fabrication procedures.

Appendix I
Time-Domain Formulation of the Microscopic Theory

The microscopic theory seems to be not well known in detail, probably because the phenomenological model has consistently produced accurate descriptions of experimental circuits. Two things may change this situation in the future. First, the theory has been recast into a time-domain formulation which makes numerical computation simpler [61]. Second, the increasing speed of practical circuits may require simulations of circuits for which the phenomenological model is too inaccurate. For these reasons we include in this Appendix a brief description of the microscopic theory.

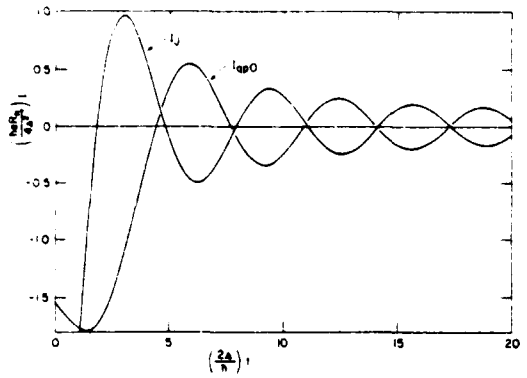

Fig. 18. The two kernels I_J and I_{qp0} in the time-domain formulation of the microscopic theory.

The time-domain formulation of the microscopic theory carries present and past information about the junction voltage in a function $U(t)$

$$U(t) = \exp(i\phi_s(t))$$

$$= \exp\left(-i\frac{e}{\hbar}\int_{-\infty}^{t} V(t')\,dt'\right). \tag{A1}$$

The function $U(t)$ is very much like a single-particle wave function. It is a solution of the time-dependent Schroedinger equation having Hamiltonian $-eV$ where V is the voltage across the junction.

The theory describes the junction current in terms of $U(t)$

$$I(t) = \frac{1}{2\pi}\,\mathrm{Im}\left\{U^*(t)\int_{-\infty}^{t} I_{qp}(t-t')\,U(t')\,dt' + U(t)\int_{-\infty}^{t} I_J(t-t')\,U(t')\,dt'\right\}. \tag{A2}$$

Here the kernels $I_{qp}(t)$ and $I_J(t)$ produce the details of the time-dependent response of the junction. The U^* denotes the complex conjugate of U.

We now examine the form of the two kernels which are plotted in Fig. 18. First I_J which describes the supercurrent reveals a logarithmic singularity (negative) just after time zero. This integrable singularity represents a very fast but not instantaneous response. If the time scale were compressed, by letting the energy gap 2Δ become large, the singularity, combined with (A2), transforms into the instantaneous current $I_0 \sin\phi$ of the phenomenological model. Somewhat after time zero, I_J reveals oscillations at the energy-gap frequency $2\Delta/\hbar$. These correspond to the resonance known as the Riedel peak shown in Fig. 5.

It is also interesting to observe that the second term of (A2) involving I_J includes a product of the form $U(t)\,U(t')$. This form tends to double the phase ϕ_s making it into the pair phase of (2). In contrast, the first term of (A2) contains the product $U^*(t)\,U(t')$ which does not double the phase ϕ_s. Thus the second term corresponds to the flow of paired electrons (the supercurrent), while the first term describes the flow of single (normal or quasi-particle) electrons.

The kernel I_{qp} is slightly more involved. This kernel contains all the information found in the current–voltage characteristic of Fig. 5. First we note that the characteristic becomes a linear resistance R_N for voltages above the energy gap. Since a pure resistance describes an instantaneous response, it appears in I_{qp} as a delta function. To simplify I_{qp} we, therefore, separate out the instantaneous response.

$$I_{qp}(t) = -2(\hbar eR_N)\,\delta'(t) + I_{qp0}(t). \tag{A3}$$

The portion of the kernel I_{qp0} is shown in Fig. 18. It also contains a peak just past time 0. This peak, however, is not as sharp as that in I_J and thus corresponds to a somewhat slower response. The oscillations at the gap frequency in I_J also appear in I_{qp0}, and correspond to the abrupt rise in current of the voltage-dependent resistance at the energy gap.

Although the time-domain formulation of the microscopic theory is conceptually equivalent to that in the frequency domain, it is particularly useful in numerical simulations [61]. As devices are fabricated which are faster than those commonly used today, simulating them may necessarily involve this formulation of the theory.

The time-domain formulation could be significantly improved in one respect. The energy-gap frequency oscillations in both I_J and I_{qp0} maintain significant amplitude to quite long times. This is a result of the sharp gap structure seen in the current–voltage characteristics. In practice, this structure is smeared over a range of voltages. As a result, the kernels I_J and I_{qp0} for practical junctions should correspondingly exhibit a faster falloff in the amplitude of the energy-gap oscillations. The development of a physical model for this falloff would make it possible to truncate the integrals of (4) after a suitable time. This would speed numerical computations and reduce memory requirements.

Appendix II
Turn-On Delay in a Single-Junction SQUID

Although not at the moment of apparent practical importance, turn-on delay in a single-junction SQUID is interesting in its own right. We shall sketch briefly how one can estimate τ_D for this case. Many mathematical details for flux entry into a SQUID may be found in [62]. Consider the case in which the junction of Fig. 4 is shunted by a superconducting loop of inductance L. This circuit is described by (6) if we add $\bar{\phi}_0\phi/L$ to the right side. The washboard potential is now given a positive net curvature, becoming a parabola with ripples. The potential energy describing this case is

$$\mathcal{U} = -\omega_p^2\cos\phi + \frac{1}{2LC}(\phi - \beta_b)^2 \tag{A4}$$

where $\beta_k = LI_k/\bar{\phi}_0$. Apart from an unimportant constant, (A4) goes to (17) as $L \to \infty$. It is clear that this SQUID will have less of a chance for switching to V_g because of the curvature of the parabola. The time delay before one or more fluxoids enter the SQUID after application of a step increase in I_b is of potential interest, however.

As I_b is raised slowly from zero, ϕ will advance from zero,

always staying in the first local minimum given by $d\mathcal{U}/d\phi = 0$. Thus ϕ is that value which solves

$$\phi + \beta_0 \sin\phi = \beta_b. \tag{A5}$$

When $d^2\mathcal{U}/d^2\phi = 0$ at the minimum, the particle will spill out, corresponding to the entrance of one (or more) fluxoids into the SQUID. Thus fluxoid entry occurs when $\cos\phi = -1/\beta_0$ and (A5) are satisfied simultaneously. The critical or threshold current for this to occur is given by

$$\beta_b^c = \phi_c + \beta_0 \sin\phi_c = \cos^{-1}(-\beta_0^{-1}) + (\beta_0^2 - 1)^{1/2}. \tag{A6}$$

Suppose that when this current is reached, it is suddenly stepped to $I_b^c(1 + \delta_0)$. If we then expand $\sin\theta$ about its initial value $\sin\phi_c$, retaining only the linear term in $\phi - \phi_c$, we find, from the generalization of (6) to the SQUID,

$$\beta_b^2\delta_0 = LC\ddot{\phi} + \frac{L}{R}\dot{\phi}. \tag{A7}$$

The term with ϕ has dropped out, leaving the same form of equation as in Section IV for the junction not shunted by inductance. If we assert, as there, that the turn-on delay time can be approximated by the time required for the phase to advance by one-half radian, we get

$$\tau_D = \omega_p^{-1}(\delta_0 f)^{-1/2} \tag{A8}$$

where $f = \beta_b^c/\beta_0 \simeq 1 + \pi/(2\beta_0) + (2\beta_0^2)^{-1}$. The approximate equality here results from expanding the right side of (A6) in powers of β_0^{-1}, and is an excellent approximation even at the lowest value of β_0 (unity) for which the system particle can be trapped away from the bottom of the parabola. Equation (A8) should be compared with (18), which it generalizes. Numerical simulations show that (A8) is quite a good approximation to the time for the rising of the first voltage pulse. The effect of the shunt inductance is to shorten the turn-on delay time.

Appendix III
Turn-On Delay in a Two-Junction SQUID

A two-junction SQUID, or interferometer, is depicted in Fig. 19(a). It is evident that such a device is inherently slower than a single junction, principally because the two junctions will not necessarily act in concert.

There is a trivial exception to this which we shall mention here, because the idea occurs again later. When the interferometer is completely symmetric, and there is no control current I_c, the bias current I_b divides equally between the two halves of the interferometer. The inductances L and damping resistors R_d draw no currents. When I_b is stepped to $2I_o(1 + \delta_0)$, one half of this passes through each junction. The junctions act together, and the turn-on delay is given by (18), (19), or (23), where ω_p still refers to the single-junction plasma frequency.

Of course, the reason for using a multijunction interferometer is because the control current allows one to set the switching threshold value of I_b over a range of values, as shown in Fig. 19(b). When $I_c \neq 0$, the analytical problem is much more difficult than for a single junction. The only published treatment of turn-on delay in a two-junction SQUID at the moment

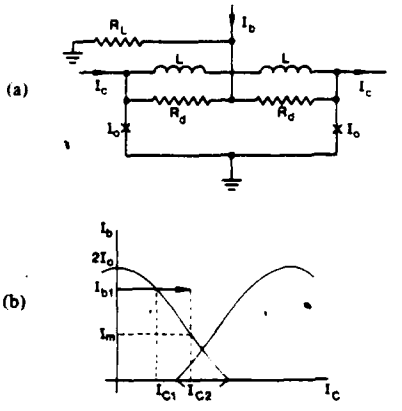

Fig. 19. (a) Two-junction interferometer, showing damping resistors R_d and a load resistor R_L. Each × represents the junction depicted in Fig. 4(a). (b) Sketch of a typical threshold curve for a two-junction interferometer, showing control stepped from 0 to I_{c2}, at bias current I_{b1}.

is that of Harris [52]. We shall here follow Harris' reasoning and give his results.

If the interferometer is heavily damped to suppress the LC resonance effects of the circuit, the interferometer is described approximately by the two equations

$$\frac{L}{R_d}\dot{\phi}_- + \phi_- + \beta_0 \sin\phi_- \cos\phi_+ = \beta_c \tag{A9}$$

$$2LC\ddot{\phi}_+ + \frac{L}{R_L}\dot{\phi}_+ + 2\beta_0 \sin\phi_+ \cos\phi_- = \beta_b \tag{A10}$$

where $\phi_\pm = \frac{1}{2}(\phi_1 \pm \phi_2)$, and the β's have been defined following (A4). One sees from (A9) and (A10) that if β_c is held constant at or below a threshold value, while β_b is stepped up, then ϕ_+ will first respond; ϕ_- will follow by virtue of the coupling between the two equations. Similarly, if β_b is fixed and β_c is stepped, ϕ_- first responds. Harris considered only the latter case.

The control current is taken as zero for $t < 0$, and I_b is fixed (for all t) at I_{b1}, so that $\phi_-(t < 0) = 0$ from (A9). At $t = 0$, I_c is stepped to a value I_{c2}, greater than the threshold value I_{c1}. Equation (A10) shows then that $\sin\phi_+$ is given approximately by $\beta_{b1}\sec\phi_-/2\beta_0$ until the time at which the latter quantity equals unity. Harris calls this time interval τ_{int} and develops an approximate expression for it, given below. At that time, ϕ_+ begins increasing rapidly, that is, the two junctions begin moving together and the interferometer tends to behave as a single junction. The time for ϕ_+ to advance from $\pi/2$ to $3\pi/2$ is designated τ_{ext}, and the total turn-on delay time of the interferometer is taken to be $\tau_D = \tau_{int} + \tau_{ext}$. For τ_{ext}, Harris simply adopts the single-junction result, in which the capacitance is twice the single-junction capacitance, and I_o is replaced by I_m, the threshold value of I_b when I_c has its final value I_{c2} (see Fig. 19(b)). Harris's approximate expression for τ_{int} is $\tau_0 + \tau_1$ where

$$\omega_0\tau_0 = \frac{1}{B}\ln\left(\frac{I_{c2}}{\Delta I_c}\right) + \frac{I_o}{\Delta I_c}\left(\phi_1 - \frac{I_{c1}}{I_o}\right) \tag{A11}$$

$$\omega_0 \tau_1 = \frac{I_o}{\Delta I_c}\left[\cos^{-1}\left(\frac{I_{b2}}{2I_o}\right) - \phi_i\right] \quad \text{(A12)}$$

$$I_{b2} = I_{b1} - 2\bar{\phi}_0 \phi_1 (2R_L C + \tau_0)/(R_L \tau_0^2) \quad \text{(A13)}$$

$$B = \beta_0^{-1} + \left[1 - \left(\frac{I_{b1}}{2I_o}\right)^2\right]^{-1/2}. \quad \text{(A14)}$$

Also, $\phi_1 = \cos^{-1}(I_{b1}/2I_o)$, $\omega_0 = R_d I_o/\bar{\phi}_0$, and $\Delta I_c = I_{c2} - I_{c1}$. Harris states that these formulas agree with the results of numerical simulations to within about 15 percent for fractional overdrives ranging from 0.1 to 1.5, and for values of R_d ranging from heavy damping to roughly critical damping.

REFERENCES

[1] E. Riedel, "Zum Tunneleffekt bei Supraleitern in Microwellenfeld," *Z. Naturforsch.*, vol. 19A, pp. 1634–1635, 1965.

[2] N. R. Werthamer, "Nonlinear self-coupling of Josephson radiation in superconducting tunnel junctions," *Phys. Rev.*, vol. 147, pp. 255–263, July 8, 1966.

[3] W. C. Stewart, "Current-voltage characteristics of Josephson junctions," *Appl. Phys. Lett.*, vol. 12, pp. 277–280, Apr. 15, 1968.

[4] D. E. McCumber, "Effect of ac impedance on dc voltage-current characteristics of superconductor weak-link junctions," *J. Appl. Phys.*, vol. 39, pp. 3113–3118, June 1968.

[5] S. Basavaiah, J. M. Eldridge, and J. Matisoo, "Tunneling in lead-lead oxide-lead junctions," *J. Appl. Phys.*, vol. 45, pp. 457–464, Jan. 1974.

[6] H. H. Zappe, "Josephson quantum interference computer devices," *IEEE Trans. Magn.*, vol. MAG-13, pp. 41–47, Jan. 1977.

[7] T. A. Fulton and R. C. Dynes, "Switching to zero voltage in Josephson tunnel junctions," *Solid State Commun.*, vol. 9, pp. 1069–1073, 1973.
T. A. Fulton, "Punchthrough and the tunneling cryotron," *Appl. Phys. Lett.*, vol. 19, pp. 311–313, Nov. 1, 1971.

[8] B. D. Josephson, "Possible new effects in superconductive tunneling," *Phys. Lett.*, vol. 1, pp. 251–253, July 1962.

[9] S. Shapiro, "Josephson currents in superconducting tunneling: The effect of microwaves and other observations," *Phys. Rev. Lett.*, vol. 11, pp. 80–82, July 15, 1963.

[10] P. Russer, "Influence of microwave radiation on current-voltage characteristic of superconducting weak links," *J. Appl. Phys.*, vol. 43, pp. 2008–2010, Apr. 1972.

[11] R. L. Kautz, to be published.

[12] D. G. McDonald, V. E. Kose, K. M. Evenson, J. S. Wells, and J. D. Cupp, "Harmonic generation and submillimeter wave mixing with the Josephson effect," *Appl. Phys. Lett.*, vol. 15, pp. 121–122, Aug. 15, 1969.

[13] D. G. McDonald, K. M. Evenson, J. S. Wells, and J. D. Cupp, "High-frequency limit of the Josephson effect," *J. Appl. Phys.*, vol. 42, pp. 179–181, Jan. 1971.

[14] D. A. Weitz, W. J. Skocpol, and M. Tinkham, "High-frequency behavior of "ideal" superconducting point contacts," *Phys. Rev. Lett.*, vol. 40, pp. 253–256, Jan. 23, 1978.
—, "Far-infrared frequency dependence of the ac Josephson effect in niobium point contacts," *Phys. Rev. B*, vol. 18, pp. 3282–3292, Oct. 1, 1978.

[15] M. Tinkham, M. Octavio, and W. J. Skocpol, "Heating effects in high frequency metallic Josephson devices: Voltage limit, bolometric mixing, and noise," *J. Appl. Phys.*, vol. 48, pp. 1311–1320, Mar. 1977.

[16] D. G. McDonald, F. R. Petersen, J. D. Cupp, B. L. Danielson, and E. G. Johnson, "Josephson junctions at 45 times the energy-gap frequency," *Appl. Phys. Lett.*, vol. 24, pp. 335–337, Apr. 1, 1974.

[17] D. A. Weitz, W. J. Skocpol, and M. Tinkham, "Niobium point-contact Josephson-junction behavior at 604 GHz," *Appl. Phys. Lett.*, vol. 31, pp. 227–229, Aug. 1, 1977.

[18] C. A. Hamilton and S. Shapiro, "Experimental demonstration of the Riedel peak," *Phys. Rev. Lett.*, vol. 26, pp. 426–428, Feb. 22, 1971.

[19] S. A. Buckner, T. F. Finnegan, and D. N. Langenberg, "Reidel singularity in Sn-Sn-oxide-Sn Josephson tunnel junctions," *Phys. Rev. Lett.*, vol. 28, pp. 150–154, Jan. 17, 1972.

[20] H. H. Zappe and B. S. Landman, "Experimental investigation of resonances in low-Q Josephson interferometric devices," *J. Appl. Phys.*, vol. 49, pp. 4149–4154, July 1978.

[21] J. Matisoo, "Subnanosecond pair-tunneling to single-particle tunneling transitions in Josephson junctions," *Appl. Phys. Lett.*, vol. 9, pp. 167–168, Aug. 15, 1966.

[22] W. Jutzi, Th. O. Mohr, M. Gasser, and H. P. Gschwind, "Josephson junctions with 1 μm dimensions and with picosecond switching times," *Electron. Lett.*, vol. 8, pp. 589–591, 1972.

[23] T. R. Gheewala, "A 30 ps Josephson current injection logic (CIL) family," *IEEE J. Solid-State Circuits*, vol. SC-14, pp. 787–793, Oct. 1979.

[24] H. H. Zappe, "A subnanosecond Josephson tunneling memory cell with nondestructive readout," *IEEE J. Solid-State Circuits*, vol. SC-10, pp. 12–19, Feb. 1975.

[25] D. J. Herrell, "A Josephson tunneling logic adder," *IEEE Trans. Magn.*, vol. MAG-10, pp. 864–867, Sept. 1974.

[26] C. A. Hamilton, F. L. Lloyd, R. L. Peterson, and J. R. Andrews, "A superconducting sampler for Josephson logic circuits," *Appl. Phys. Lett.*, vol. 35, pp. 718–719, Nov. 1, 1979.

[27] C. A. Hamilton, "A sampling circuit and method therefor," U.S. Patent Application 853 354, 1977, pending.

[28] S. M. Faris, "Generation and measurement of ultrashort current pulses with Josephson devices," *Appl. Phys. Lett.*, vol. 36, pp. 1005–1007, June 1980.

[29] D. B. Tuckerman, "A Josephson ultrahigh resolution sampling system," *Appl. Phys. Lett.*, vol. 36, pp. 1008–1010, June 1980.

[30] A. J. Dahm, A. Denenstein, T. F. Finnegan, D. N. Langenberg, and D. J. Scalapino, "Study of the Josephson plasma resonance," *Phys. Rev. Lett.*, vol. 20, pp. 859–863, Apr. 15, 1968.

[31] A. V. Svidzinskii and V. A. Slyusarev, "Contribution to the theory of tunneling in superconductors," *Sov. Phys.–JETP*, vol. 24, pp. 120–123, Jan. 1967.

[32] A. I. Larkin and Yu. N. Ovchinnikov, "Tunnel effect between superconductors in an alternating field," *Sov. Phys.–JETP*, vol. 24, pp. 1035–1040, May 1967.

[33] R. E. Harris, "Cosine and other terms in the Josephson tunneling current," *Phys. Rev. B*, vol. 10, pp. 84–94, July 1, 1974.

[34] —, "Josephson tunneling current in the presence of a time-dependent voltage," *Phys. Rev. B*, vol. 11, pp. 3329–3333, May 1, 1975.

[35] T. A. Fulton and D. E. McCumber, "dc Josephson effect for strong-coupling superconductors," *Phys. Rev.*, vol. 175, pp. 585–586, Nov. 1968.

[36] D. M. Ginsberg, R. E. Harris, and R. C. Dynes, "Strong-coupling correction to the low-frequency electrical conductivity of superconductors and Josephson junctions," *Phys. Rev. B*, vol. 14, pp. 990–992, Aug. 1, 1976.
R. E. Harris, R. C. Dynes, and D. M. Ginsberg, "Strong-coupling correction to the jump in the quasi-particle current of a superconducting tunnel junction," *Phys. Rev. B*, vol. 14, pp. 993–995, Aug. 1, 1976.

[37] D. G. McDonald, E. G. Johnson, and R. E. Harris, "Modeling Josephson junctions," *Phys. Rev. B*, vol. 13, pp. 1028–1031, Feb. 1, 1976.

[38] S. Shapiro, P. H. Smith, J. Nicol, J. L. Miles, and P. F. Strong, "Superconductivity and electron tunneling," *IBM J. Res. Devel.*, vol. 6, pp. 34–43, Jan. 1962.

[39] A. B. Zorin and K. K. Likharev, "Current-voltage characteristics of low capacitance Josephson junctions," *Sov. J. Low Temp. Phys.*, vol. 3, pp. 70–71, Feb. 3, 1977.

[40] W. A. Schlup, "Solution of the Werthamer equation at finite temperatures," *Phys. Rev. B*, vol. 18, pp. 6132–6138, Dec. 1978.

[41] D. G. McDonald and R. L. Peterson, "Design of a Josephson-junction picosecond pulser," *J. Appl. Phys.*, vol. 48, pp. 5366–5369, Dec. 1977.

[42] R. E. Harris, "Intrinsic response time of a Josephson tunnel junction," *Phys. Rev. B*, vol. 13, pp. 3818–3821, May 1976.

[43] S. Basavaiah and R. F. Broom, "Characteristics of in-line Josephson tunneling gates," *IEEE Trans. Magn.*, vol. MAG-11, pp. 759–762, Mar. 1975.

[44] V. Ambegaokar and A. Baratoff, "Tunneling between superconductors," *Phys. Rev. Lett.*, vol. 10, pp. 486–489, June 1, 1963; Erratum, *Phys. Rev. Lett.*, vol. 11, p. 104, July 15, 1963.

[45] J. H. Greiner *et al.*, "Fabrication process for Josephson integrated circuits," *IBM J. Res. Devel.*, vol. 24, pp. 195–205, Mar. 1980.

[46] J. M. Baker, C. J. Kircher, and J. W. Matthews, "Structure of tunnel barrier oxide for Pb alloy Josephson junctions," *IBM J. Res. Devel.*, vol. 24, pp. 223–234, Mar. 1980.
[47] J. M. Eldridge and J. Matisoo, "Fabrication of variable current density Josephson junctions," U.S. Patent 3 816 173, June 11, 1974.
[48] T. R. Gheewala, "Design of 2.5 μm Josephson current injection logic (CIL)," *IBM J. Res. Devel.*, vol. 24, pp. 130–142, Mar. 1980.
[49] J. Niemeyer and V. Kose, "Observation of large dc supercurrents at nonzero voltages in Josephson tunnel junctions," *Appl. Phys. Lett.*, vol. 29, pp. 380–382, Sept. 15, 1976.
[50] R. F. Broom, W. Jutzi, and Th. O. Mohr, "A 1.4 mil^2 memory cell with Josephson junctions," *IEEE Trans. Magn.*, vol. MAG-11, pp. 755–758, Mar. 1975.
[51] S. B. Kaplan, "Acoustic matching of superconducting films to substrates," *J. Low Temp. Phys.*, vol. 37, pp. 343–365, 1979.
[52] E. P. Harris, "Turn-on delay of Josephson interferometer logic devices," *IEEE Trans. Magn.*, vol. MAG-15, pp. 562–565, Jan. 1, 1979.
[53] H. H. Zappe, "Minimum current and related topics in Josephson tunnel junction devices," *J. Appl. Phys.*, vol. 44, pp. 1371–1377, Mar. 1973.
[54] R. L. Peterson and D. G. McDonald, "Picosecond pulses from Josephson junctions: Phenomenological and microscopic analyses," *IEEE Trans. Magn.*, vol. MAG-13, pp. 887–890, Jan. 1977.
[55] D. B. Sullivan and J. E. Zimmerman, "Mechanical analogs of time dependent Josephson phenomena," *Amer. J. Phys.*, vol. 39, pp. 1504–1517, Dec. 1971.
[56] S. H. Dhong and T. Van Duzer, "Minimum-width control-current pulse for Josephson logic gates," this issue, pp. 1965–1973.
[57] W. Anacker, "Josephson tunneling devices–A new technology with potential for high-performance computers," in *AFIPS Conf. Proc.: Fall Joint Computer Conf.*, vol. 41, pp. 1269–1278, Dec. 1972.
[58] J. C. Swihart, "Field solution for a thin-film superconducting strip transmission line," *J. Appl. Phys.*, vol. 32, pp. 461–469, Mar. 1961.
[59] R. L. Kautz, "Picosecond pulses on superconducting striplines," *J. Appl. Phys.*, vol. 49, pp. 308–314, Jan. 1978.
[60] —, "Miniaturization of normal state and superconducting striplines," *NBS J. Res.*, vol. 84, pp. 247–259, May 1979.
[61] R. E. Harris, "Numerical evaluation of the response of a Josephson tunnel junction in an arbitrary circuit," *J. Appl. Phys.*, vol. 48, pp. 5188–5190, Dec. 1977.
[62] R. L. Peterson and R. I. Gayley, "Multiple magnetic flux entry into SQUIDs: A general way of examining the cos ϕ conductance," *Phys. Rev. B*, vol. 18, pp. 1198–1206, Aug. 1, 1978.

The extraordinary performance of Josephson-junction circuits for scientific measurements, and the suitability of similar circuits for large scale integrated electronics, presage the emergence of a new technology.

Donald G. McDonald

The pioneers of superconducting electronics are accumulating an impressive record of achievement. For example, they have now gained the high-performance lead in the important field of digital electronics. Logic delays of 13 picoseconds and switching times of 9 picoseconds have been experimentally demonstrated.[1] The same basic devices, Josephson junctions, also make the most sensitive microwave detectors, the most sensitive magnetometers (or current sensors) and the most stable voltage sources. Although each of these developments is an important independent accomplishment, the *combination* of these developments in a single technology merits special attention.

To gain a perspective of research in superconducting electronics during the past fifteen years, consider the *variety* of accomplishments beyond those mentioned above. In the lowest frequency band of the electromagnetic spectrum this research has centered on the development of current comparators of very high accuracy, on the extension of accurate thermometry to very low temperatures, on new techniques for gravitational, geomagnetic and biomagnetic measurements, and most recently, on gravitational-wave detection. In the midrange of frequencies, from the radio band through the microwave band, emphasis has been given to accurate measurements of power and attenuation, to the development of superconducting-cavity stabilized oscillators, to parametric amplifiers, to accurate waveform measurements of fast transient signals, to microwave frequency analog-to-digital converters, and (with particularly heavy emphasis) to integrated circuits for logic and memory. In the highest frequency band for which superconductivity is useful, from millimeter waves to the infrared, advances have been made in the sensitivity of millimeter-wave heterodyne detectors for astrophysical measurements, in broad-band frequency synthesis, and in the measurement of molecular constants at CO_2-laser frequencies. When these developments are compared with the best techniques at ambient temperatures, improvements in sensitivity, accuracy, speed, or resolution of factors of 10 to 100 have been common. Two devices, each an excellent example of modern superconducting electronics, are illustrated in figures 1 and 2.

What needs to be recognized from the foregoing is the broad significance of low-temperature electronics. Although it is not entirely evident from the discussion thus far, we will see that all of the most basic components of a general-purpose electronic technology have been developed in the superconducting realm. Thus, with some reservations, we can begin to think about making almost any critical electronic instrument or system with superconducting integrated circuits.

The availability of an accurate model for a Josephson junction, and the accurate control of circuit parameters resulting from the development of integrated circuit fabrication methods for superconductors,[2] together mean that basic circuits can be accurately modeled and, therefore, optimized. In a practical sense it is this last development (fabrication methods) that brings superconducting electronics within striking distance of the fundamental physical limits to measurements in two areas: energy sensitivity and single photon detection.

In speculating on the future of superconducting electronics one cannot ignore the fact that no liquid-helium-temperature technology, for any application whatever, has succeeded in a major way by emerging from the research environment for broader use. No one can say whether or not superconducting electronics will succeed, but we will show how this technology overcomes an important practical barrier to the continuation of long-term trends of electronics toward higher speed and increased miniaturization. Thus we see superconducting electronics becoming a significant challenge to established semiconductor electronics.

My main purpose here is to sketch the conceptual basis for superconducting electronics and to discuss the status and implications of current research. Instead of describing complex circuits I will emphasize fundamental ideas and relationships to more familiar phenomena. At the practical level superconducting electronics has a simple and elegant theory; however, it is theory unlike anything that preceded it. Testimony to its originality comes from the Nobel prizes bestowed on its creators: John Bardeen, Leon Cooper, J. Robert Schrieffer, Ivar Giaever and Brian Josephson. All but Giaever are theoretical physicists.

Superconductors

The abrupt transitions of some metals (lead, tin, and niobium, for example) from a normally conducting state to a state of zero electrical resistance, or superconductivity, below a critical transition temperature T_c is basic to any discussion of superconductivity. A second elementary property is the exclusion of electrical currents and magnetic flux from the interior of superconductors; they are both largely confined to a surface layer 10^{-5} cm thick, called the penetration depth.

In normal metals the current density $\mathbf{j}$ is related to the applied electric field $\mathbf{E}$ by Ohm's Law, $\mathbf{j} = \sigma\mathbf{E}$, where σ is the conductivity. The conductivity is a real number for frequencies up to the

A highly sensitive SQUID, shown in the center, surrounded by its external coupling coils. This computer-enhanced color illustration is an artist's impression of a device made by Michael Cromer and Pasquale Carelli at the National Bureau of Standards. Figure 1

Don McDonald is a staff scientist in the Cryoelectronic Metrology Group of the National Bureau of Standards, Boulder, Colorado.

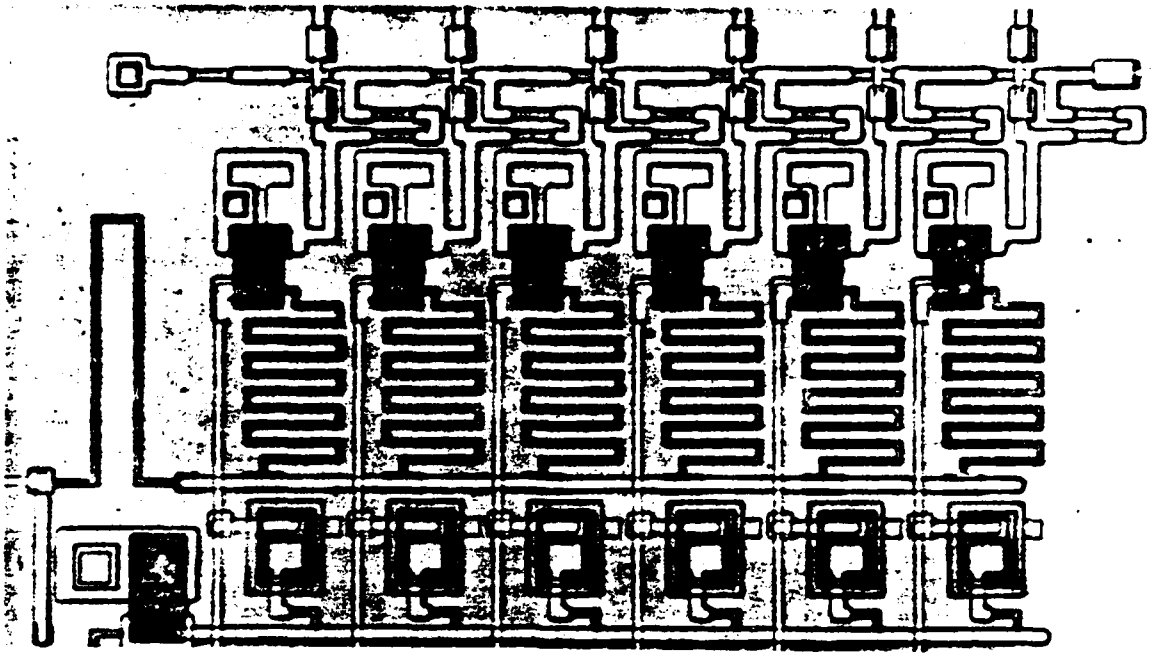

A six-bit analog-to-digital converter that uses six identical SQUIDs as current comparators. This device, developed by C. A. Hamilton and Frances L. Lloyd of NBS, operates at a conversion rate of 2×10^9 samples per second and an output data rate of 12×10^9 bits per second—nearly an order of magnitude faster than the fastest semiconductor devices. Figure 2

order of 10^{14} Hz. Thus for an alternating **E** field of modest frequency the current and voltage are in phase and, as a result, power is dissipated in the metal. For a superconductor similar logic leads to the conclusion that if the power dissipation is to be zero, the current and voltage must be out of phase by 90°, which means that σ must be an imaginary number.

But if high-frequency currents are imposed on superconductors, small amounts of power *are* dissipated. So the general case requires a complex conductivity

$$\sigma = \sigma_1 + i\sigma_2$$

where σ_1 is characteristically much less than σ_2. The two terms for the conductivity naturally give rise to the two-fluid model of a superconductor in which σ_1 is the conductivity of a normally conducting fluid and σ_2 is the conductivity of a dissipationless fluid, or superfluid.

For normal conductors the conductivity can be used to calculate the resistance of a wire:

$$R_n = (1/\sigma)(l/A)$$

where l is the length of the wire and A is its cross-sectional area. If a complex conductivity is used in a similar fashion, one obtains both a resistance and a reactance. For a superconductor the phase of the reactance indicates that it is inductive in character with inductance L_s given by

$$L_s = \frac{1}{\omega}\frac{\sigma_{2\omega}}{\sigma_{1\omega}^2 + \sigma_{2\omega}^2}\left(\frac{l}{A}\right) \qquad (1)$$

where ω is the angular frequency. The ω subscript on σ_1 and σ_2 implies a frequency dependence of these quantities. Equation 1 is applicable only if the transverse dimensions of the superconducting wire are small enough to ensure a uniform current density—in other words, for transverse dimensions less than the penetration depth mentioned earlier.

To gain physical understanding of this inductance we consider a simple model of the superfluid component of superconductors. The charge carriers are "superconducting electrons" with mass m, charge e, and number density n, all moving with velocity v_s. They have a kinetic energy $(1/2)\,nmv_s^2(l/A)$. Equating the inductive energy $(1/2)L_s i^2$ to the kinetic energy and using the usual expression for the current, $i = nev_sA$, we obtain:

$$L_s = \frac{m}{ne^2}\frac{l}{A} \qquad (2)$$

Detailed analysis shows that this expression for L_s is the low-frequency limit of the more general expression in equation 1. From this simple derivation, however, we see that energy is stored in a superconductor in the form of kinetic energy of superconducting electrons. The inductance L_s, which we now call the *kinetic inductance*, is a manifestation of this energy storage. Thus superconductivity does not simply refer to a large conductivity; it refers to a large *imaginary* conductivity, which may be alternatively described as a kinetic inductance. Of course, any superconductor will also have magnetic inductance (determined by the detailed geometry), which must be added to L_s.

A piece of superconducting wire in a circuit can usually be described as having no resistance but finite magnetic and kinetic inductances. In fact the magnetic inductance numerically dominates the kinetic inductance in most situations. The kinetic inductance dominates only in conductors of very small cross-sectional area (it is proportional to $1/A$) and in Josephson junctions, both of which are important in microelectronics.

Before turning to the subject of Josephson junctions we will extend our description of superconductivity by discussing magnetic flux quantization. From a conceptual point of view the original flux quantization experiments and their interpretation are the critical link between the classical superconductivity of Kamerlingh Onnes (1911) and the modern superconductivity epitomized by Josephson's theory (1962).

Magnetic flux quantization

Imagine taking a circular ring of superconductor, initially at a temperature above its transition temperature

T_c, and applying a magnetic field perpendicular to the plane of the ring. Then cool the ring below T_c and remove the externally applied field. Because of Faraday's Law and the perfect conductivity of the ring, a permanently "trapped" maghetic field will exist in the hole of the superconductor. This field is produced by a permanently circulating supercurrent around the ring.

The classical (pre-quantum) analysis of this experiment predicts that the magnitude of the trapped flux should be proportional to the strength of the applied magnetic field; however, in 1950 Fritz London predicted a different result, based on quantum theory. Because the microscopic theory of superconductivity had not been developed at that time, his argument was heuristic in nature.

He postulated that superconductivity was the result of a "condensation" in momentum space such that the motion of the superfluid could be described by a single mean-value momentum vector. With this simplification the properties of the superfluid were then assumed to be the same as those of a typical single particle of mass m, charge q, and velocity $\mathbf{v}_s$. The momentum of this particle in a magnetic field of vector potential A is

$$\hbar\mathbf{k} = m\mathbf{v}_s + q\mathbf{A} \qquad (3)$$

in SI units. The wave function of the superfluid was taken to be of constant amplitude throughout the superconductor but of variable phase. We denote the wave function as $\Psi = |\Psi|e^{i\theta(r)}$ with the phase $\theta(r) = kr$.

London noted that if one considers the phase of the wave function at points along a circular path P inside a ring, as in figure 3a, then the basic requirement that the wave function must be single valued at each point along P is a significant constraint. In particular the change in phase for a complete trip around P must be an integral multiple of 2π:

$$\oint_P \mathbf{k}\cdot d\mathbf{r} = 2\pi n, \quad n = 0,1,2,... \qquad (4)$$

(This equation is also used in the Bohr-Sommerfeld theory of the hydrogen atom.) If the path P is chosen well inside the superconductor, then $\mathbf{v}_s$ is zero everywhere along P, because supercurrent exists only in a thin surface layer of the ring, as mentioned earlier. Consequently, equations 3 and 4 together give

$$\hbar^{-1}\oint_P q\mathbf{A}\cdot d\mathbf{r} = 2\pi n \qquad (5)$$

Using the general result that the integral of A around a closed path is the flux Φ through the path, we finally obtain

$$\Phi = nh/q = n\phi_0 \qquad (6)$$

This result predicts that flux through the ring will be quantized in units of h/q. It was later shown that $q = 2e$ for a superconductor, rather than just e as London thought, so the quantum of magnetic flux is $\phi_0 \equiv h/2e = 2.07\times10^{-15}$ Wb.

The wave function for the superconductor with ten flux quanta through the ring is illustrated in figure 3b. It is a ten-turn helix on the surface of a torus. For a change of one flux quantum through the ring the number of turns of the helix must change by one.

In 1961, Bascom S. Deaver and William M. Fairbank, and R. Doll and M. Näbauer, showed experimentally that magnetic flux through superconducting rings was indeed quantized as discussed above. These experiments, combined with London's insightful theory, endowed superconductors with a new characteristic, a quantum phase factor for the macroscopic system. This abstract quality might well have fallen into obscurity had it not been for Josephson's discovery of the phase dependence of tunneling currents between superconductors. This discovery occurred about one year after the successful flux-quantization experiments, but apparently it was not stimulated by those experiments.[3] However, Josephson's ideas, in the hands of other physicists, rather quickly transformed the concept of magnetic flux quantization to one of practical importance.

Josephson junctions

Without Josephson junctions superconducting electronics would be of little interest. These junctions are the essential superconducting elements for producing power gain at high speed, a vital function in electronics.

Josephson junctions most commonly take the form of two thin films of superconducting metals separated by a very thin layer of insulator, as illustrated in figure 4a. Experimentally it is found that such devices will conduct electrical current with zero voltage drop across their terminals, as was first reported by Philip W. Anderson and John M. Rowell. Above some maximum level of current, called the critical current I_c (typically about 1 mA), voltage does appear across the terminals of the device.

The physical basis for this behavior derives from the fact that the wave function, which describes the properties of the superconductor, extends slightly beyond the surface of the metal. Thus, if the insulating layer separating the two superconductors of figure 4 is thin enough (about 1 nm), the wave functions of the two superconductors can overlap in space, and thereby physically couple the two systems. Under these circumstances an electrical current can pass through the insulator,

Microscopic theory

The current–voltage characteristic of a Josephson junction is a plot of the average current in a junction versus the applied voltage. It has two branches, which are conceptually separable and are derived from the components of the two-fluid model of a superconductor. In the microscopic theory of superconductivity, by John Bardeen, Leon Cooper and Robert Schrieffer, a superfluid current is described by paired electron states, or the flow of so-called "Cooper pairs." A normal fluid current is described by unpaired electrons, the so-called "quasiparticles." At $T = 0$ K all electrons are paired and there are no quasiparticles, if the superconductor is in thermodynamic equilibrium.

In the current–voltage characteristic shown above right we first consider the supercurrent, which is the current ranging from zero to a maximum value of I_c, all at zero voltage. For voltages greater than zero, but less than the energy-gap voltage V_g, the amplitude of the supercurrent is unchanged but it is rapidly oscillating, at 484 MHz/microvolt, and averages to zero. Thus the supercurrent does not contribute to the current–voltage characteristic for $V > 0$.

The remainder of the characteristic results from entirely different processes. Between $V = 0$ and V_g there is no mechanism for transporting direct current at $T = 0$ K, so the device behaves as an insulator. When the applied voltage reaches the energy-gap voltage, sufficient energy is available from the electric field to break pairs of electrons and produce a quasiparticle current. Thus the righthand portion of the characteristic is referred to as the "quasiparticle branch."

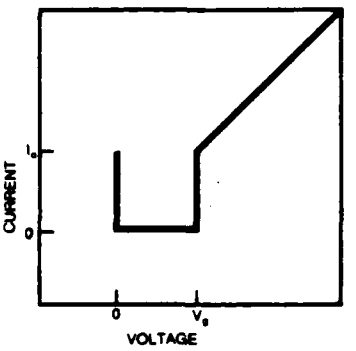

A number of complicating features are omitted from this brief discussion in order to emphasize the most important concepts. An actual current–voltage characteristic at $T = 4$ K is illustrated in figure 6a.

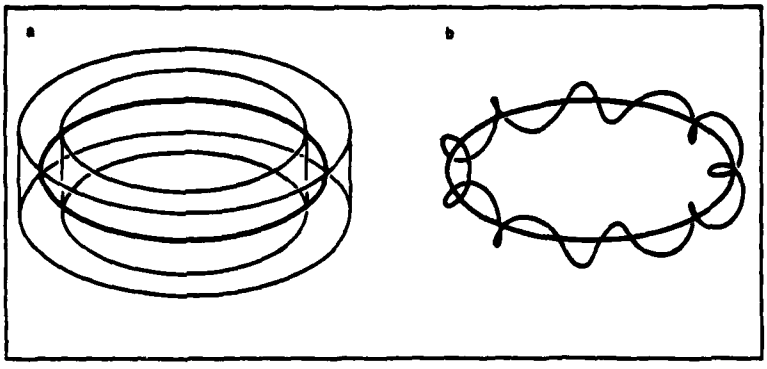

Superconducting ring (part a), with the path of integration (called P in the text) shown in color. Part b shows the wave function describing the system when ten flux quanta are trapped in the ring. Allowed states must have an integral number of wavelengths around P. Figure 3

by the mechanism of quantum-mechanical tunneling, even though the insulator is not a conductor in the classical sense.

Josephson's discovery was not the discovery of tunneling between superconductors, which had already been observed by Giaever, but rather the theoretical prediction that a supercurrent could tunnel through an insulating barrier. According to the theory of superconductivity a supercurrent is a flow of paired electrons. The conventional wisdom prior to Josephson was that the correlated tunneling of a pair of electrons would be a process of very low statistical probability and, therefore, unobservable. Josephson showed that due to the special properties of the superconducting state, pair tunneling has essentially the same probability as single-particle tunneling.

The practical description of the tunneling supercurrent is in terms of two simple equations. These equations both involve θ', the difference in phase from one side of the tunneling barrier to the other, of the macroscopic wavefunction first introduced in the discussion of magnetic flux quantization. The equations are:

$$\frac{d\theta'}{dt} = \frac{2e}{\hbar} V(t) \tag{7}$$

and

$$I_s = I_c \sin \theta' \tag{8}$$

Equation 7 says that the time rate of change of θ' is proportional to the instantaneous voltage across the tunneling barrier, with the proportionality constant being 484 MHz/microvolt. Equation 8 says that the tunneling supercurrent I_s is zero if θ' is zero and reaches a maximum value of I_c for $\theta' = \pi/2$.

In particular we note that these equations permit non-zero current with zero applied voltage. We also note that if $V(t)$ is a constant, other than zero, then θ' increases linearly in time and produces a sinusoidally oscillating current I_s. Further discussion of Josephson junctions is given in the box on page 39.

Just as we described superconductors in terms of an effective inductance, we find a similar description for Josephson junctions. Combining the elementary relationship $V = L_J\, dI_s/dt$ (where L_J is the inductance of a Josephson junction) with equations 7 and 8, we obtain

$$L_J = \frac{\phi_0}{2\pi I_c \cos \theta'} \tag{9}$$

We recognize that this is not a magnetic inductance, because it does not depend on geometry; it is the kinetic inductance of the superfluid in the Josephson junction.

From $\int I_s V\, dt$ the energy stored in L_J is found to be

$$E_J = -\frac{\phi_0 I_c}{2\pi} \cos \theta' \tag{10}$$

Equation 10 tells us that as the phase θ' changes, the energy stored in the Josephson junction is modulated between $\pm \phi_0 I_c/2\pi$. For a typical junction the modulated energy is approximately 10^{-18} J. From this property we should expect that superconducting electronics will be useful only if we are dealing with quantities of energy comparable to or smaller than this characteristic Josephson energy. Thus, superconducting electronics is intrinsically "low-power" electronics, but not impractically low.

For example, the thermodynamic fluctuation energy at room temperature is $kT \sim 4 \times 10^{-21}$ J, which is considerably smaller than the Josephson energy, and therefore not generally disruptive to superconducting electronic systems.

The Josephson inductance is important in determining the maximum speed of response of Josephson junctions. At very high frequencies the shunt capacitance of a junction electrically shorts L_J, which makes the junction ineffective in the circuit. The small size of L_J (about 0.3 pH), however, gives a sufficiently low impedance compared with the capacitive reactance that full Josephson responses[1] can occur on time scales as short as 2 picoseconds.

SQUIDs

In the experiments on magnetic flux quantization described earlier, the quantized state of the superconducting ring could be changed only by raising the temperature of the superconductor above its transition temperature, which is a time-consuming process. The invention of the superconducting quantum interference device (or "SQUID") by Robert C. Jaklevic, John Lambe, Arnold H. Silver, and James E. Mercereau in 1964 eliminated this require-

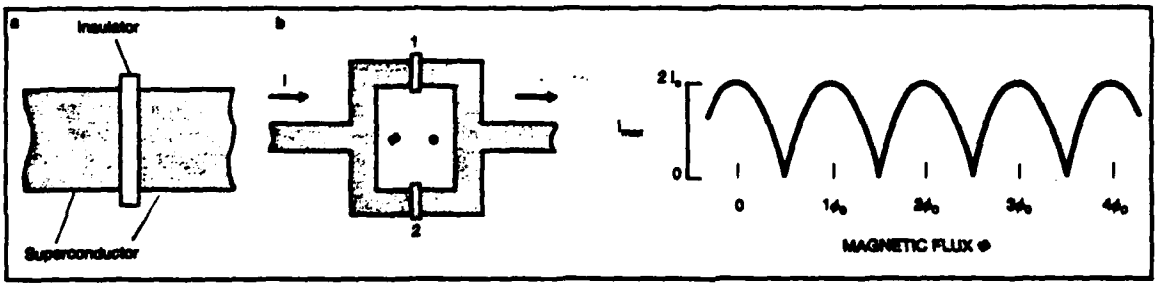

Josephson junction (a) and SQUID (b), shown very schematically. The SQUID consists of two Josephson junctions connected in parallel in a superconducting loop. Figure 4

The maximum current I_{max} that a SQUID will conduct, shown as a function of magnetic flux Φ through the SQUID loop, in the limit of small loop inductance. $I_{max} = 2I_c \cos|\pi\Phi/\phi_0|$. Figure 5

ment and also eliminated the need for a conventional magnetometer to sense the quantized state of the ring. In SQUIDs the quantized states are observed through a periodic dependence of their critical current on applied magnetic field, as we will discuss shortly.

The significance of SQUIDs resides primarily in the fact that they provide a practical means for utilizing magnetic flux quantization in a variety of applications. SQUID magnetometers, based on the theory and design of James E. Zimmerman and Silver, have been made with extremely high sensitivity—around 10^{-14} T. Although early work focused on this unique sensitivity, more recent developments for integrated circuit applications of SQUIDs, pioneered by Hans H. Zappe, emphasize high-speed operation of these devices—operation on a time scale of 10 to 100 ps.

A simple SQUID is illustrated in figure 4b. It consists of a superconducting loop interrupted by two Josephson junctions. In these devices the kinetic inductance of the junctions is made comparable to the magnetic inductance of the loop, so that the junctions have a major effect on the dynamics of the circuit.

If the junctions were not in the loop, that is, if the loop were just a continuous film of superconductor, then the magnetic flux inside the loop would be $\Phi = n\phi_0$, as in equation 6. The corresponding phase shift of the wavefunction around the loop in this case is

$$2\pi n = 2\pi(\Phi/\phi_0) \tag{11}$$

With Josephson junctions in the loop this last equation becomes

$$2\pi n = 2\pi(\Phi/\phi_0) + \theta'_1 - \theta'_2 \tag{12}$$

where θ'_1 and θ'_2 are the phase shifts across the respective Josephson junctions. The transport current I through the SQUID is given by the sum of the currents in the two junctions:

$$I = I_c(\sin\theta'_1 + \sin\theta'_2) \tag{13}$$

The maximum value that I can have under any circumstances is $2I_c$, corresponding to equal phase shifts of $\pi/2$ in each junction. This situation occurs for $\Phi = n = 0$, for example. With flux through the loop one junction will reach its critical current before the other if the *external current is increased*. The maximum current through the SQUID with zero voltage drop, I_{max}, occurs when either junction reaches its critical current. Combining equations 12 and 13 and solving for I_{max} yields the form of the essential character of SQUID response. The resulting pattern, shown graphically in figure 5, is often referred to as an "interference" pattern because of its similarity to optical interference patterns. The important result is that I_{max} is a *periodic function* of the flux through the SQUID, with a periodicity of ϕ_0.

The high sensitivity of SQUID magnetometers comes in part from the small value of ϕ_0, which means that the interference pattern provides a finely graded measuring scale for magnetic flux. Also important is the low noise level of the device, which allows a sensitivity many orders of magnitude greater than ϕ_0.

A fundamental way of analyzing the noise performance of a magnetometer is in terms of its energy sensitivity. The relevant quantity is $S_\Phi/2L$, where S_Φ is the spectral density of the square of the magnetic flux noise in the loop of the SQUID at low frequencies, and L is the inductance of the loop. In 1977, Claudia D. Tesche and John Clarke[4] predicted theoretically that a SQUID *should* achieve an energy sensitivity of approximately $h/2 = 3.3\times10^{-34}$ J/Hz. This value is very close to $\hbar$, which is the maximum energy sensitivity per Hz obtainable in any quantum-mechanical system, according to the Heisenberg uncertainty principle.

This theoretical prediction stimulated experiments in several laboratories beginning with a major advance to a sensitivity of 145 $\hbar$ by E. L. Hu *et al.* in 1978, a further advance by Mark B. Ketchen and Richard F. Voss to 5$\hbar$ in 1979, and culminating in two experiments[5] reaching very near $\hbar$ in 1980. The swiftness of these advances attests to the skill of the researchers and the innate qualities of superconducting methods. We believe that no other technology has produced a device of comparable sensitivity.

These impressive results should stimulate further refinement of the theory regarding ultimate practical limitations. In particular a theory is needed for the rising spectrum of $1/f$ noise, which dominates at frequencies below the tens of kHz range, where the maximum sensitivity is obtained.

Circuits

In the foregoing discussion we have described the elementary properties of the unique components of superconducting electronics: Josephson junctions and SQUIDs. The first applications of these devices were to magnetometers, radiation detectors and voltage standards. Very early however, in fact less than two years after Josephson's original publication, Rowell's patent application on logic and switching recognized the broader potential applications of Josephson junctions. In 1966 Juri Matisoo published the first experimental results with an emphasis on digital electronics. He reported measurements of the switching speed from the pure supercurrent branch to the quasiparticle branch of the current–voltage curve (see figure 6a). The high-speed switching that he observed (faster than 800 ps) stimulated a more extensive research effort, which has greatly enlarged the potential arena for applications of superconducting electronics.

We might reasonably ask what the ultimate functional scope of superconducting technology could be? In digital logic systems it is relatively easy to answer this question because a sufficient requirement for performing logic is the availability of the three functions of Boolean algebra—AND, OR and NOT—all of which have been implemented in superconducting technology. Extending this line of thought we might ask if *all of* the functional operations normally performed by electronics can also be performed by superconducting devices? Unfortunately we know of no rigorous way of answering this question but an intuitive and practical answer is that if components are available for detection, amplification, logic, and memory, then most general purpose circuits, both analog and digital, can be built.

In the table on page 42 we summarize the highlights of such basic developments. For each of the functional areas there has been a variety of developments but, for brevity, we describe only a single device or circuit in each area.

For detection we note that the device most widely used for this purpose in conventional electronics is the diode rectifier. The equivalent device in superconducting electronics is a detector biased on the quasiparticle nonlinearity of a tunnel junction's current–voltage characteristic (see the box on page 39). This device has reached its highest development in the reference given in the table. The quoted responsivity corresponds to 0.52 electrons in the output of the device for each incident photon. Thus the practical device is within a factor of two of the so-called quantum limit of one electron per photon. (One electron per photon is believed to be the maximum output a tunneling device can have.) In addition to a good quantum efficiency, the noise-equivalent power given in the table is the lowest ever published for a microwave video detector. Thus, measured against other practical devices, the performance is excellent. It is nevertheless clear that the noise performance can still be considerably improved with already developed fabrication methods that reduce the leakage current.

Although the research efforts for detectors are at microwave frequencies and above, in general electronics one is usually interested in lower-frequency detectors. Device theory says that the responsivity will be essentially the same at audio frequencies, for example,

so we view this video detector as a general-purpose device.

Moving on to amplification, we ask what superconducting device is most nearly equivalent to the conventional transistor? A SQUID amplifier, shown schematically in the table, plays this role. This is the same basic circuit as a SQUID magnetometer. As discussed earlier the recent trend in research on SQUID magnetometers has focused on their energy sensitivity, which implicitly recognizes that they have power gain, although they have not generally been viewed in this light. The SQUIDs designed for maximum energy sensitivity, which we discussed as magnetometers, have not had an efficiently coupled input coil. In Michael Cromar and Pasquale Carelli's work cited in the table, however, a highly sensitive SQUID was tightly coupled to a relatively large-size but low-inductance input coil, giving an energy sensitivity of around $71\hbar$ and a power gain as listed in the table. This was an important step forward, but considerably more development is needed (related primarily to bandwidth and dynamic range of operation) before SQUIDs can routinely be used as amplifiers.

The next function of interest is logic. Logic and memory circuits are the main products of the commercial integrated circuit industry, so it is not surprising that these functions have received far more study and development than the preceding two functions.

Josephson junctions in binary logic circuits act as threshold detectors. The threshold condition for switching the circuit is that the sum of the two input currents must exceed the Josephson junction critical current. Figure 6 illustrates the simplest implementation of a logic function. As might be expected the more sophisticated implementation of superconducting logic involves more complex circuits, but the basic threshold switching idea remains.

The leading developments in this field have been by the groups at IBM Research Laboratories and at Bell Telephone Laboratories. Through the years these groups have devised a number of distinct approaches to logic circuits. However, at the present time

Highlights of developments in superconducting electronics

FUNCTION	SCHEMATIC	PHYSICAL MECHANISM	NOTES
Detection	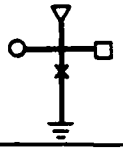	Rectification by the quasiparticle nonlinearity.	Measured current responsivity[a] of 3500 amps of output current per watt of input power at 36 GHz. Noise equivalent power = $2.6 \pm 0.8 \times 10^{-16}$ W/Hz$^{1/2}$
Amplification	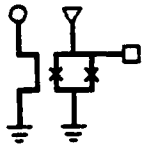	Magnetic modulation of the SQUID critical current by the input signal.	The energy sensitivities per unit bandwidth of SQUID amplifiers are approaching the quantum-mechanical limit for this quantity (at audio frequencies). Power gains of the order of 6×10^6 have been achieved in single devices.[b]
Logic	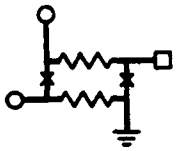	Switching produced by drive currents exceeding the junction critical current.	The fastest superconducting logic produced so far is a two-input OR gate with a switching delay of 13 ps when fabricated with 2.5-micron linewidth lithography.[c] Designs emphasizing simplicity of fabrication and improved miniaturization properties yield an estimated 40 ps switching delay for fully loaded circuits.[d,e] The power dissipation per gate is about 3 microwatts. These circuits provide a basis for a computer with a 2 nanosec logic cycle time.[f]
Memory	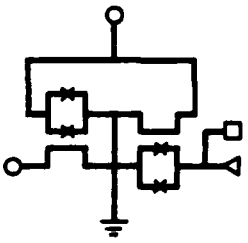	Information stored by flux trapping in the large superconducting loop.	Memory compatible with the above high-speed logic utilizes the quantized flux state of a superconductor. Two flux quanta are inserted for a 1 and no quanta for a 0. In present design work a one-bit memory cell is expected to have a current transfer time of about 35 ps (time to go from a to b in figure 7) when fabricated with 2.5-micron minimum linewidths. Overall memory access time for reading one bit is no more than about 500 ps on a 4K-bit chip having 6 mW of dissipation per chip.[g]
		Symbols used in the schematics are: ○ input terminal ▽ bias terminal □ output terminal X Josephson junction	

References

a. P. L. Richards, T. M. Shen, R. E. Harris, F. L. Lloyd, Appl. Phys. Lett. 36, 480 (1980).
b. M. W. Cromar, P. Carelli, Appl. Phys. Lett. (to be published). Also see J. M. Jaycox, M. B. Ketchen, Proc. 1980 Applied Spectroscopy Conference, to be published in IEEE Transactions on Magnetics.
c. T. R. Ghiswala, IEEE J. Solid-State Circuits SC-14, 767 (1979).
d. T. A. Fulton, S. S. Pei, L. N. Dunkleburger, Appl. Phys. Lett. 34, 709 (1979).
e. T. R. Ghiswala, A. Mukherjee, Int. Electron Devices Meeting, Washington, D. C. (1979).
f. W. Anacker, IBM J. Res. Develop. 24, 107 (1980).
g. S. M. Faris, W. H. Henkels, E. A. Valassakis, H. H. Zappe, IBM J. Res. Develop. 24, 143 (1980).

there is a convergence of approaches that have considerable similarity. The latest results are summarized in the table. The schematic shown there for logic (and also for memory) is a simplification of the actual circuit.

Finally we turn to the memory function. We will briefly discuss only the present form of the highest speed random-access memory (cache memory) that is being developed as large-scale integrated circuits. The storage of binary information is conveniently accomplished with the flux-trapping phenomena discussed earlier. Two features of this form of information storage are the zero power dissipation in memory when no reading or writing is occurring and the fact that it is "nonvolatile," which means that the stored information is not lost if the computer is turned off. In addition it operates at sufficient speed to be compatible with the very high-speed Josephson logic circuits. Some details of memory-cell operation are described in figure 7.

In the table we have identified the unique physical mechanism used in each of the functional areas. Because the mechanisms are different in each case we begin to get a feeling for the richness of phenomena available in superconductivity. The practical importance of these effects becomes clear when we note that in all four functional areas superconducting electronics has extraordinary performance, in fact performance beyond that of any other technology.

To appreciate the broader picture more fully, however, we must briefly take up one additional topic: miniaturization in electronics. This topic is put in perspective by the present situation in commercial electronics, in which circuit power dissipation is seen to be of major importance. The highest-speed large-scale computer of today has 400 000 logic gates. To avoid overheating in this system there are only two gates in each integrated circuit package; so there are 200 000 separate integrated circuits for logic. Compare this situation with the other extreme of miniaturization, which is a microprocessor with about 20 000 logic gates in a single miniature package. To make a microprocessor system roughly comparable in complexity to the high-performance logic unit would require 20 microprocessors or just 20 integrated circuits. (The emphasis here is on a crude comparison of levels of integration; no suggestion is intended that it is practical to interconnect 20 microprocessors for the required logic of the large computer.) The cost of these 20 circuits is only a few thousand dollars, whereas the cost of the higher-performance logic system is on the scale of millions of dollars. To a significant degree this difference comes from differences in costs of packaging and assembling a miniaturized system as compared with one that could not be miniaturized because of high power dissipation. Part of the cost difference also arises from the volume of production, which favors microprocessor technology over that for high-speed logic systems. It is fully expected that there will be reductions in the power requirements for semiconductor logic in the future. On the other hand, as computers get faster there is a natural need for increased memory size, which produces increasing problems of power dissipation.

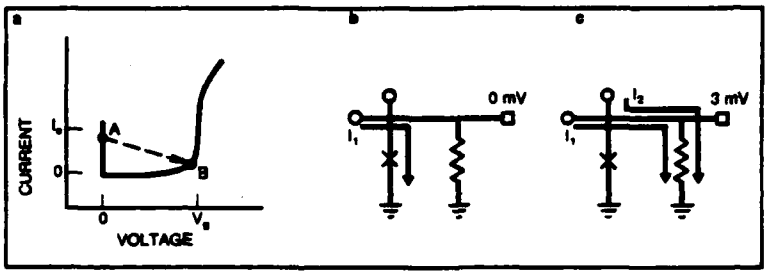

Switching of a simple AND gate. Initially only one current I_1 is present. It has a magnitude less than I_c; also the Josephson junction is a state A of the current-voltage characteristic shown in part a. The path of this current in the AND circuit, shown in color in part b, is entirely through the junction, and the result is a zero voltage output. If a second current, I_2, of comparable magnitude is also applied, the critical current of the junction is exceeded and it switches to the energy gap voltage V_g. In this situation the current in the junction after switching depends on the value of the load resistance. If the resistance is properly selected the junction will switch to point B of the characteristic (a), where the junction current is much less than in the zero voltage state. Thus, to a good approximation, both input currents are directed to the load resistance, as in part c, resulting in a 3-mV output. The circuit is reset to zero voltage by reducing I_1 and I_2 to zero. Figure 6

One of the virtues of superconducting technology is that it achieves high speed without high power dissipation in either logic or memory. In fact, the speed of superconducting technology exceeds the speed of the fastest conventional technology and simultaneously dissipates orders of magnitudes less power.[6] Thus the principal barrier to miniaturization of high-speed electronics is eliminated in this technology. In what follows we will consider the physical reasons for this performance.

Basis for performance

Is it simply an accident that superconducting electronics has outstanding performance in *all four* of the functional areas of electronics, or is there a basic reason why this should be so? We might say that superconductivity is the reason for the good performance, but that would be a rather nebulous response because superconductivity has many facets. The role of superconductivity in superconducting electronics is to provide the physical mechanism for making things happen. The specific question we will address is why does it work so well? To discuss this question we will examine the features of the technology that are of the greatest practical importance, namely the low power dissipation, the high speed, the high sensitivity and the low noise.

Detection, amplification, logic and memory all utilize nonlinearities for their practical realization. By nonlinearity we mean a nonlinear relation between an input parameter and an output parameter. The simplest case is for a two-terminal device in which there is a nonlinear relation between the input current and the resulting voltage, as in a Josephson junction.

The fact that the nonlinearities of superconducting devices occur at very low energy, generally below 5 meV, is of fundamental practical importance, producing both low power dissipation and, to a substantial extent, the high speed of these devices. It is important to recognize that such low-energy nonlinearities are effective only at low temperatures.

Electrons in solids have fluctuations in their energies of the order of a few kT. If this fluctuation energy is substantially greater than the range of energy over which a nonlinearity exists, then the nonlinearity will in effect be averaged out by the fluctuations. A basic requirement for a nonlinearity to be physically effective with a change in terminal voltage from zero to V is that eV should not be less than kT. (As an example note that the large quasiparticle nonlinearity in a Josephson junction occurs over an energy range around 8 kT for $T = 4$K). This relationship is a restriction on the minimum voltage at which an electronic technology can operate and, consequently, sets the scale for power dissipation.[7] For devices with the same impedance but operating at different temperatures T_1 and T_2, the ratio of the *minimum* power dissipations is

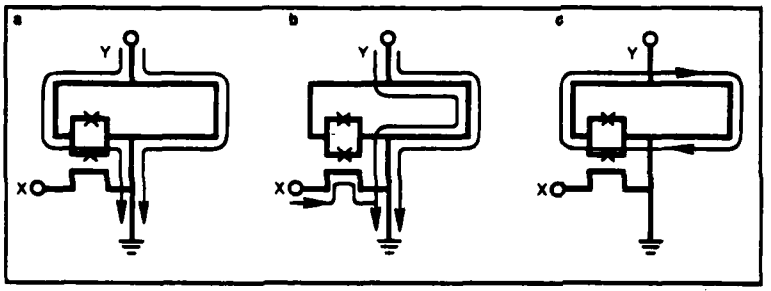

Operation of a memory cell consisting of a superconducting loop with an inserted SQUID. If flux is trapped in the loop it is interpreted as "1," and the absence of trapped flux is a "0." Consider the writing of a 1 in a cell initially in the 0 state. The writing sequence begins with the application of a Y current as shown in part a. This current naturally divides itself between the two sides of the superconducting loop according to their relative inductances. The current in the SQUID in the left-hand branch of the main loop is arranged to be less than the SQUID critical current. Next, an X current is applied. It is inductively coupled to the SQUID and reduces the SQUID's critical current below the level of the applied Y current. This causes the SQUID to switch temporarily to the voltage state, which diverts its current to the other side of the loop, as in b. If the X and Y currents are now turned off, a persistent current is established in the loop as shown in c, resulting in a 1 state. Reading of the 0 or 1 states is done with a nearby second SQUID on the right-hand side of the memory cell (see table, page 42), which simply detects whether or not there is flux in the loop. Figure 7

$P_1/P_2 = (V_1/V_2)^2 = (T_1/T_2)^2$. According to this formula a reduction in power dissipation by a factor of about 5000 is achievable on going from 300K to 4 K, if optimal devices are used in both cases.

Lower power dissipation implies less heating of the substrate, the importance of which has already been emphasized. To complete this argument one must also consider heat transfer from the substrate to the surrounding medium as Robert Keyes[7] has done. This process is about a factor of 20 less favorable at low temperatures, so the effective decrease in power dissipation is about a factor of 250 rather than 5000. Nevertheless it remains an important factor for electronics, and it illustrates the importance of a low-temperature environment.

A primitive model for the speed of typical electronic devices reveals how low-energy nonlinearities also contribute to higher-speed operation. Consider a model in which the terminals of a device must make an excursion in voltage across its intrinsic nonlinearity. The time that this will take is given approximately by CV/i, where C is the capacitance between the output terminals, V is the necessary voltage change, and i is the current available to drive the change in voltage.

In superconducting devices the voltage change is typically 3 mV. For contrast we note that for room-temperature devices, even in unsaturated semiconductor logic, the corresponding voltage is about 600 mV. Thus, low-voltage operation gives an intrinsic speed advantage to superconducting devices. Such operation is possible only at low temperatures.

The high sensitivity of SQUID magnetometers depends upon the small size of the flux quantum. As we have already discussed, flux quantization is a manifestation of a coherent quantum-mechanical state extending over macroscopic distances. Superconductivity is not the only such state. The coherence of lasers and the long-range order of magnetic materials may be similarly described.[8] Thus we cannot assert that a low-temperature environment is required for a macroscopic quantum state. What we can assert is that a low temperature is required for the observation and use of macroscopic quantum states with small spacings between energy levels. It is the small energy spacing between the quantized flux states (or actually the small barrier between states) that produces the high sensitivity of SQUIDs. An additional factor is the low noise level of Josephson junctions. There is nothing conceptually extraordinary about the noise in Josephson junctions; both the usual Johnson noise and electronic shot noise are present as in other devices. But of course the low-temperature environment reduces the Johnson noise by a factor of 100 below that of ambient temperature devices. Thus we find that both factors responsible for the high sensitivity of SQUIDs are in fact made possible by the low-temperature environment in which they operate.

We conclude that the basis for the good performance of superconducting electronics in the four functional areas is primarily the low temperature of operation.

Future prospects

Superconducting electronics should be viewed as a technology potentially applicable to any critical instrumentation problem that requires the highest possible performance in either speed or sensitivity. Considering the sophisticated and relatively mature development of conventional electronics, we should all be impressed with the result that superconducting technology, even in its present immature form, has the best performance in the most fundamental areas of both analog and digital electronics.

We have attributed the good performance of this technology to its low-temperature operation. On this basis it seems likely that if superconducting electronics is optimally implemented then no ambient temperature technology will give comparable performance. A critical question, however, is: How closely can ambient temperature circuits approach the performance of superconducting circuits? No one knows what the ultimate answer will be because both technologies are still advancing. A related question is: Can the performance of other electronic technologies be greatly improved by cooling? This is a complex issue to discuss, but Keyes[7] has addressed the question for electronics based on semiconductors and on magnetic and optical materials. His general conclusion is that reduced operating temperatures are beneficial in many ways. Whether the performance of these systems can be made comparable to that of superconducting electronics remains an open question.

Perhaps foremost among the practical questions about superconducting integrated circuits are those relating to reliability of fabrication processes and durability of the devices after fabrication. There is a tendency for the very thin tunneling barriers in Josephson junctions to change with time when stored at room temperature and a tendency for the mechanical stresses of temperature cycling to 4 K to cause electrical changes in junctions. Most of the circuits discussed here were made of lead-alloy superconductors. The successful fabrication and operation of a 2048-bit main memory development chip was the most severe test of these methods thus far.[9] Competing with lead-alloy circuits are more recent developments with niobium. A report on junctions with niobium base electrodes and lead-alloy counter electrodes[10] gives failure probabilities of less than 2×10^{-6} failures per Josephson junction per thermal cycle to 4 K. Advances in this area look promising.

Another problem, unique to this technology, is magnetic flux trapping at inhomogeneities in the superconducting films. Such flux can greatly alter the performance of superconducting circuits. Flux trapping occurs spontaneously as superconductors are

cooled in a magnetic field, even in very small fields. It can also be produced by thermal gradients that develop as the circuits are being cooled to 4 K. Efforts are underway to solve this problem.

Miniaturization, which is of great importance for integrated circuits, poses interesting questions. Superconducting circuits are presently being developed mostly with 2.5-micron minimum linewidth lithography, much the same as commercial semiconductor circuits. As the linewidth is reduced, performance is expected to improve significantly[11]. However, as the geometry becomes sufficiently small (films about a tenth of a micron thick), new effects become significant. The basic description of Josephson tunnel junctions is not expected to change but the kinetic inductance of the circuit external to the junctions will become increasingly significant—both in transmission lines and in SQUIDs. Physically this means that energy storage in SQUIDs, for example, shifts away from magnetic energy toward kinetic energy of the electrons. How important this will be has not been worked out.

When devices are made smaller there will be a tendency to want an increase in the junction critical current density so as to maintain the Josephson coupling energy and ensure stability against thermal fluctuations. Increased current density increases the importance of nonequilibrium between the quasiparticle and pair distributions. The effect of nonequilibrium on device performance has not been quantitatively explored. It is perhaps most interesting for noise performance.

Of course semiconductor technology also encounters new problems with increased miniaturization. A specific area where miniaturization decidedly favors superconductivity is in the properties of the microstrip transmission lines that interconnect high-speed devices. Richard L. Kautz[12] has shown that, within the context of high-density integrated circuits, further miniaturization of normal metal lines will produce poor transmission properties for pulses having widths of 100 ps or less. The superior properties of superconducting transmission lines may be of decisive importance in the competition between very high speed technologies.

For large-scale integrated circuits the prospects for superconductivity are sufficiently promising that the design of prototype superconducting computers is underway. Matisoo has recently summarized this work.[13] There are reasonable prospects for a superconducting machine about fifty times faster than the general-purpose machines of today.

Many opportunities for further developments exist in analog superconducting electronics, but the importance of these developments is more difficult to summarize because the possibilities are so varied. We will therefore focus somewhat arbitrarily on the interface between analog and digital circuits, that is, on analog-to-digital converters, which are circuits of technological importance in many areas of work.

In figure 2 we illustrate an advanced superconducting analog-to-digital converter design that emphasizes high-speed performance. Equally important is the development of designs for high-accuracy converters. The precision of the best commercially available devices is limited by the instability of their semiconductor based voltage references, which is a few parts in 10^6. In superconducting technology one can use the Josephson voltage reference, initially developed by Donald N. Langenberg, William H. Parker and Barry N. Taylor, which is known to be at least a factor of 100 better than its semiconductor counterpart. If this reference is combined with a superconducting current comparator and the necessary digital circuitry, the resulting analog-to-digital converter can have the same precision as the Josephson voltage reference. Thus an improvement by a factor of 100 over conventional technology is feasible, but as physicists are prone to say, the engineering details have not been worked out.

What is perhaps more fascinating to physicists is that the maximum achievable precision of the Josephson voltage reference is simply unknown. This is significant not only for the physics involved but also for practical reasons as well. Measurement systems of the highest precision commonly operate on the basis of observing changes between a reference level and the quantity of interest. Thus an improved reference would allow one to observe physical effects that are presently unobservable, in phenomena as varied as solid-state physics and geophysics, for example.

Recent work by Kautz[14] on the Josephson voltage reference is notable in this connection. He showed that the basic mechanism of phase lock between the Josephson self-oscillation and the external drive-oscillator can be maintained without a significant break for at least six hours at a frequency of 25 GHz, which corresponds to 5×10^{14} continuous cycles. This experimental work, combined with the accompanying theory, suggests that essentially perfect phase lock is achievable with a Josephson junction. This in turn implies that, barring the intervention of other effects, it should be possible to define voltage as precisely as frequency, the most accurately measurable physical quantity. The real problem that remains is the possible "other effects." No such effects have been identified, although there is evidence[15] that thermodynamic nonequilibrium processes may necessitate a correction factor for the Josephson voltage reference.

It is clear that basic SQUID systems are still not adequately understood and should be more thoroughly explored. The status of the most sensitive energy detector is unique and of fundamental importance to experimental science. Within the framework of Claude Shannon's celebrated ideas for information transfer one should recognize that the most sensitive energy detectors are also the most sensitive *information* detectors. Thus, since information is the goal of all experiments, it is clear that the most critical experiments of all kinds should incorporate these new SQUIDs when applicable.

Over what bandwidth can SQUIDs be made the most sensitive detectors? How should direct feedback (without conventional electronics) around the SQUID be used? No one knows. In fact these questions lead us to mention recent work in which it was shown that a superconducting heterodyne mixer, operating at 36 GHz, can very nearly detect a single photon.[16] This is a second area where superconducting electronics closely approaches a fundamental limit for measurements. Since this work was done with a Josephson junction (which is thought of as an electric-field detector) and not a SQUID (which is thought of as a magnetic-field detector), it raises the interesting problem of determining the best spectral region for using SQUIDs and for using Josephson junctions as sensors. No definitive answer can be given yet.

In concluding this discussion it is fitting to broaden the perspective and to consider the development of electronics from a more philosophical point of view. I shall ignore such technical details as the different materials used in producing electronics devices and consider somewhat more generally what is happening in electronics. Since the 1950's conventional electronics has progressed dramatically, largely by advances in miniaturization, which has many ramifications but which we describe only as a major change in the dimensional length scale of devices and circuits. Because this change was so useful it suggests that one should consider other radical shifts in the primitive physical variables of electronics. The two radical changes that have been most extensively studied in the last two decades are changes in frequency and in temperature. The shift in frequency, to the optical region, has resulted in fiber optics and associated optical circuits, for which the main broad application appears to be communications over medium and long distances. On the other hand the shift in temperature

to the cryogenic regime has led to superconducting electronics, a technology best adapted to the microscale world of miniaturized integrated circuits. Thus the major radical alternatives to conventional electronics are seen to be functionally complementary. Maybe at some time in the future these radical technologies will be joined.

But regardless of the course that future commercial technology takes, it should be abundantly clear that superconducting electronics presents a demanding challenge to the technology of semiconductors. It is reasonable to claim, at least for the foreseeable future, that superconducting electronics will be the pre-eminent technology for high performance—for high speed, for high precision, and for high sensitivity.

References

1. For a review with emphasis on high-speed measurements, see D. G. McDonald, R. L. Peterson, C. A. Hamilton, R. E. Harris, R. L. Kautz, IEEE Trans. Electron Devices, ED-27, 1945 (1980).
2. J. H. Greiner, C. J. Kircher, S. P. Klepner, S. K. Lahiri, A. J. Warnecke, S. Basavaiah, E. T. Yen, John M. Baker, P. R. Brosious, H.-C. W. Huang, M. Murakami, I. Ames, IBM J. Res. Develop. 24, 195 (1980).
3. B. D. Josephson, Science 184, 527 (1974).
4. C. D. Tesche, J. Clarke, J. Low Temp. Physics 29, 301 (1977).
5. R. F. Voss, R. B. Laibowitz, M. B. Ketchen, A. N. Broers, Conference Digest, Second International Conference on Superconducting Quantum Devices, Berlin, May 1980, page 94; M. W. Cromar, P. Carelli (to be published in Appl. Phys. Lett.).
6. T. R. Gheewala, IEEE Trans. Electron Devices, ED-27, 1857 (1980).
7. R. W. Keyes, Proc. IEEE 63, 740 (1975).
8. M. O. Scully, in *Coherence and Quantum Optics* (L. Mandel, E. Wolf, eds.) Plenum, New York (1973); page 69.
9. R. F. Broom, P. Gueret, W. Kotyczka, Th. O. Mohr, A. Moser, A. Oosenbrug, P. Wolf, IEEE J. Solid-State Circuits, SC-14, 690 (1979).
10. R. F. Broom, S. I. Raider, A. Oosenbrug, R. E. Drake, W. Walter, IEEE Trans. Electron Devices, ED-27, 1996 (1980).
11. H. H. Zappe, Proceedings of NSF Workshop on Opportunities for Microstructure Science, Engineering and Technology, Arlie, Va. (1975); page 209.
12. R. L. Kautz, J. Research NBS 84, 247 (1979).
13. J. Matisoo, Scientific American, May 1980, page 50.
14. R. L. Kautz, Appl. Phys. Lett. 36, 386 (1980).
15. J. Clarke, M. Tinkham, Phys. Rev. Lett. 44, 106 (1980).
16. T. M. Shen, P. L. Richards, R. E. Harris, F. L. Lloyd, Appl. Phys. Lett. 36, 777 (1980); see also PHYSICS TODAY, August 1980, page 19. □

DESIGN LIMITATIONS FOR SUPERCONDUCTING A/D CONVERTERS

C. A. Hamilton and Frances L. Lloyd

Abstract - This paper reviews the principle of A/D conversion using superconducting quantum interference and describes the results obtained with this technique. At an accuracy of four or six bits the design of such converters is straightforward. Higher accuracy requires careful consideration of numerous design constraints including critical current uncertainty, power supply regulation, turn-on-delay, signal line crosstalk, and the threshold curve critical points. The implications of these constraints are analyzed with respect to an example design for an 8-bit converter.

INTRODUCTION

DC SQUIDs (Superconducting QUantum Interference Device) are being extensively developed for use as logic gates in digital computers. A characteristic of these devices, which is not used in the computer application, is the periodic dependence of their switching threshold on an input control current. This periodicity offers a unique method for using a set of dc SQUIDs to perform A/D conversion [1,2,3]. Figure 1 outlines the basis of this method.

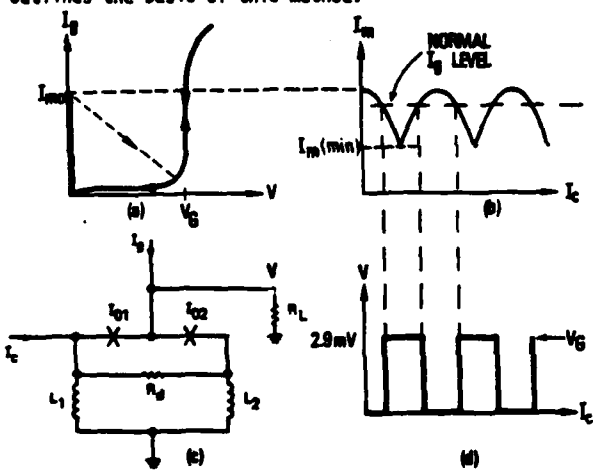

Fig. 1(a). The I-V curve of a double junction SQUID, (b) the dependence of the critical current I_m on a control current I_c, (c) the circuit diagram of a SQUID, and (d) the input-output characteristic of a SQUID comparator.

The circuit for a dc SQUID is shown in Fig. 1(c). The X's represent Josephson tunnel junctions with their attendant shunt capacitance. Since this device is basically two junctions in parallel, it has an I vs. V curve which, as shown in Fig. 1(a), is like that of a single Josephson tunnel junction. For currents below the maximum threshold current, I_{mo}, the device has zero voltage drop. When I_{mo} is exceeded, the SQUID switches very rapidly (~30 ps depending on overdrive) along the load line to the energy gap voltage (V_G = 2.9 mV). Quantum interference of the superconducting phase around the SQUID loop causes the threshold current I_m to have a periodic dependence on the magnetic flux through the SQUID loop. This is shown in Fig. 1(b) which plots the threshold current I_m versus a control current I_c which is directly injected through the SQUID inductance L_1. The curve repeats each time the injected current induces an additional flux quantum (ϕ_o = 2.07 x 10^{-15} Webers) into the SQUID loop. The periodicity ΔI_c is thus given by $\Delta I_c = \phi_o/L_1$. By applying a signal, I_c, to the control input and pulsing the SQUID current I_q to the level shown by the dotted line in Fig. 1(b) one obtains the input-output characteristic of Fig. 1(d). The SQUID can thus be used as a comparator whose digital output is a periodic function of its analog input I_c. This is exactly the property required in an A/D converter. To see why this is true we have listed, in Table I, A/D converter output codes in both binary and Gray code as a function of the analog signal input. It can be readily seen from this table that each digital output (e.g. the LSB - least significant bit) is a periodic function of the signal input with the period changing by a factor of two from one bit to the next. This is true in both binary and Gray code. Gray code has the advantage that only one bit changes as the signal passes through each quantizing threshold.

Analog Signal	Binary Code	Gray Code
0	000	000
1	001	001
2	010	011
3	011	010
4	100	110
5	101	111
6	110	101
7	111	100

Table I. Digital output codes of an A/D converter as a function of signal input.

Figure 2(a) is the circuit diagram for a 6-bit converter using this idea. The required variation in periodicity is achieved by using a resistor ladder to divide the input signal by a factor of two for each successive SQUID. The resulting set of binary weighted signal currents are injected into six identical SQUIDs. Another variation of this circuit uses a magnetically coupled signal with variable mutual inductance to achieve the binary ratios [2,3].

When a conversion is to be made, a pulse is applied to the power supply line so that all six SQUIDs are biased to the level shown in Fig. 1(b). Each SQUID for which this bias level exceeds the threshold curve will switch to the voltage state producing a 2.9 mV pulse on its output line. These pulses are a digital representation of the analog signal. For continuous operation the supply line is driven by a pulse train or at the highest speeds by an offset (monopolar) sine wave. This A/D converter operates in a fully parallel fashion and requires only one SQUID comparator for each bit of accuracy. Figure 2(b) is a photograph of the circuit.

Manuscript received March 23, 1981.
Supported by the U. S. Office of Naval Research under contract number N00014-80-F-0012.
C. A. Hamilton and Frances L. Lloyd are with the National Bureau of Standards, Electromagnetic Technology Division, Boulder, Colorado 80303 U.S.A.

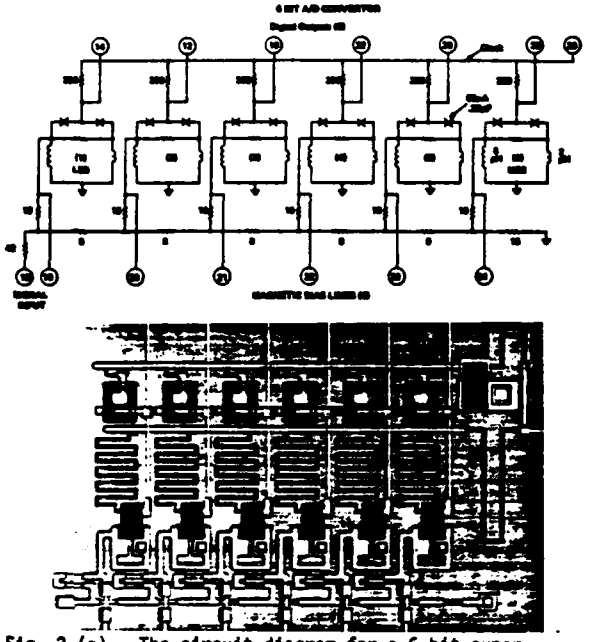

Fig. 2 (a). The circuit diagram for a 6-bit superconducting A/D converter and (b) a photo of the circuit. Minimum linewidth is 5 μm.

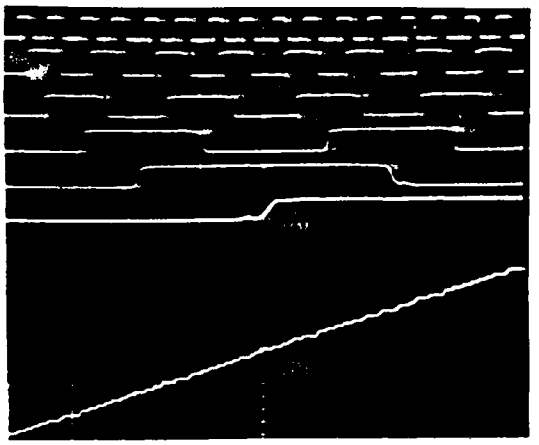

Fig. 3 (A). The six digital outputs as a function of signal input, and (B) the analog value of the output as a function of the signal (staircase function).

Fig. 4. The digital output data on one of the six output lines as a function of time. Sixteen successive samples are shown.

Experimental Results

Figure 3(a) shows the 6 bit patterns as a function of analog signal level. Note that the output is in Gray code so that perfect alignment of the threshold levels is not required. In Fig. 3(b) the Gray code is converted back to an analog signal. The monotonic staircase verifies that the resolution of the converter is ± 1 LSB.

Crosstalk between the chip leads causes considerable difficulty in testing this device at very high speed. For this reason a mount has been designed in which the pads on the chip are pressed against the ends of 8 coplanar striplines which are etched on G-10 circuit board. Six millimeters away from the chip each stripline pair converts to 50 ohm coax. The coax shields are tied together only at the superconducting ground plane on the chip. Capacitive crosstalk is minimized by maintaining sufficient space between the striplines and other metal parts of the sample holder.

The maximum operating frequency of the present converter design is 4 GHz. We are currently not able to fully verify the operation of the converter at this rate. However, by synchronizing a signal waveform with the 4 GHz power supply, it is possible to use a sampling oscilloscope to observe the digital data on the output lines. Figure 4 shows the data on one of the six output lines for 16 successive samples of a 4 *ns* wide signal ramp. It is clear that the full utilization of this A/D converter will require either a greatly improved sample holder and interface electronics or some data rate reduction on the chip.

DESIGN CONSIDERATIONS

Let us now look at the design considerations for this type of A/D converter. In particular we shall consider extending the present design to N = 8 bit resolution. The design goals for this converter, in order of importance will be (1) to achieve a monotonic output code, (2) to reduce the probability of single bit errors to an acceptable level and (3) to maximize the speed of operation. Here the term "single bit error" refers to an error in the value of the output code which is equal to 1 part in 2^N of the full scale value. It is important to note that by using Gray code small errors in the switch points of any of the N bits result only in single bit errors in the output code. In contrast, if binary code were used, an error in the switch point of any bit leads to an output error equal to the weight of that bit. e.g. half of full scale for the MSB. This, of course, is the reason for using Gray code.

To be useful, the final design must be compatible with a particular set of design rules. These design rules specify, among other things, a minimum linewidth and the thickness of various dielectric layers. This leads to a maximum achievable line impedance. For example, if the minimum linewidth is 5 μm and the dielectric thickness is 500 nm of SiO then the maximum line impedance is about Z_o = 15 Ω. This is a good starting point for the design of an 8-bit A/D converter.

Critical Current

If the SQUID comparators are to drive output lines of impedance Z_o to a voltage near V_g, then the minimum bias current I_o is given by V_g/Z_o. Since the normal bias level is about 75% of I_{mo} we can calculate a minimum value of I_{mo}

$$I_{mo} = \frac{V_g}{.75\, Z_o} \approx 0.25 \text{ mA.} \qquad (1)$$

Critical Current Uncertainty

There is another constraint on I_{no} which results from the fact that thermal noise in the output load resistors can lead to premature switching of any SQUID which is biased near its threshold curve. The effect of the noise may be described by drawing the threshold curve as a band which represents the region of bias over which switching is uncertain during the sampling time. The relative width of this band is strongly dependent on the value of the critical current. In order to prevent single bit errors, the width of the band at the normal bias level must be less than one part in 2^N of full scale for every SQUID comparator. This is shown in Fig. 5 which plots a portion of the threshold curves for the LSB and MSB SQUID comparators in an 8-bit converter. The problem is most difficult for the MSB comparator since the slope of its threshold curve is so small. The effect is readily observed in the experimental data of Fig. 3(A). This data represents an average over many samples so that the slope between transitions is a measure of the switch point uncertainty. For the MSB this slope spans a region about equal to 1/64 of full scale. This converter will therefore make a significant number of single bit errors.

The problem can be analyzed quantitatively by using Fig. 6 which is a plot of the lifetime τ of the zero voltage state of a single junction as a function of critical current for several different bias levels varying from 96.8 - 99.8% of the theoretical critical current [4]. These curves correspond to the single bit error threshold for bits 4 through 8 of an 8-bit converter. The time τ may be interpreted as the time which can be spent at the specified bias level before an error (premature switching) occurs. As an example, let us specify a single bit error rate less than 10% for a converter operating at 500 MHz in which the peak bias level is maintained for only about 5% of each cycle. The required value of τ then is $\tau = 0.05/(0.1 \times 5 \times 10^8) = 1$ ns. Figure 6 shows that the minimum critical currents for comparators 6, 7, and 8 are about 0.4, 1 and 3 mA respectively. The minimum critical current of lower order bits is dictated by loading considerations as described previously. The curves of Fig. 6 have been derived on the basis of a single junction whereas the converter uses double junction SQUID devices. Since a theory for the SQUID case doesn't presently exist we shall assume that the single junction result is adequate.

SQUID β_L

Another important parameter which must be chosen for the SQUID comparators is the value of $\beta_L = 2\pi (L_1 + L_2) I_o/\phi_o$. β_L is a measure of the number of flux quanta which can be stored in the SQUID loop. Figure 7 shows threshold curves for three different values of β_L [5]. The multiple lobes of the curves correspond to different numbers of flux quanta in the SQUID loop. If the operating point crosses the dashed portion of the curve the number of the flux quanta will change without switching to the voltage state. If the operating point crosses the solid portion of the curve, switching to the voltage state will occur. The ends of the solid lines are called the critical points. When operated in an A/D converter, the SQUID is biased to the level shown by the dashed line. The regions of this bias line below the threshold curve must fall inside the critical points to avoid spurious switching. For very low β_L one obtains the curve of Fig. 7(c) which has excellent immunity to spurious switching but due to the low inductance it has poor sensitivity to control current (large lobe separation). For large β_L as in Fig. 7(a) the sensitivity

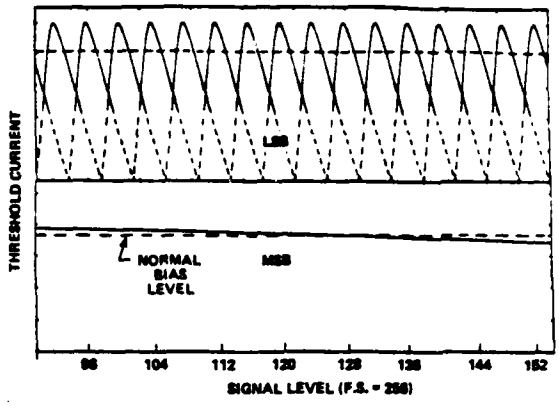

Fig. 5. A portion of the threshold curves for the LSB and MSB SQUID comparators in an 8-bit A/D converter.

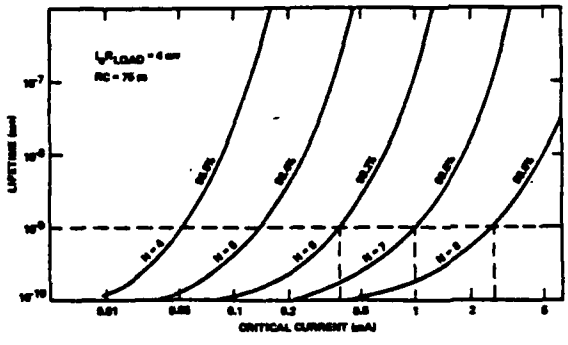

Fig. 6. The lifetime of the zero voltage state as a function of bias level and critical current.

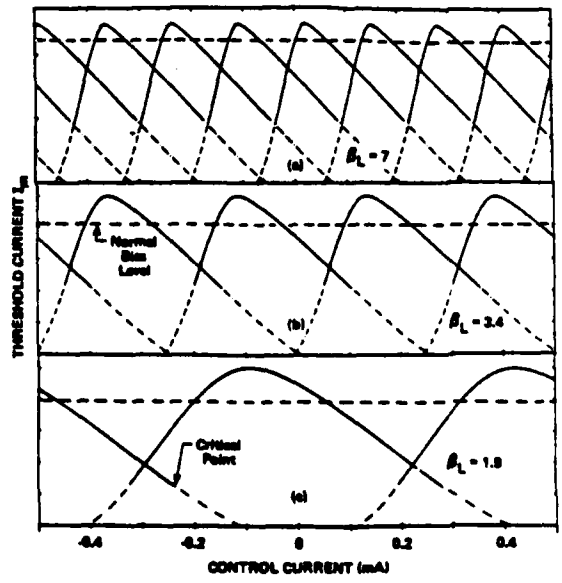

Fig. 7. Threshold curves for three different values of β_L. In each case $I_{o1} = I_{o2} = .125$ mA and the junction capacitances are 2.5 pF.

is high but overlap of the lobes allows spurious switching which is highly dependent on the past history of the SQUID. An acceptable compromise is for $\beta_L = 3.4$ as in Fig. 7(b).

The skew in the threshold curves of Fig. 7 is caused by making the value of L_1 much larger than L_2. This is done to increase the sensitivity of the comparator. In all three curves of Fig. 7 the damping resistor, R_d, is chosen by simulation to produce minimum overlap of the solid portions of the curve. The load resistor $R_L = Z_0$ is chosen to satisfy (1).

SQUID Comparator Design

With the results obtained so far it is possible to design a set of SQUID comparators for an 8-bit A/D converter. Table II is such a design. Each row of this table gives the design values for the n^{th} comparator where n (column 1) varies from 1 (LSB) to 8 (MSB). The second column shows the required number, n_ℓ, of threshold curve lobes for a full scale signal swing. This value is based on Gray code output and can be readily found by extending Table I. Column three gives the critical current, $I_o = I_m/2$, of each junction. These values are controlled by the previously described conditions of loading and critical current uncertainty. Column four is the total SQUID inductance and is based on $\beta_L = 2\pi (L_1 + L_2)I_o/\phi_o = 3.4$. The fifth and sixth columns show how this inductance is somewhat arbitrarily distributed between L_1 and L_2. Sensitivity is enhanced by maximizing L_1 especially for the lower order bits. Column 7 is the amount of signal current required to drive each SQUID through n_ℓ lobes of its threshold curve. The sum of column 7 is therefore the total full scale signal current, i.e. 40 mA. This is used to calculate column 8 which shows the fraction of signal current, f_n, directed to each SQUID.

Realizability

It is now important to consider whether the values in Table II can be realized with sufficient accuracy. In particular the values of I_o, L_1, and f_n must be achieved with an accuracy on the order of $1/2^8$ or 0.4%. In the present state of Josephson technology it is quite out of the question to control junction critical currents to 0.4%. However, it is possible to add an adjustable dc bias current to the gate current of each SQUID to appropriately set the switch points. This approach was used successfully with the 6-bit converter and should be extendable to 8-bits. A second set of bias currents can also be injected into the control input of each SQUID. These currents are used to adjust the phase of the threshold curve in order to compensate for local trapped flux or other magnetic fields.

In the case of the L_1 inductance values it is only necessary to achieve the ratios with high accuracy. It is expected that this can be done by increasing the size of the structures to reduce the effect of lithographic errors. Note that the most critical SQUIDs (1-4) are all identical. Also, errors in the inductance values of the last two bits can be completely compensated using the adjustments previously described.

The signal current division factors, f_n, have been contrived to come out as rational fractions. The required signal current division can therefore be accomplished by a simple set of identical resistors. This has the advantage that the division ratio becomes insensitive to the resistor value and lithography runout errors cancel to first order. Experience with the 6-bit converter has shown that current division to the necessary accuracy can be achieved. Figure 8 shows one way in which the desired division ratios could be realized using 29 identical resistors. If we choose R = 20 ohms, the signal input impedance is $Z_{in} = 0.4R = 8\ \Omega$ and the full scale signal voltage range is 320 mV.

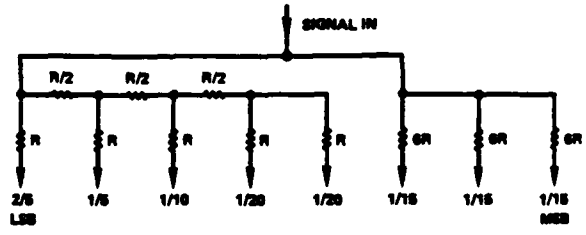

Fig. 8. A resistor network for achieving the current division ratios of Table II. Twenty-nine resistors of value R are required.

POWER SUPPLY REGULATION

Since all of the SQUID comparators are driven from a common power supply, it is imperative that this supply have a low enough impedance to prevent error causing crosstalk. From the point of view of power supply regulation, an 8-bit A/D converter can be described by the circuit of Fig. 9. I_s and G_s are the input supply current and the regulating conductance, respectively, the G_i are the conductances to each SQUID and the V_i are the voltages across the 8 SQUIDs. The supply bus voltage V is given by

$$V = \frac{I_s + \Sigma V_i G_i}{G_s + \Sigma G_i} . \qquad (2)$$

1 n	2 n_ℓ	3 I_o	4 $L_1 + L_2$	5 L_1	6 L_2	7 I_n(f.s.)	8 f_n	9 R_{supply}
1	64	0.125 mA	9 pH	8.28 pH	.72 pH	16 mA	2/5	304 Ω
2	32	0.125	9	8.28	.72	8	1/5	304
3	16	0.125	9	8.28	.72	4	1/10	304
4	8	0.125	9	8.28	.72	2	1/20	304
5	4	0.250	4.86	4.14	.72	2	1/20	152
6	2	0.5	3.10	1.55	1.55	2.67	1/15	76
7	1	1.0	1.55	.77	.77	2.67	1/15	38
8	0.5	2.0	.78	.39	.39	2.67	1/15	19

Table II. Design values for the SQUID comparators in an 8-bit A/D converter.

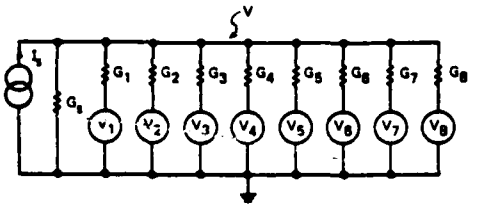

Fig. 9. Equivalent circuit for the A/D converter power supply.

The minimum value of V occurs when all the SQUIDs are in the zero voltage state where $V_1 = 0$. The maximum of V occurs when all the SQUIDs are in the voltage state where $V_1 = V_g$ the energy gap voltage. The worst case variation of V therefore is

$$\Delta V = V_{max} - V_{min} = \frac{V_g \Sigma G_1}{G_s + \Sigma G_1} \quad . \tag{3}$$

In order to avoid LSB errors due to supply variations $\Delta V/V$ must be less than $S/2^N$ where $S = 0.7$ is the slope of the threshold curve (dI_m/dI_c) at the operating point. This gives

$$\frac{V_g \Sigma G_1}{V(G_s + \Sigma G_1)} < \frac{S}{2^N} \quad . \tag{4}$$

We can now define a total bias current for all eight SQUIDs $I_b = V \Sigma G_1$ to obtain

$$\frac{V_g I_b}{V^2(G_s + \frac{I_b}{V})} < \frac{S}{2^N} \quad . \tag{5}$$

Limiting values in this equation are obtained by setting the equality and solving for V. An approximate solution for $G_s >> G_1$ is

$$V = \sqrt{\frac{2^N V_g I_b}{S G_s}} \quad . \tag{6}$$

There is some latitude in choosing G_s. Lower values improve the match to the room temperature supply but at the same time increase V and consequently increase power supply crosstalk at the chip mount. Power dissipation is largely independent of G_s and is approximately given by

$$P_s = 2^N V_g I_b / S \quad . \tag{7}$$

As an example assume $I_b = 6$ mA, $S = 0.7$, $V_g = 3$ mV, $N = 8$ and $G_s = 2$ Ω. This gives $V = 57$ mV and a power dissipation of 6.6 mW. Thus the required regulation (0.3%) can be achieved with a purely resistive regulator which dissipates only modest power. The values of the supply resistors $(R_1 = 1/G_1)$ are given by $R_1 = V/.75(2I_o)$ and are computed for our example case in the last column of Table II.

ADDITIONAL CONSIDERATIONS

Signal Line Crosstalk

When any SQUID switches there will be a transient voltage across its L_1 which may propagate to other SQUIDs causing them to switch erroneously. The maximum value of this transient voltage depends strongly on junction capacitance and is best determined by simulation. If we assume a junction capacitance of 20 pF/mA (critical current density of about 200 A/cm^2) it is found to be about 0.2 mV. Using the resistor network of Fig. 8, it can be shown that such a voltage transient at any SQUID is insufficient to cause a significant change in the threshold of any other SQUID. However, if junctions with much lower capacitance are used, these transients are larger and can cause errors. This is a reason to use the slowest (low critical current density, large area) junctions consistent with other design requirements.

Turn-On-Delay

In an 8-bit A/D converter some of the comparators will be required to switch with very small overdrive which may lead to substantial turn-on-delay [6]. If this turn-on-delay exceeds the gate current time, errors may occur. This problem may be considered in terms of a modified threshold curve which plots the boundary between the superconducting and voltage state for some specific gate current pulse width, e.g., a 1 ns pulse. If one now selects a new slightly higher gate current amplitude which intersects this modified threshold curve at the 50% duty cycle points, the effect of turn-on-delay is fully compensated.

Aperture Time

In order to make an accurate conversion, the signal applied to the converter must not change during the conversion time. This is normally accomplished by preceeding the converter with a sample and hold circuit. Suppose that this circuit averages the signal over an aperture time τ_a and then delivers this average value to the A/D converter. We may then ask how large τ_a may be before single bit errors occur between the averaged sample and an instantaneous sample. The answer may be found by averaging a sine wave, $\sin(2\pi Bt)$, at the signal bandwidth limit, B, over a time $T-\tau_a/2$ to $T + \tau_a/2$ and solving for the value of τ_a for which the average does not differ from $\sin(2\pi BT)$ by more than one part in 2^N. One finds that τ_a must satisfy the equation

$$1 - \frac{\sin \pi B\tau_a}{\pi B\tau_a} < \frac{1}{2^N} \tag{8}$$

for which an approximate solution is

$$\tau_a < \frac{1.6}{f_s} 2^{-(N/2)} \tag{9}$$

where $f_s = 2B$ is the Nyquist sampling rate and N is the number of bits in the conversion. Thus for an 8-bit converter operating at 500 MHz, $\tau_a = 200$ ps. Because of the large signal voltage and dynamic range in the present design, it is unlikely that an adequate sample and hold circuit could be implemented in superconducting technology. It should, however, be possible using a fast semiconductor technology.

An alternative approach is to require that the signal not change by more than one part in 2^N during the conversion time. The resulting requirement on conversion time is

$$\tau_c < 1/\pi f_s 2^{N-1} \quad . \qquad (10)$$

For N = 8 and f_s = 500 MHz, τ_c = 5 ps. Since 5 ps is far too little time to make a conversion, this approach is not very promising.

High Field Effects

The comparator for the LSB of our 8-bit converter is required to have 64 identical lobes in its threshold curve. In SQUIDs driven by external magnetic fields, flux penetrating the junctions leads to a decrease in the lobe amplitude after many cycles. However, by building the SQUID comparators on a superconducting ground plane the junctions are completely shielded from the field due to injected signal current. This is readily verified experimentally where more than 64 lobes have been observed with no detectable change in amplitude.

Limiting Speed

The entire reason for considering a superconducting A/D converter is the expectation that it will be very fast. An estimate of how fast is therefore appropriate. Suppose that we assume a monopolar power supply of the form $1+\sin 2\pi f_s t$. Let us somewhat arbitrarily divide a cycle into four parts as shown in Fig. 10. The active time, assumed to be about 20% of a cycle, consists of the turn-on-delay, the SQUID risetime and the time required to transfer data out. As mentioned previously a slight overdrive can be used to keep the turn-on-delay small, i.e. less than 20 ps. Assuming the SQUIDs are loaded according to (1) the risetime is Z_0C where C is the total capacitance of the two junctions. For 200 A/cm^2, 20 pF/mA junctions this risetime is 75 ps and a similar time would be required to transfer data out. The necessary active time is therefore about 170 ps which corresponds to a cycle time of 850 ps.

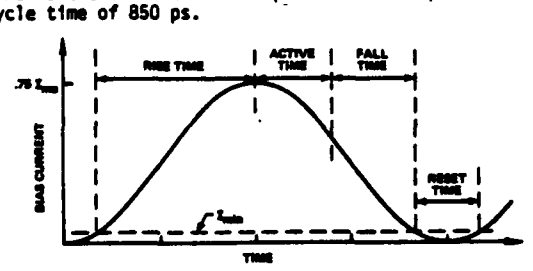

Fig. 10. One cycle of the power supply waveform.

The reset time is defined as the time during which the bias current is below I_{min} where I_{min} is the minimum current for which the junction can remain in the voltage state. I_{min} for a single junction is given by [7]:

$$I_{min} \approx \sqrt{2}\, I_o/\omega_p RC \quad , \qquad (11)$$

where the plasma frequency ω_p is:

$$\omega_p = \sqrt{2eI_o/\hbar C} \quad , \qquad (12)$$

and R is the resistive load. Assuming that the SQUID can be treated like a single junction the value of I_{min}/I_{max} is the same for all eight SQUID comparators of Table II and is about .05. This makes the reset time about 17% of a cycle.

The reset time must be long enough to ensure that all SQUIDs will reset with a high degree of probability. This problem has been studied extensively for power supplies which pass linearly through zero [7]. Although no results exist for our case, the fact that the supply lingers near zero should improve the reset probability. Simulations show that if the reset time is more than about $3Z_0C$ the SQUIDs will reset with high probability. For the SQUIDs in our A/D converter design $3Z_0C$ = 225 ps. Since this must be equal to or less than 17% of a cycle, the minimum cycle time is determined by the reset time and is 1.3 ns. This corresponds to a maximum sampling frequency of 760 MHz. Since both the active time and the reset time scale as junction capacitance, faster operation can be achieved by using lower capacitance (higher critical current density) junctions. However, as mentioned previously this may lead to errors due to crosstalk on the signal line. Also, as the junction areas decrease, lithography runout errors become more significant. It therefore becomes more difficult to achieve the desired critical current values.

SUMMARY

The principle of using SQUID comparators to perform A/D conversion has been reviewed. Experimental results with such a device have shown a monotonic output with 6-bits of accuracy. High speed testing suggests operation is possible at sampling rates of 4 GHz. A thorough analysis has been made of the design considerations for such converters using as an example an 8-bit converter with projected operation to sample rates of 760 MHZ. It has been found necessary to use large critical current SQUIDs to overcome the effects of noise in the comparators for the more significant bits. Adequate power supply regulation can be achieved with a simple resistive shunt. Turn-on-delay, signal line crosstalk, and high field effects have little influence on the design. The most important factor determining speed of operation is the time necessary to reset the SQUIDs between conversion cycles.

ACKNOWLEDGEMENTS

The authors are indebted to Donald B. Sullivan, Richard E. Harris, and Richard L. Kautz for discussions which contributed to this work.

REFERENCES

[1] H. H. Zappe, "Ultrasensitive Analog to Digital Converter Using Josephson Junctions," IBM Tech. Disc. Bull., Vol. 17 pp. 3053-3054, 1975.

[2] R. E. Harris, C. A. Hamilton, and F. L. Lloyd, "Multiple-Quantum Interference Superconducting Analog-to-Digital Converter," Appl. Phys. Lett., Vol. 35, pp. 720-721, 1979.

[3] C. A. Hamilton and Frances L. Lloyd, "A Superconducting 6-Bit Analog-to-Digital Converter with Operation to 2 x 10^9 Samples/Second," IEEE Electron Dev. Lett., Vol. EDL-1, pp. 92-94, 1980.

[4] R. L. Kautz, "On a Proposed Josephson Effect Voltage Standard at Zero Current Bias," Appl. Phys. Letters, Vol. 36, pp. 386-388, 1980.

[5] R. L. Peterson and C. A. Hamilton, "Analysis of Threshold Curves for Superconducting Interferometers," J. Appl. Phys., Vol. 50, pp. 8135-8142, 1979.

[6] E. P. Harris, "Turn-on-Delay of Josephson Interferometer Logic Devices," IEEE Trans. Mag., Vol. MAG-15, pp. 562-565, 1979.

[7] Robert E. Jewett and Theodore Van Duzer, "Low-Probability Punchthrough in Josephson Junctions," IEEE Trans. Mag., Vol. MAG-17, pp. 599-602, 1981.

DISTRIBUTION LIST

FOR

TECHNICAL REPORTS

CONTRACT NUMBER N00014-81-F-0048

	ADDRESSEE	NUMBER OF COPIES
1.	Office of Naval Research, Code 414Y 800 North Quincy Street Arlington, VA 22217 ATTN: Max N. Yoder	4
2.	Office of Naval Research Branch Office 1020 East Green Street Pasadena, CA 91106 ATTN: Richard G. Brandt	1
3.	TRW-Defense & Space Systems Group One Space Park Redondo Beach, CA 90278 ATTN: Arnold H. Silver	1
4.	IBM Corporation Federal Systems Division 2-L250 18100 Frederick Pike Gaithersburg, MD 20877 ATTN: Bryan C. Troutman	1
5.	TRW Defense Space Systems Group One Space Park Redondo Beach, CA 90278 ATTN: D. Claxton	1
6.	University of California Dept. of Electrical Engineering and Computer Science University of California Berkeley, CA 94720 ATTN: Ted Van Duzer	1
7.	Naval Research Laboratory, Code 2026 4555 Overlook Avenue, S.W. Washington, D. C. 20375	1
8.	Naval Research Laboratory, Code 6854 4555 Overlook Avenue, S.W. Washington, D. C. 20375	1

9. Data Acquisition Research
Tektronix
P. O. Box 500
Beaverton, OR 97077 — 1

10. University of California
Lawrence Livermore Laboratory
Livermore, CA 94550
ATTN: Joe Balch — 1

11. Hewlett-Packard
1501 Page Mill Road
Palo Alto, CA 94304 — 1

12. Texas Instruments, Inc.
P. O Box 5936
Dallas, TX 75222
ATTN: William Wiseman — 1

13. National Bureau of Standards
325 Broadway - Room 2137
Boulder, CO 80303
ATTN: Donald B. Sullivan — 4

14. Defense Documentation Center
Cameron Station Bldg. 5
Alexandria, VA 22314 — 12

15. A. G. E. D.
9th Floor
201 Varick Street
New York, NY 10014 — 1

16. Office of Naval Research, Code 6854
800 N. Quincy Street
Arlington, VA 22217 — 1

17. Department of Defense
R03
Fort Meade, MD 20755
ATTN: F. D. Bedard — 1

18. Lab for Physical Science
4928 College Ave.
College Park, MD 20740
ATTN: Nancy K. Welker — 1

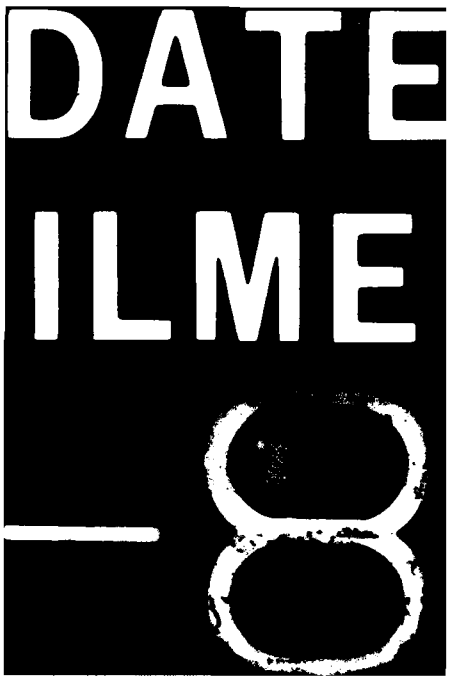
DATE
ILME
8